NANOSTRUCTURES AND PROPERTIES OF BLENDS OF HOMOPOLYMER AND ELASTOMERIC BLOCK COPOLYMER NANOPARTICLES

A Dissertation
Presented to
The Academic Faculty

by

Sungwon Ma

In Partial Fulfillment
of the Requirements for the Degree
Doctor of Philosophy in the
School of Polymer, Textile, and Fiber Engineering

Georgia Institute of Technology
August 2010

NANOSTRUCTURES AND PROPERTIES OF BLENDS OF HOMOPOLYMER AND ELASTOMERIC BLOCK COPOLYMER NANOPARTICLES

Approved by:

Dr. Yonathan Thio, Advisor
School of School of Polymer, Textile and Fiber
Georgia Institute of Technology

Dr. Seung Soon Jang
School of School of Materials Science and
Georgia Institute of Technology

Dr. David G. Bucknall
School of School of Polymer, Textile and Fiber
Georgia Institute of Technology

Dr. Vladimir Tsukruk
School of Polymer, Textile and Fiber
Georgia Institute of Technology

Dr. Anselm Griffin
School of School of Polymer, Textile and Fiber
Georgia Institute of Technology

Date Approved: June 21, 2010

ACKNOWLEDGEMENTS

First of all, I would like to express my gratitude to my advisor, Dr. Yonathan Thio for his guidance and for teaching me the ways of research.

I also would like to thank Dr. Anselm Griffin, Dr. David Bucknall, Dr. Vladimir Tsukruk, and Dr. Seung Soon Jang for their suggestions and for serving my committee members. I also would like to thank Dr. Parachuru for helping me to understand yarn testing.

Many thanks go to Dr. Jasmeet Kaur for helping to understand nanocomposites and Dr. Mihir Oka who is my group member for DMA, tensile tester, and nanoparticles. I also would like to thank Dr. Han Gi Chae for guiding and advising my research and Mrs. Beom-Jin Yoon, Young Ho Choi, Se Hoon Chang, Seung Geol Lee, Jihoon Lee, Ikjun Choi, Jae Ik Choi, Ram, and Sarang Deodhar, as well as Ms. Michelle Schlea for their help and friendship.

I am grateful to my parents, brother, and sister-in-law for their endless love, support, and patience.

TABLE OF CONTENTS

LIST OF TABLES

LIST OF FIGURES

SUMMARY

This thesis is on the topic of nanostructures and properties of blends of homopolymer and elastomeric block copolymer nanoparticles. The objectives of this thesis are: 1) to synthesize elastomeric nanofibers and nanosheets morphology utilizing the self-assembly of PS-b-PI copolymer and cold vulcanization process; 2) to study the viscoelastic properties of blends of polystyrene and the elastomeric nano-objects; 3) to investigate the morphology effect in elastomeric nano-object blends; 4) to study the control of crosslinking density of nanofibers and viscoelastic behavior using dynamic mechanical test; 5) to synthesize nanofibers having different PI core size using lamellar PS-b-PI copolymer by adding neat polystyrene; 6) to understand the effect of the core PI size and morphology in blends.

Chapter 1 presents the motivation and objectives as well as scope of the thesis. Overall introduction and brief review of literature of block copolymer, blends, nanocomposites, and viscoelastic properties are given in chapter 2. Synthesis and characterization of elastomeric nanofibers and nanosheets as well as PCM (partially crosslinked multi-junction) samples are introduced in chapter 3. Nanofibers and nanosheets were synthesized by cold vulcanization process using S_2Cl_2 crosslinking reagent resulting from self-assembly property of PS-PI block copolymer. The crosslinking reaction was confirmed by FT-IR using characterization peak of double bond of isoprene and by DSC using T_g point of polyisoprene. The blend samples for DMA were prepared by solvent casting method with varying weight percent of the nanoparticles.

Chapters 4 and 5 present results of rheological behavior and the effect of morphology between the elastomeric nanofiber and nanosheet blends. The critical volume concentration was investigated by percolation threshold theory for rod and disk. The characterization of nanofibers and nanosheets was carried out by SEM images. Nanofiber and nanosheet blends showed nanofiller effect and their structural change between 5 and 10 wt%, as fitted using Cross-Williamson three parameter model and calculated by percolation threshold theory.

Thermo-mechanical properties of two shapes of elastomeric nanoparticles, nanofibers and nanosheets, were measured using dynamic mechanical analysis to study the morphology effects in blends; the results are presented in chapter 6. The morphology of the nanoparticles was imaged by SEM and the nanoparticle morphologies in the blends were also characterized from fracture surface of DMA sample by SEM. In the nanofiber blends, storage and loss modulus increased with increasing filler loading in the terminal region. Tan δ results also showed that the value decreased with increasing nanofiber loading because the nanofiber morphology prevented the motion of neat PS. The moduli in the nanosheet blends indicated the values were similar to nanofiber blends in the terminal region but the value between 90 ^{o}C and 125 ^{o}C (T_g of neat PS) showed opposite result compared to nanofiber blends. Normalized tan δ values are plotted in terms of T - T_g in order to understand the effect of crosslinking filler and morphology. The study of activation energy using frequency sweep has been explored as well.

In chapter 7, the crosslinking density and morphology of nanofillers were investigated resulting in three elastomeric block copolymer nanofillers: fully crosslinked nanofiber (FCF), fully crosslinked multi-junction nanofiber (FCM) and partially

crosslinked multi-junction sample (PCM) using dynamic mechanical analysis. For comparison with these nanofillers, uncrosslinked PS-PI block copolymer (UBC) have been studied as well. The crosslinking density is calculated by measuring the change in intensity of the double bond peaks using FT-IR spectroscopy. The blends are prepared by solvent casting by mixing neat polystyrene and four nanofillers: FCF, FCM, PCM, UBC. The thermo-mechanical properties and morphology of the blends were characterized by dynamic mechanical analysis (DMA) and scanning electron microscope (SEM). DMA results show that the modulus increase with increasing filler loading in the terminal region in case of both PS/FCM and PS/FCF systems and the rate of increase is related to the crosslinking density. These results are interpreted as the effect of crosslinking density and the free volumes of fillers in blends.

In chapter 8, rheological properties of two nanofibers with the same PS block length but different core PI size are discussed. One type of nanofibers was synthesized and blended with polystyrene by the method described in chapter 3. Binary blending method, which is to blend a homopolymer and a diblock copolymer, was used in order to generate the other type of nanofibers morphology from lamellar PS-b-PI copolymer. The storage and loss moduli increased with increasing nanofiber loading. In order to study the core PI size and morphology effect, zero-shear viscosity and relaxation time are investigated. The values are obtained from three parameter Cross-Williamson model.

In chapter 9, conclusions and recommendations for future works are discussed.

CHAPTER 1

INTRODUCTION

1.1. Motivation and objectives

Block copolymers have been designed and used in many fields, for example, improving mechanical[1-5] and rheological properties[6-8], biomedical research[9-12] as well as electrical applications[13, 14]. Research on the self-assembly of block copolymers have contributed in areas such as those involving nanocomposites, nanowires, nanoparticle cages, drug-delivery systems. Research in recent decades has shown that self-assembly technique for block copolymers is a very useful way of fabricating micro and nano scale structures. By controlling the volume fractions of each block, various nanostructures can be created: spherical, cylindrical, lamellae, etc.[15, 16]. The structures assumed by self-assembly of block copolymers, however, cannot be maintained in melt, solution or suspension when blending with other polymers. Hence, the uses of self-assembled morphologies are limited to bulk or thin film of block copolymers. To maintain the self-assembled block copolymer structure in diverse processing conditions is one important issue in these research fields.

Hashimoto *et al*.[17-21] and many others[22-24] have studied the blends of block copolymers with homopolymers. The study[19] showed that the morphologies of the blends could be controlled by varying the molecular weight of the two polymers or their individual composition. However, blends of crosslinked copolymers combined with homopolymer have not been reported in the literature.

Moreover, many researchers have discussed the factors which affect the physical properties of blends[25, 26]. One of the important factors is the shape effect of nanofiller such as sphere, cylinder, and lamellar. Since physical properties of nanocomposites and blends strongly depend on the morphology and shape of nanofillers, the mechanical and rheological properties can be significantly changed by those filler morphologies. Many carbon based or inorganic fillers such as CNT, clay, and $CaCO_3$ are used as fillers for blending[27-29]. Some papers have explored elastomeric nanoparticles[30, 31] which are thermoplastics homopolymer. However, there are no detailed studies about elastomeric organic nanofillers which have cylindrical or lamellar morphology. Therefore, the approach of this thesis is to focus on verifying the morphology of self-assembled structure resulting from the crosslinking reaction and to investigate the effect of nanostructures in blends of crosslinked block copolymer with homopolymer.

This research project is focused on the mechanical and rheological properties of blends of crosslinked and uncrosslinked poly(styrene)-*b*-poly(isoprene) copolymer with neat polystyrene. Investigation of the blends of elastomeric nanoparticle with homopolymer and behavior of the nanoparticle in the system will provide the basic knowledge to understand and design future research associated with generating various nanoparticle morphologies as well as self-assembled and crosslinked system of block copolymers in blends. Furthermore, the method of generating various elastomeric nanoparticle morphologies is discussed.

1.2. Scope of dissertation

The main objective of this thesis is to study the blends of polystyrene with crosslinked PS-*b*-PI and with uncrosslinked PS-*b*-PI. Chapter 2 introduces and reviews relevant concepts for block copolymers, polymer blends, vulcanization, and viscoelastic properties. In chapter 3 and 4, the preparation of cylindrical and lamellae elastomeric nanoparticle and their viscoelastic properties are discussed. In chapter 5, the comparison of the morphologies between cylindrical and lamellar shaped elastomeric nanoparticle in blends is discussed. The effects of crosslinking density and shape on blends in terms of rheological and dynamic mechanical properties are discussed in chapter 6 and chapter 7, respectively. In chapter 8, effect of controlled core PI size in blends is studied.

CHAPTER 2

BACKGROUND

2.1. Block copolymer

2.1.1. Introduction

Block copolymers are a class of polymers that consists of two or more distinct contiguous parts. They can be polymerized by controlled synthesis methods where the molecular structure can be designed as diblock, triblock, random multiblock, arm starblock, etc. as shown in Figure 1.

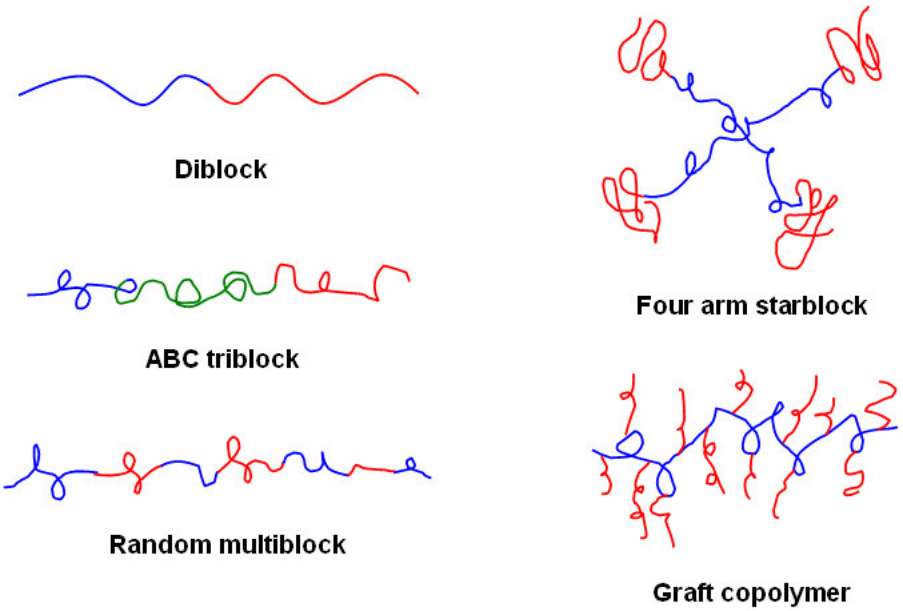

Figure 1. Various types of block copolymer architectures.

Block copolymers are also useful industrially because they allow a wide variety of hybrid properties by the choice of the blocks. As an example, thermoplastic elastomers are block copolymers which consists of a rubbery part (polybutadiene or polyisoprene)

and glassy domains (usually polystyrene). They are used in improving impact strength of thermoplastics, compatibilization and pressure-sensitive adhesion in the solid states and surfactant in solution states[32]. Useful reviews of these applications of block copolymer are available in books edited by Goodman[33, 34] and review articles by Riess *et al.*[35] for the solid state while the solution state application are reviewed by Schmolka[36] and Nace[37].

2.1.2. Melt behavior of block copolymer

In the melt, block copolymers can undergo self-assembly into various morphologies to minimize their free energy. Typically, block copolymers remain a homogenous mixture above a temperature called the order-disorder transition (ODT) temperature, but self-assemble below the ODT. The domain sizes of ordered structures are determined by the radii of gyration of the blocks, typically in the order of nanometers. The microphase separation behavior of block copolymers is usually characterized by three main parameters: the interactions, the length of the blocks, and the composition, as will be explained below.

The first main factor governing microphase separation is incompatibility between blocks. Below ODT, the blocks tend to segregate and lead to the microphase separation into nanoscale domains. The phase behavior is determined by the Gibbs free energy of mixing, which has two main components: energetic interaction between blocks (enthalpic term) and chain disorder (entropic term). This thermodynamic driving force is often described using the interaction parameter which was introduced by Flory-Huggins [38, 39]. The factor is often simply expressed as

$$\chi = \frac{A}{T} + B \tag{1}$$

where A and B are enthalpic and entropic coefficient, respectively.

The other main factors are the volume fraction of blocks and the degree of polymerization (N) which is defined by the number of segments in the block copolymer chain. The volume fraction is used instead of mole fraction because, unlike the thermodynamics of mixtures of small molecules, the molecules in a polymer mixture may occupy very different sizes of volume. Based on the above concepts, block copolymer phase behavior is usually generated using a phase diagram which is expressed by the combination of χN and volume fraction[15, 16, 32, 40].

The volume fraction of each block determines the morphology of ordered structure such as spheres, cylinders, bicontinuous networks, perforated layers, and lamellae[41]. According to strong and weak segregation theory[42, 43], χ and N act together to determine the morphology. Higher χ values represent strong separation and higher N (longer chain length) causes expansion of periodic size of block copolymer. Thus, the degree of incompatibility, χN, decides ordered or disordered structure in block copolymer system. In describing the degree of incompatibility of block copolymer, the terminology of segregation limit is commonly used: when χN is close to $(\chi N)_{ODT}$, the block copolymer is said to be in a weak segregation limit. At higher χN, it is said to be strongly segregated as shown in Figure 2.

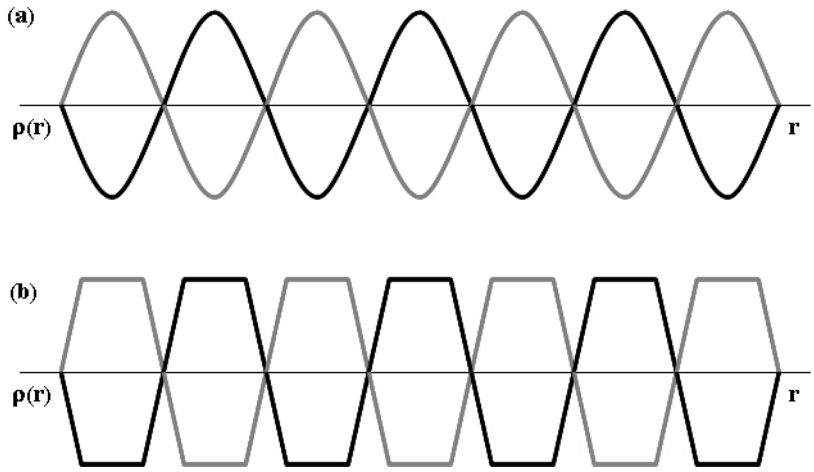

Figure 2. Composition profiles of A and B components in the weak segregation limit (a) and strong segregation limit (b).

Many researchers[40, 42-50] have made predictions of the order-disorder transition temperature for block copolymer systems. Helfand and Wasserman[42-45, 47] used statistical thermodynamic theory for free energy and domain size of block copolymer system. Leibler[40] established a theory for the microphase separation properties in block copolymers using a random phase approximation method introduced by de Gennes[51].

The theoretical and experimental studies on the phase separation of PS-***b***-PI copolymer are reviewed by Bates[15]. Figure 3 shows PS-***b***-PI copolymer phase diagram generated from theory[15] and experiments[41]. The theoretical phase diagram was predicted by self-consistent mean field theory[48, 52, 53]. It can be seen that the two phase diagrams are similar with acceptable amount of error. Both theoretical and experimental phase diagram of PS-***b***-PI linear block copolymer also show that χN and volume fraction determine the phase structure of the block copolymer.

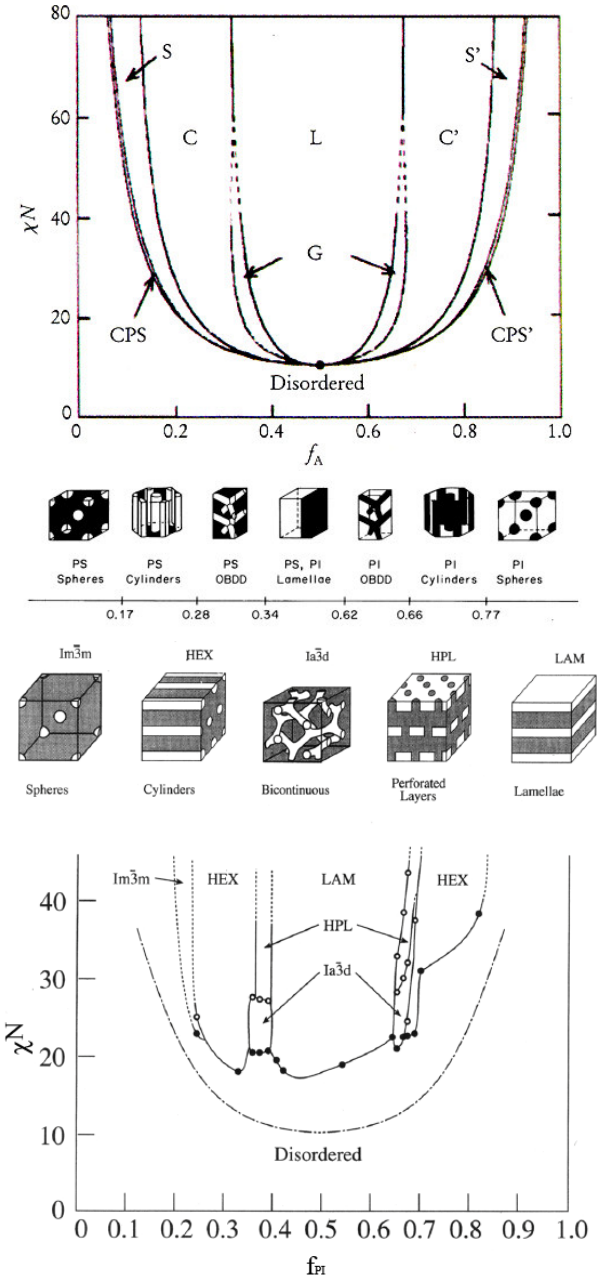

Figure 3 Theoretical[15] and experimental[41] phase diagram for polystyrene-polyisoprene (PS-***b***-PI) diblock copolymer and effect of various compositions on the ordered structures in PS-***b***-PI diblock copolymer. (f_A indicates volume fraction of PS block in PS-***b***-PI copolymer)

2.1.3. Self-consistent field theory of block copolymers

The critical challenge in theoretical modeling of block copolymer is how to predict the phase morphologies of block copolymers. One of the most useful theories of phase

separation of block copolymer is the self-consistent field theory (SCFT) by Edwards in the 1960s[54]. This theoretical work was developed by Helfand in 1975[42] and Hong *et al.* in 1981[55] contributing to the theory for treating block copolymers. In 1980s, weak-segregation and strong-segregation regime are reported by Leibler[40] and Ohta *et al.*[56] using an approximate analytical theory. Currently numerical methods are also used in an effort to solve the mean-field equation in order to obtain exact numerical solutions developed by Matsen and Schick in 1994[52]. Recently, some researchers have used the self-consistent field theory which included Gaussian fluctuations in ordered phase and numerical methods for analyzing phase behavior of block copolymers.

2.2. Blends and composites of block copolymer and nanoparticles

2.2.1. Introduction

In the last decade, quantitative information for the blends of block copolymers has been derived. Empirical studies of blends of block copolymers have been done, e.g. by Hashimoto[17-21, 57] and Winey[23, 58, 59]. Matsen[60, 61] provided detailed phase diagrams using self-consistent mean field theory[62] for the blends of block copolymers and homopolymers.

Homopolymer blends with block copolymers are also an attractive research area for applications such as compatibilizers and thermoplastic elastomers. In these applications, the block copolymer can be used for reducing the interfacial tension between homopolymers due to segregation of block copolymer. Polymer blends which involve two or more homopolymers and block copolymers have an interaction between the macro and micro separated homopolymers and block copolymer. These separation

properties are closely related to the length of the polymers chain and the composition of the blends. Many blend compositions are studied in academic and industrial areas.

In the case of blends of A type homopolymer and AB type diblock copolymer, block copolymer can dissolve homopolymers around the point which the phase separation occurs[63]. The condition for these phase separation behaviors is closely related to the relative chain lengths. For example, the relative chain length can be expressed by $\alpha = N_{Ah}/N_{Ac}$, where N_{Ah} is the degree of polymerization of the A homopolymer and N_{Ac} is the degree of polymerization of the A block on AB diblock copolymer[32].

There are a variety of possibilities of blends regarding homopolymers with block copolymers (i.e. A homopolymer/ABC triblock copolymer[64], AB diblock/AC diblock copolymer[65], AB diblock/ABA[66] or ABC triblock copolymer[67], and so on), but in this thesis, the blends of PS(A) homopolymer with PS-PI(AB) diblock copolymer is studied, with cold vulcanization utilizing elastomeric nanoparticles.

2.2.2. Polymer nanocomposites

If polymer and nanoparticles are mixed to form a heterogeneous structure, the physical properties of the composite depend on the physical properties of constituent materials, the size of nanoparticles, interaction between nanoparticle and polymer, as well as the morphology of nanoparticles[68]. Nanoparticles such as CNT, clay, gold, silver nanoparticles etc. have been studied because of their large surface area and physical properties. In addition, by controlling and modification of morphologies of the

nanoparticles, the specific properties may be modified for various purposes, e.g., mechanical, electrical, optical, and medical applications.

One advantage of using nanoparticles in polymer is to provide considerable changes in terms of physical properties at low weight fraction of nanoparticle. In order to accomplish the large changes in physical properties of nanocomposite material, several factors are important: 1) particle-particle and particle-matrix interaction, 2) percolation thresholds at low volume fraction, 3) large particle number densities (up to ~10^{20} cm^{-3}), 4) large interfacial area (10^7 cm^2cm^{-3}), and 5) the shape of nanoparticles[68].

Many studies on nanocomposites have been conducted intensively over several decades. The first synthesis study of polymer-clay nanocomposite material was performed in 1987 by researchers at the Toyota Polymer Research and Development Lab using exfoliation method of nylon-6 and clay for mechanical and thermal properties[69, 70]. Polymer–CNT(Carbon nanotube) nanocomposites are also an emerging research area because of the outstanding mechanical and electrical properties of CNT.

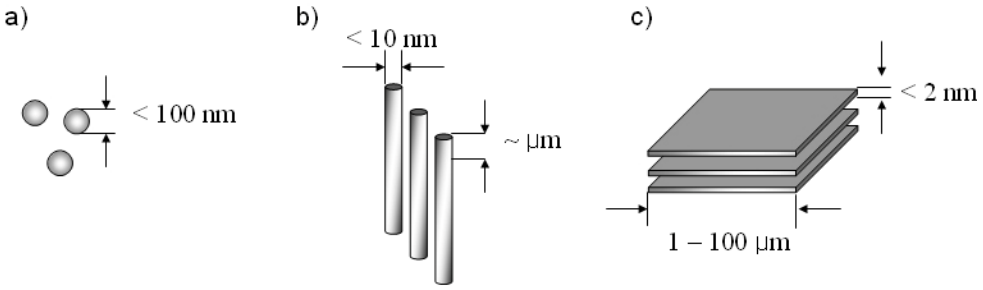

Figure 4. Various shapes of nanoparticles: a) Sphere type (e.g. ceramics, C_{60}, $CaCO_3$, gold and silver particles), b) Rod type (e.g. Carbon nanofiber, single/multi-walled carbon nanotube), and c) Platelet type (e.g. Montmorillonite and Graphite/Graphene)

2.2.3. Block copolymer nanocomposites

In the case of block copolymer nanocomposites, the geometrical structures of self-assembled block copolymer can act as a template for nanoscaled inclusions in terms of special localization and alignment. In a particular study, Fredrickson and Bicerano[71], have shown the barrier properties of polymer-clay hybrid system to depend on alignment of clay nanoparticle composites having well aligned nanoclay particles required significantly lower clay loading as compared composites having random clay dispersion for achieving similar barrier properties[71]. In addition, some theoretical studies[72, 73] regarding alignment effect suggested that the modulus of perfectly aligned clay composites can increase up to an of magnitude more than randomly oriented clay composites. These studies suggest that not only the distribution of nanoparticles in polymer matrix but also the morphological ordering of nanoparticles in the matrix is important factor for influencing the physical properties. Thus, introduction of nanostructures into block copolymer template has received much attention.

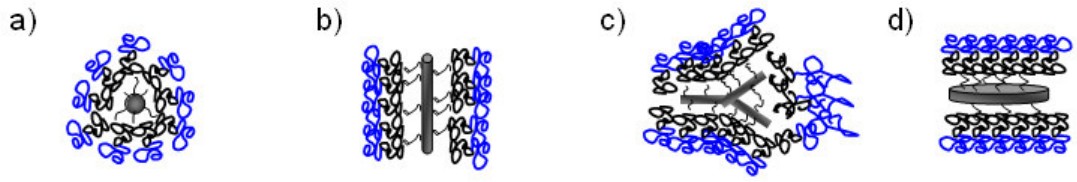

Figure 5. Schematic illustration of block copolymer chain arrangement in nanoparticle and diblock copolymer. (a) dot/sphere, (b) rod/cylinder, (c) tripod/gyroid, and (d) disc/lamellae[68].

2.2.4. Polymer particles

The use of rigid inorganic nanoparticles, such as glass fibers and clay nanoparticles, to modify the properties of homopolymers or block copolymer has been an active area of research[74-76]. On the other hand, the study of rubber-modified polymers – mainly for impact or toughening applications[77, 78] – has mostly been limited to the spherical geometry of the rubber inclusions in macro-scales, which is the preferred minimum energy geometry under most mixing conditions. Polymer particles in blends have been studied for their toughening mechanism as exemplified in recent reviews and articles by Mangaraj, Rajeev, and Yee[79-81]. Lee et al.[26] have explored the structure-property relationship for the blends. In addition, many studies have looked at silica, clay, and $CaCO_3$ as inorganic fillers in polymer nanocomposites[28, 29, 82]. While many studies have been conducted for rubber toughening properties using elastomeric particles having spherical shaped, there have been no systematic studies for blends of homopolymer and elastomeric nanoparticles having cylindrical and sheet morphologies in the literature,

The use of nanoparticles synthesized by crosslinked block copolymer provides us with a method to explore the role of geometry in rubber-modified systems without interpenetrating polymeric networks (IPN) at higher volume fraction. In particular, the effect of elastomeric nanoparticles in homopolymers on the surrounding polymer matrix has not been reported in the literature.

2.3. Fabrication of block copolymer nanoparticles

2.3.1. General vulcanization

Vulcanization is a process of modifying rubber or elastic material by introducing sulfide bonds resulting in a 3-D crosslinked structure. These sulfide bonds increase the elasticity of the material and reduce the plasticity. Since the first discovery of rubber vulcanization by Charles Goodyear in 1839, the vulcanization process and technology have developed further to be used in many industrial and research areas. The use of sulfur to crosslink natural rubber (NR), styrene-butadiene rubber (SBR), butadiene rubber (BR), and other polymers having unsaturated carbon group has been studied. Vulcanization could also be accomplished without elemental sulfur using some sulfur compounds and their derivatives, i.e. sulfur-donor compounds, which include thiuram, thiourea, demercapto, and S-Cl compounds[83]. A typical process of vulcanization uses high temperature of around 170 ^{o}C or electron beams such as UV radiation, γ-rays and ultrasonic waves. In this study, S-Cl sulfur compounds will be used for vulcanization of block copolymers at room temperature.

2.3.2. Cold vulcanization

It is possible to accomplish vulcanization at room temperature using sulfur monochloride (S_2Cl_2). Glazer[84] has reported a cold vulcanization process in polyisoprene. In this method[84], the S_2Cl_2 crosslinking reagent was first vaporized at room temperature and then used to cure the isoprene units by creating sulfide bonds. The same group[85, 86] had also studied the kinetics and mechanism of cold vulcanization process between rubber and sulfur monochloride.

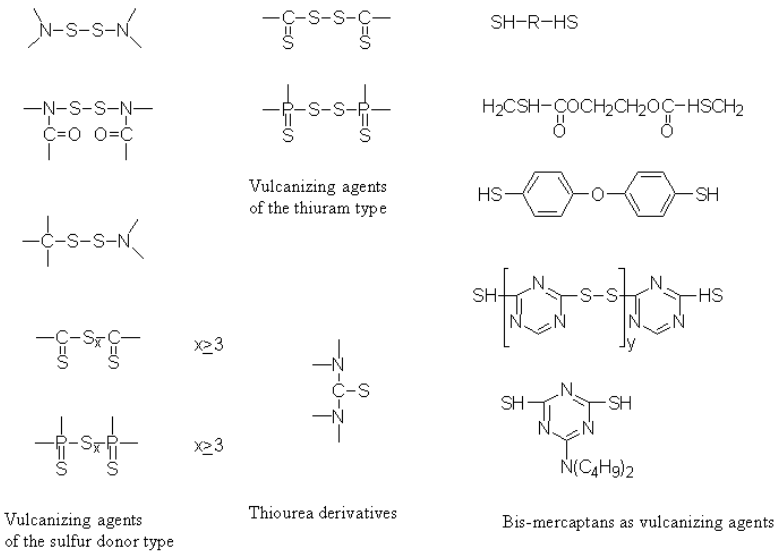

Figure 6. Compounds with sulfur-bearing functional groups[83].

2.3.3. Fabrication of elastomeric nanoparticles

Elastomeric nano-domains are formed by phase separation of PS-PI block copolymer and maintained by crosslinking reaction of the polyisoprene block, which acts as a core structure. These nanoparticles have potential applications as nanocomposites, membranes, tissue engineering materials, etc. Block copolymer nanoparticles can be obtained by employing the phase separation properties of block copolymers. For example, two common methods to obtain cylindrical morphology from block copolymer are 1) the use of a selective solvent[87] to create cylindrical micelles and 2) self-assembly in the bulk[88] to form hexagonal packed cylindrical domains. Most strongly segregated diblock copolymers which have approximately 70:30 volume fraction will construct hexagonally packed cylindrical structures[15]. In order to maintain cylindrical structure, selective crosslinking can be used, as exemplified by the use of S_2Cl_2 as crosslinking

agent for the cylindrical domains by Liu *et al.*[89]. Their study demonstrated that PS-*b*-PI copolymer (30 vol%, isoprene) formed hexagonally packed cylindrical morphology and the isoprene units were crosslinkable by S_2Cl_2 thereby generating block copolymer nanoparticles.

Based on the method, nanofiber and nanosheet structures are generated. Block copolymer self-assembly is one of the most facile methods to generate various nano sized morphologies such as sphere, cylinder, gyroid, and lamellar. Figure 7 is schematic illustration of PS-b-PI morphologies from different PS and PI volume fraction and crosslinking reaction. For example, the three different morphologies shown can be used to generate sphere, fiber, and sheet nanostructures.

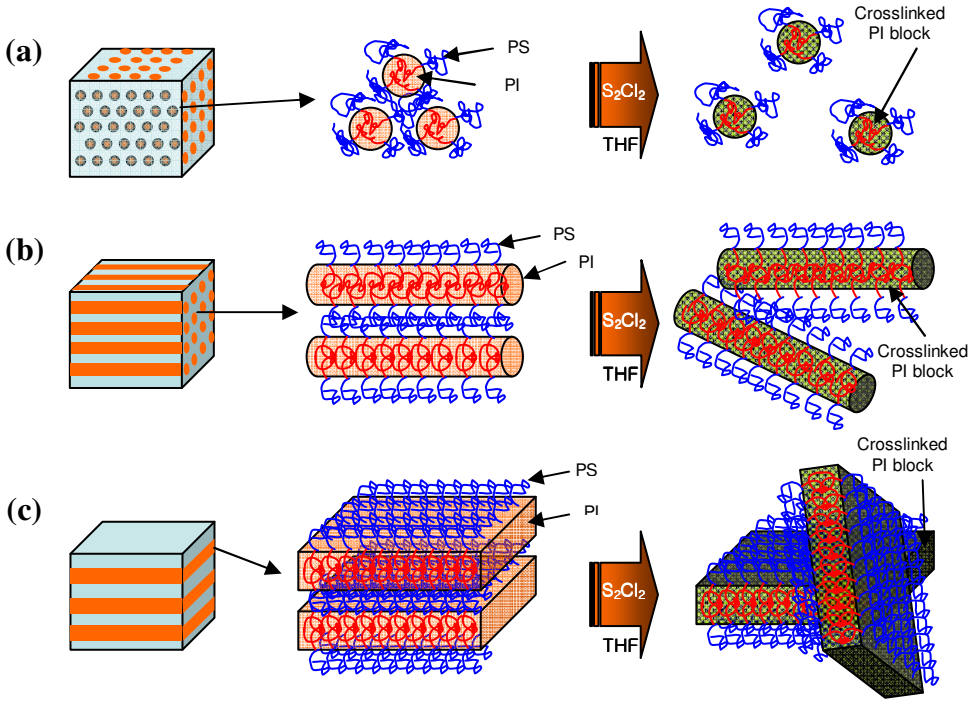

Figure 7. Schematic illustration of PS-PI morphologies of nanoparticles. Sphere (a), cylinder (b), and lamellar (c) shaped structures and crosslinked morphologies.

2.4. Viscoelastic properties in blends and composites

2.4.1. Introduction

Polymers exhibit viscoelastic properties, which depends on temperature and rates. Elastic materials can store their mechanical energy as potential energy, whereas viscous fluid dissipates the mechanical energy as heat when viscoelastic materials are deformed. The investigation of these energy variations in a wide range of temperature or rates has proven to be very useful for studying the physical properties of viscoelastic materials such as glass transition temperature, relaxation spectra, crystallinity, molecular orientation, and morphology of block copolymer. In addition, the study of these structure-property relationships of viscoelastic materials can be extended to polymer blends and composites. In this thesis, rheology and dynamic mechanical analysis will be discussed.

2.4.2. Rheology

Rheology is the study of flow and deformation[90, 91]. Many researchers[6-8, 92-98] have studied the fundamental relations between force and deformation in polymeric blends and composites. Rheological properties provide information about thermo-mechanical properties such as viscosity, relaxation time, material function, and molecular weight. Rheology has been utilized as a quantitative tool to study polymer blends system containing organic or inorganic nanoparticles[92, 93, 98]. In some cases of polymer blends and composites, particle dispersion is a major concern. The incorporation of nanostructured fillers in polymer matrix contributes to a significant improvement in the viscoelastic properties[99]. The filler shape and morphology can affect both linear and

non-linear viscoelastic properties in polymer blend or composite systems[99]. Hence, rheology has been applied as a tool to study the effect of filler in the blend or composites systems.

Rheology could also be extended toward the analysis of ordered structure in copolymer systems. Han *et al.*[100, 101] identified the order-disorder transition temperature (ODT) in the block copolymer system using rheology. In particular, they studied the relationship between dynamic moduli ($G'(\omega)$ or $G''(\omega)$) and angular frequency(ω) under isothermal condition and plotted storage modulus as a function of loss modulus to determine the ordered or disordered state using a modification of Doi-Edwards model[102].

One way to characterize the microphase separation of block copolymer is to study the flow behavior of the polymers. In addition, the flow properties are highly sensitive to the structure, size, shape and surface property of the particles. Hence, the study of rheology in polymer systems is a very useful way to understand their properties.

2.4.3. Dynamic mechanical analysis.

Dynamic mechanical analysis can be used as the determination of the dynamic mechanical properties of polymeric materials. There are relationships between the dynamic properties and the structural factors such as crystallinity, molecular weight, crosslinking, molecular structures, and compositions. In addition, the analysis results can be affected by temperature, pressure, time, and frequency, and type of deformation.

The dynamic mechanical properties are determined by the dynamic storage modulus (E'), the loss modulus (E''), and $\tan \delta = E''/E'$ resulting from nondestructive tests.

These tests measure the changes of these properties during the deformation of polymeric materials in terms of the factors such as temperature, frequencies, amplitude, and oscillation.

Dynamic mechanical analysis is very useful method to do dynamic studies for polymer blends or composites from single polymeric system to complex multi-blending such as thermoplastic blends, organic-inorganic nanocomposites, and crosslinked rubber.

CHAPTER 3

SYNTHESIS AND CHARACTERIZATION OF ELASTOMERIC NANOOBJECTS AND PREPARATION OF BLENDS

3.1. Introduction

Rubber vulcanization has been used to generate thermoplastic elastomeric nanoparticles that have a spherical shape resulting from the surface tension in the blends[31]. Various studies have been performed over several decades in order to understand the toughening mechanisms of rubber and fracture behavior[78, 103]. The majority of the studies focused on spherical rubber particles with diameters of several microns. In this chapter, the nanofiber structures and the nanosheet morphologies are generated by cold vulcanization using a modification of the approach by Liu *et al*.[89]. In addition, synthesis of elastomeric nanoparticles, especially nanofibers and nanosheets, is discussed. The detailed characterization methods and preparation of blended samples are also reported.

3.2. Preparation of nanofibers, nanosheets, and their blends

3.2.1. Materials

Polystyrene-b-polyisoprene copolymers were obtained from Polymer Source Co. Ltd. and the properties are given in Table 1. Sulfur chloride (S_2Cl_2) and polystyrene of $\overline{M}_w$=350,000 g/mol (PDI: 2.06) were purchased from Aldrich. Materials and solvents were used as received.

Table 1. Characterization data of PS-b-PI copolymers. Volume fractions of polyisoprene were calculated from specific volume of PS and PI[100, 104].

	Mn(Kg/mol)	$Tg(^oC)_{DSC}$		PDI	PI content	
Polymer	PS-*b*-PI	PS part	PI part	M_w/M_n	Vol. fraction	Morphology
SI23	23-*b*-8.0	101.6	-68.9	1.07	0.23	Cylinder
SI43	31.6-*b*-28	91.4	-62.3	1.06	0.43	Lamellar

3.2.2. Synthesis of nanofibers and nanosheets

The nanoparticle synthesis was carried out by following the methodology described by Liu *et al*[89] with a few modifications. 1g of PS-*b*-PI block copolymers was dissolved in toluene as 15 wt% solution. The solution was cast into a glass dish with diameter of 90 mm and dried under N_2 environment for 3 days. The dried film and S_2Cl_2 were placed in the same glass chamber for a week. The film was later dried in a vacuum oven in order to remove excess S_2Cl_2. The nanofibers were dispersed in THF by vigorous stirring for a week.

Nanoparticles and gel were separated by centrifugation at 3,000 rpm. The supernatant was first precipitated using methanol and filtered and dried afterwards. The gel was sonicated for 12 hours to release the entangled fiber. The crosslinked PS-*b*-PI fiber obtained from gel was precipitated using methanol. The filtration and drying were carried out for 24 hours at room temperature under vacuum.

The nanoparticles ranging from 0.5 to 10.0 wt% were used to prepare the blend samples with neat PS. The particles were initially swelled in toluene for 24 hours to

achieve better dispersion of fillers in solution. The swelled nanoparticles were later mixed with polystyrene. Total concentration of the solution was 10 % by weight. Oxidation of the polyisoprene block was prevented by the addition of 1 % by weight of 2-6-di-tert-butyl-4-methyl-pheonl (BHT) in the polyisoprene block[105]. A solvent casting method was used to make films from the blends. The solution of the blends was first poured into an aluminum dish and then dried for 3 days at room temperature. The evaporation of the residual solvent in the cast film was carried out in a vacuum oven at 80 ^{o}C for 24 hours.

3.2.3. Preparation of blends

Table 7 shows blend sample data with the weight fraction of polyisoprene. The nanofibers and nanosheets were prepared to blend with neat polystyrene at concentrations of 0.5 – 10 wt%. In order to compare the effect of crosslinked PS-b-PI in the blends, neat polystyrene with uncrosslinked PS-b-PI blends samples were prepared as well. To improve the mixing, the nanofibers and nanosheets were first swelled in toluene for 24 hours and then neat polystyrene was added. The blend films were prepared using a solvent casting method and aluminum foil was used as dishes for drying. The cast films were dried at room temperature for 2 days. In order to completely dry, the films were placed in a vacuum oven and dried above 100 ^{o}C for 24 hrs. The samples for the mechanical and rheological tests were prepared using a compression molding machine.

Table 2. Sample codes of blends of nanoparticle and block copolymer with PS as well as blended weight percent of PS-b-PI and calculated PI weight percent.

Sample code	PS-b-PI: wt%	PI: wt%	Sample code	PS-b-PI: wt%	PI: wt%
PS/fiber and PS/SI23	0.5	0.13	PS/sheet and PS/SI43	0.5	0.23
	1	0.26		1	0.47
	2	0.51		2	0.93
	5	1.32		5	2.38
	10	2.81		10	4.99

3.3. Control of crosslinking density in nanofibers

3.3.1. Material

Materials used in this section are the same as described in Section 3.2.1.

3.3.2. Synthesis

Due to the self-assembling properties of block copolymer, different geometries were obtained by cold vulcanization which was described in Section 3.2.2. such as fully crosslinked nanofibers (FCF) and fully crosslinked nanofibers having multi-junction points (FCM). They were separated using sonication for 12 hours and centrifugation at 3000 rpm.

In order to control the crosslinking density, a modification of the method published by Liu *et al.*[89] was used. To synthesize partially crosslinked samples (PCM), completely dried PS-b-PI samples were prepared using the same method described in

Section 3.2.2. The S_2Cl_2 crosslinking reagent was diluted using hexane as 3 wt% in order to carry out the crosslinking reaction slowly[106]. Prepared hexane solution was placed into the same chamber. The sample was exposed to the solution for different times (1, 3, 7, 24, 49, and 120 hrs). The same procedure described in Section 3.2.2 was used to obtain final product.

3.3.3 Preparation of blends

The fillers were used for preparing blended samples using a solvent casting method. The fillers were first swelled in toluene for a day and neat PS was then dissolved in same solution with vigorous stirring for an additional day. The concentration of the mixture was 10 wt%. The solution was poured into the dish made of aluminum foil. The samples were dried for 3-4 days in the hood. The residual solvent was removed under the vacuum at 100 ^{o}C for 12 hours. The dried samples were pressed and cut in preparation to test viscoelastic properties. The sample codes are listed in Table 3. Sample preparation of blends used in this section was discussed in section 3.2.3.

Table 3. Blends of neat PS with nanofiber and with uncrosslinked PS-b-PI having 0.23 volume fraction of polyisoprene. A range of concentration is from 0.5 to 10 wt%

Sample Code	Description	Crosslinking Time	S_2Cl_2 Concentration	Relative crosslinking density
FCF	fully crosslinked nanofiber	168 hrs	100 wt%	100%
FCM	fully crosslinked multi-junction	168 hrs	100 wt%	100%
PCM	partially crosslinked multi-junction	24 hrs	3 wt%	78%
UBC	uncrosslinked block copolymer	N/A	N/A	0%

3.4. Core PI size control of nanofibers

3.4.1. Material and synthesis

1 g of PS-PI block copolymer which has a 31,500-28,000 molecular weight (g/mol) was dissolved in toluene and 3.29 g of neat PS having 35,000 molecular weight (g/mol) were also dissolved in the same solution in order to generate a cylindrical morphology from lamellar morphology. The solution was dried in a glass dish for 3-4 days. The sample was crosslinked for a week and swelled. Finally, the sample was precipitated and filtered. Table 4 shows the sample codes and characteristic information.

Table 4. characteristics of PS-b-PI copolymer

sample	Morphology	MW(PS-PI)	MW of neat PS	Final morphology
Nanofiber-A	cylinder	23000-8000	N/A	cylinder
Nanofiber-B	lamellar	31500-28000	35000	cylinder

3.4.2. Preparation of blends

Sample preparation of blends used in this section is identical to the one described in section 3.2.3.

3.5. Characterizations

3.5.1. Equipment

The fracture surfaces of the blended samples were imaged using LEO 1530 scanning electron microscopy. A gold coating was applied for all SEM samples. The images were obtained by thermally assisted field emission scanning electron microscopy applying 5 keV using the In-Lens detector.

The dynamic rheological values were measured by an AR2000 (TA Instrument) using 25 mm diameter parallel plates. Samples were tested between 160 ^{o}C and 200 ^{o}C with a step of 10 ^{o}C. All tests were carried out in the frequency range of 0.01 – 100 Hz (0.0628 – 628 rad/s) with a strain of 0.05%.

The samples for dynamic mechanical analysis (DMA) were compression molded from solvent casted films using a hot press machine at 150 ^{o}C. The film thicknesses were maintained between 0.4 and 0.5 mm. The DMA was carried out in tension mode under a constant heating rate of 2 ^{o}C/min and at a frequency of 2 Hz. The temperature range was from 35 ^{o}C to 160 ^{o}C.

Fourier transform infrared spectroscopy (FT-IR) was performed using a Perkin-Elmer Spectrum One equipped with auto image microscope. The spectra were recorded using 128 scans at a resolution of 4 cm^{-1} in the range between 4000 and 600 cm^{-1}. The FT-IR samples were prepared using KBr with press machine.

Glass transition temperatures of the samples were measured by differential scanning calorimetry (DSC). The results were collected in the range from -90 to 150 ^{o}C at a heating rate of 10 ^{o}C/min using TA instrument model TA 800.

3.5.2. Characterization of nanofibers and nanosheets

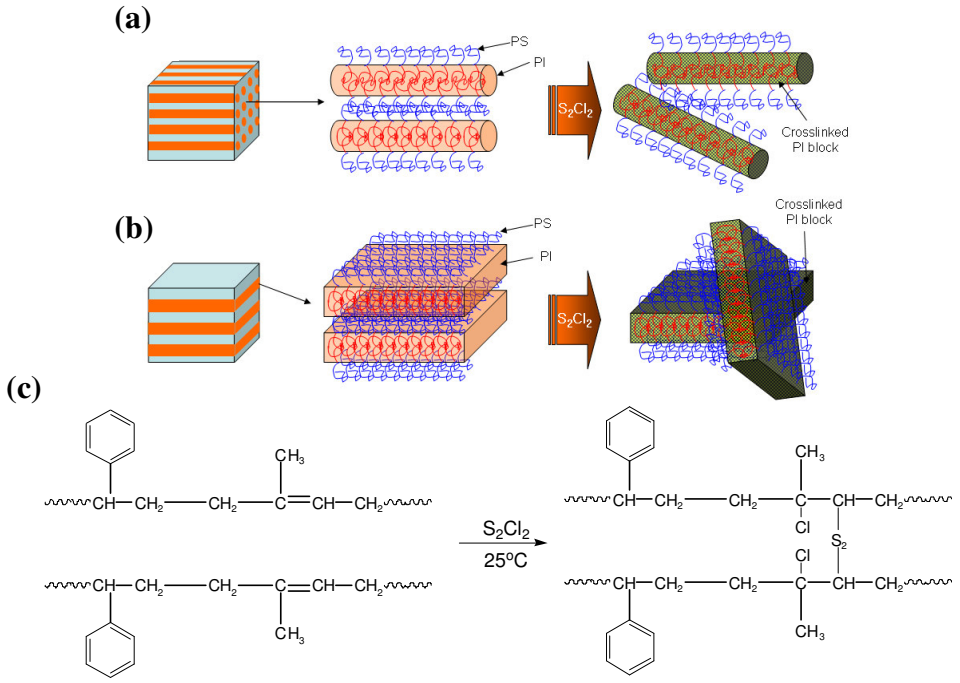

Figure 8. The sketch of cold vulcanization process from cylinder (a) and lamellar (b) morphology using S_2Cl_2 crosslinking agent and the chemical reaction of cold vulcanization (c).

Figure 8 (a) and (b) show a schematic illustration of two morphologies of the PS-b-PI copolymer. The self-assembled cylindrical PS-b-PI structure consists of PS (70 vol.%) as a shell and PI (30 vol.%) as a core due to their volume fraction. When the S_2Cl_2 crosslinking agent is applied, double bonds in the isoprene block make a sulfur linkage between two backbone chains. Finally the crosslinked cylindrical building block can be obtained in the form of fiber. In the case of lamellar PS-b-PI by maintaining 50/50 volume fraction, sheet shaped block copolymer particles are obtained. Figure 8 (c) shows the chemical reaction occurring in the crosslinking reaction.

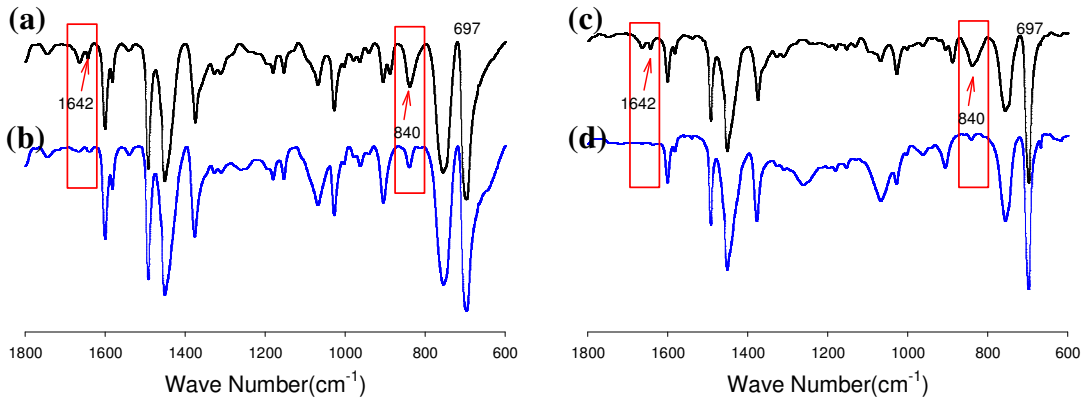

Figure 9. FT-IR spectra of (a) SI23 before crosslinking reaction and (b) fiber after crosslinking reaction of cylindrical morphology, (c) SI43 having lamellar morphology before crosslinking reaction and (d) sheet after crosslinking reaction.

The detection of the double bond peak of isoprene at 1642 cm^{-1} was carried out using FT-IR. The intensity of the double bond peak in isoprene is decreased after the crosslinking reaction as shown in Figure 9. FT-IR spectra of the two morphologies of PS-b-PI before and after the crosslinking reaction are shown in Figure 9. In order to do a quantitative comparison, the 697 cm^{-1} peak of a mono-substituted phenyl ring was used as a reference[107]. Two characteristic peaks which indicate the double bond in polyisoprene are decreased after the crosslinking reaction as shown in Figure 9.

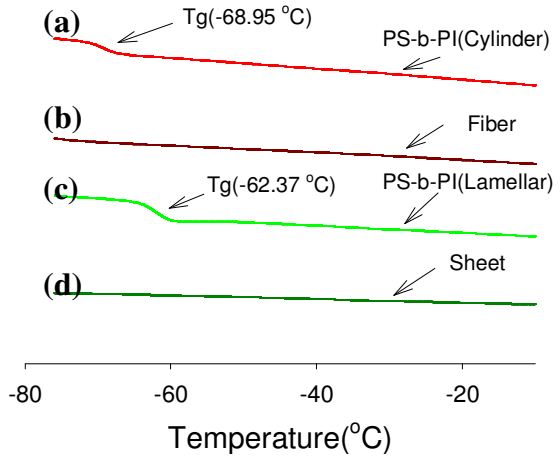

Figure 10. Heat flow plot at low temperature range for PS-b-PI samples of before and after crosslinking reaction. From top to bottom (a) SI23, (b) crosslinked SI23, (c) SI43, and (d) crosslinked SI43.

Differential scanning calorimetry (DSC) was used as another characterization tool for confirming crosslinking reaction. In Figure 10, the glass transition temperature (T_g) of an uncrosslinked PS-b-PI sample is -68.5 °C resulting from the motion of the isoprene chain whereas after the crosslinking reaction, the T_g is not detected as seen in Figure 10 (b). In the case of the PS-b-PI having lamellar morphology, the T_g of isoprene is also not identified by DSC after the crosslinking reaction as seen in Figure 10 (d). These results suggest that the crosslinking reaction was successfully accomplished by the S_2Cl_2 crosslinking reagent at room temperature.

CHAPTER 4

VISCOELASTIC PROPERTIES OF BLENDS OF POLYSTYRENE AND CROSSLINKED POLYSTYRENE-POLYISOPRENE NANOFIBER

4.1. Introduction

This chapter reports the study on the viscoelastic properties of blends of crosslinked and uncrosslinked PS-*b*-PI copolymer with neat polystyrene. Maintaining the self-assembled block copolymer structures in diverse processing conditions will provide various possible potential applications. The investigation of viscoelastic behavior of the blends of PS-*b*-PI nanofibers with the homopolymer provides the basic knowledge to understand and design future research in self-assembled and crosslinked systems of block copolymers. In addition, this study could contribute to understanding the blends of homopolymers with block copolymers containing a rubbery part in terms of mechanical and rheological property changes.

4.2. Result and Discussion

4.2.1. Crosslinking process

The crosslinking process using cold vulcanization was discussed in Chapter 3. The diffusion of S_2Cl_2 in the PS-*b*-PI film can affect the crosslinking density. Liu *et al.*[89], observed diffusion of S_2Cl_2 vapor in a relatively thick PS-*b*-PI film. Their results confirm

that the choice of film with thickness below 5 mm in this experiment was sufficient to allow uniform crosslinking density in the bulk.

4.2.2. Characterization of PS-*b*-PI Nanofibers

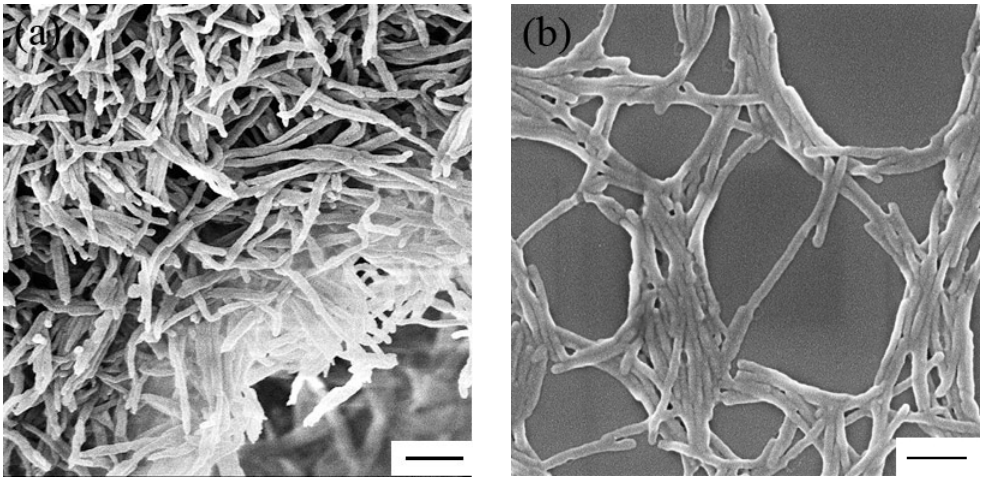

Figure 11. SEM micrographs of PS-*b*-PI nanofibers (a) in the bulk and (b) spincoated from dilute suspension on silicon wafer. Each scale bar indicates 300 nm.

Figure 11 (a) and (b) show SEM micrographs of prepared nanofibers and their morphology. A number of individual nanofibers can be observed from the images in Figure 11 (a) and (b). The nanofiber length is on the order of several microns measured by manually using SEM images whereas the diameter of the fibers is about 35 nm. Liu *et al*.[89] reported a value of 21 nm for the diameter of the PS-*b*-PI cylindrical morphology using the same molecular weight of PS-*b*-PI. Their lower diameter value was based on the uncrosslinked domain size measured using TEM. The difference in the observed diameters is likely due to the processing effect where solvents will separate the nanofibers from each other and swell them. The polystyrene outer layer structure dries

first and becomes glassy thereby preventing the swollen isoprene core from shrinking during drying.

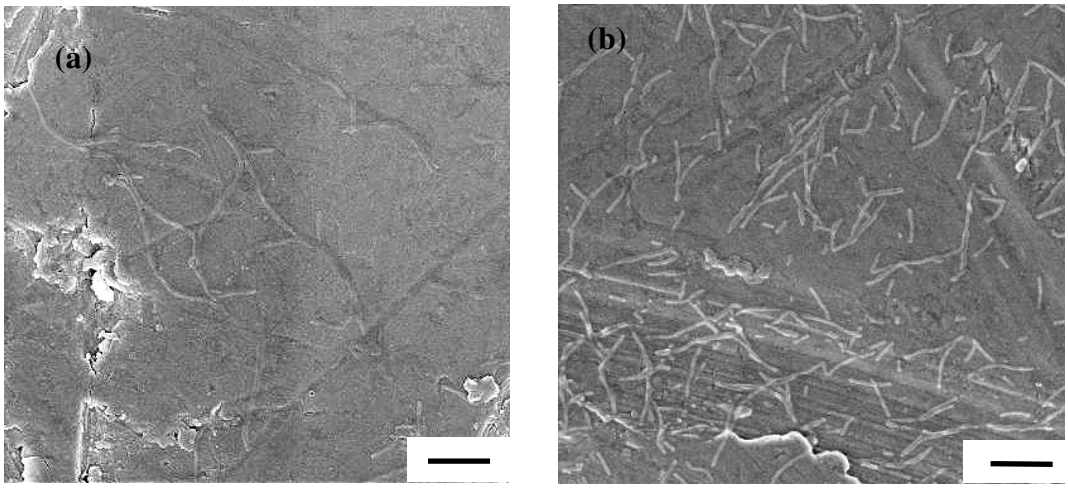

Figure 12. SEM images of PS-PI nanofibers (a) long length and broad distribution and (b) short length and narrow distribution. Each scale bar indicates 1 μm.

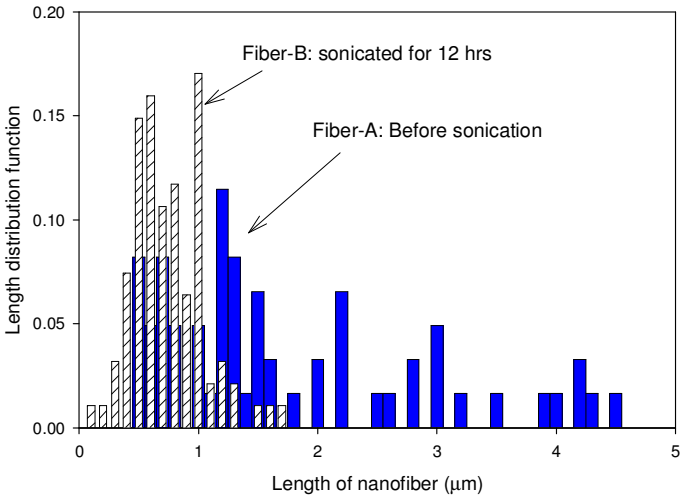

Figure 13. Nanofiber length distribution profile for long and short fibers. Thin bars with stripes indicate the sample before sonication for separate the size distribution and thick bars show the sample that was applied for 12 hrs using sonicator.

After the separation of nanofibers from the bulk in a suspension, sonication was performed to obtain two different length distributions of. Depending on the sonication

time, two nanofiber samples were prepared: one with an average length of ~1.7 µm and the other with average length of ~ 0.7 µm. Figure 12 (a) shows that the longer nanofiber population has a broad distribution. The short nanofibers were prepared using a sonication method of the S_2Cl_2 treated PS-*b*-PI film as shown in Figure 12 (b). In order to compare the length profile, each nanofiber length was measured manually from SEM images. Figure 13 gives the result of the length distribution function in terms of fiber length. Only long fibers having lengths between 2 and 5 µm were removed from the unsonicated fiber after sonication for 12 hours. This suggests that the stress from the ultrasonic power breaks longer fiber before affecting the shorter fibers. The center of the fiber was likely the weakest point where the fracture could occur. In this chapter, only the nanofibers with a narrow length distribution were reported as shown in Figure 13 in order to minimize the effect of length distribution.

4.2.3. Rheological investigation

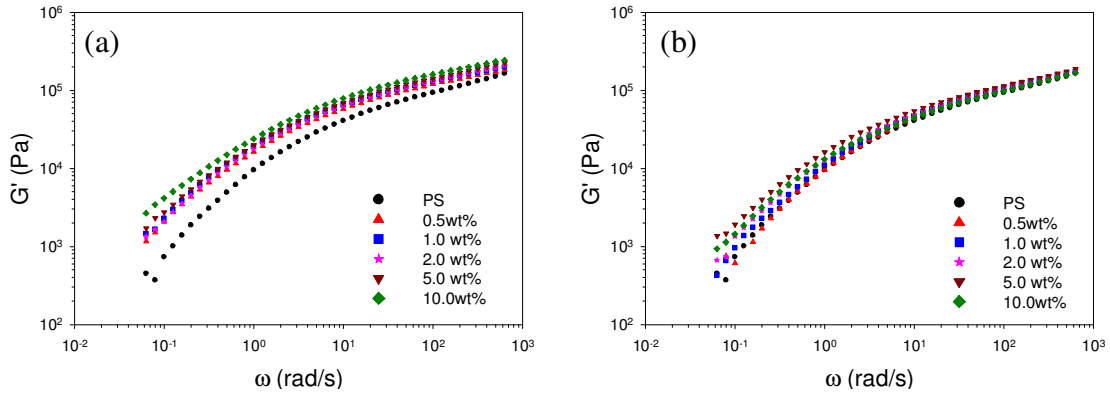

Figure 14. Variation of storage modulus of the blends of nanofiber (a) and PS-*b*-PI copolymer (b) with neat PS at 180 °C.

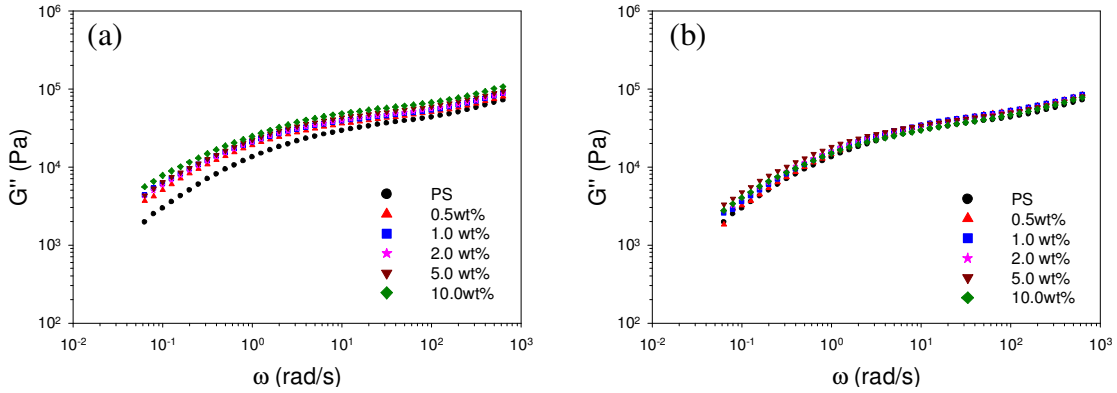

Figure 15. Loss modulus graphs of the blends of fiber-B (a) and PS-*b*-PI copolymer (b) with neat PS at 180 ^{o}C.

The incorporation of nanostructured fillers into the polymer matrix contributes to a significant change in the viscoelastic properties[8, 92, 93, 98]. The filler shape and morphology can affect both the linear and non-linear viscoelastic properties in polymer blends or composites systems. Rheology could also be extended toward the analysis of ordered structures in copolymer systems. The blends of nanofibers and PS-*b*-PI copolymer with PS were studied to understand the relationship between the nanofibers and PS in terms of rheological properties. Figure 14 and 15 show storage and loss moduli as a function of angular frequency. The tests were conducted at 180 ^{o}C with 0.05 % strain. The storage moduli of the nanofiber blends increased with the increase in the nanofiber contents over the frequency ranges as shown in Figure 14 (a).

The rheological values at 180 ^{o}C indicate that the moduli are changed by increasing nanofiber filler contents compared to uncrosslinked copolymer blends. In order to understand the viscoelastic properties, a wide range of temperature (160 ^{o}C – 200 ^{o}C) were used to obtain the rheological data.

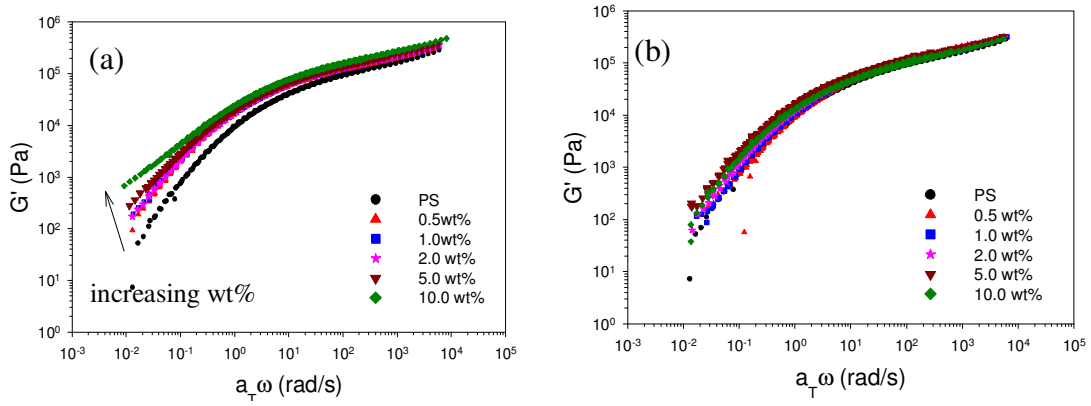

Figure 16. The master curves of the storage modulus for nanofiber (a) and copolymer blends (b) with PS.

A master curve of time-temperature superposition was made by using the WLF method[108] to calculate the shift factor. Figure 16 shows the master curves of time-temperature superposition of the dynamic storage moduli for the two blends as a function of frequency. In the blends of the crosslinked copolymer with PS, the dynamic moduli were not increased with increasing copolymer content. Only blends of fiber/PS shows an increased modulus value while increasing the fiber content.

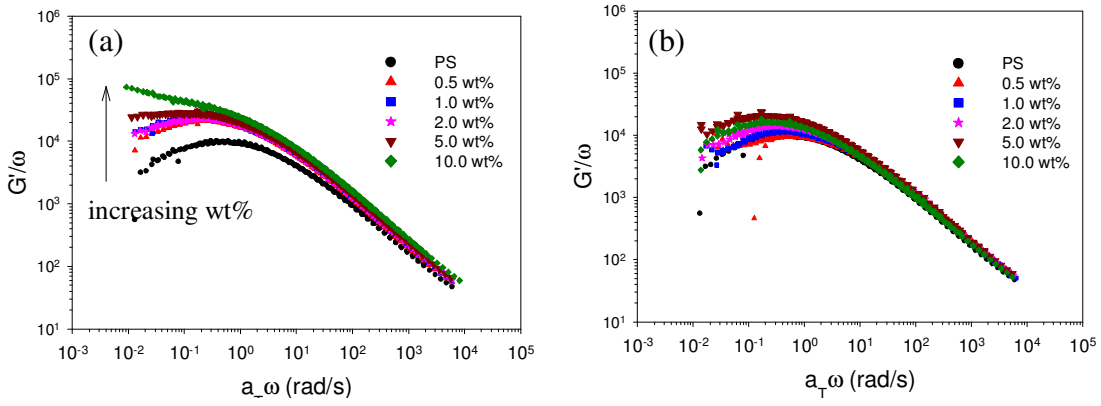

Figure 17 The dynamic elasticity coefficient of the blends of PS-*b*-PI fiber (a) and copolymer (b) with PS in terms of angular frequencies. To plot the coefficient graph, master curve data of G′ and frequency were used.

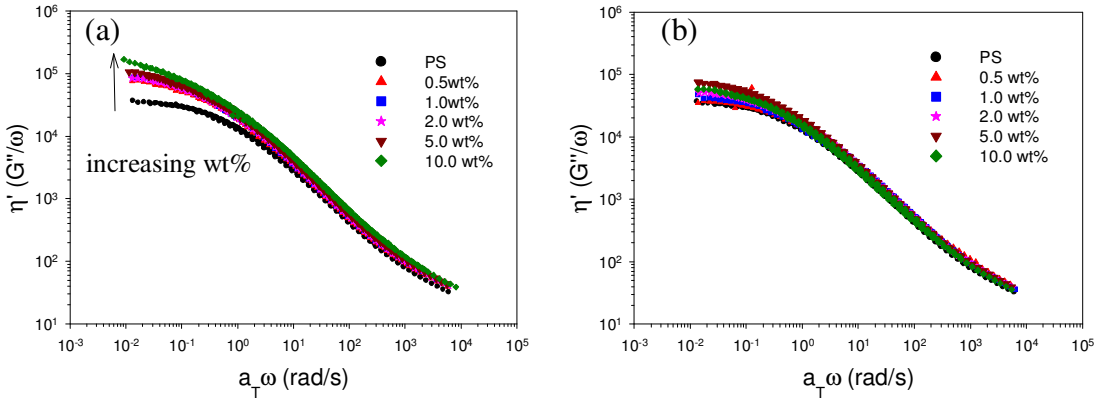

Figure 18 The dynamic viscosity of blends of PS-b-PI fiber (a) and PS-*b*-PI copolymer (b) with PS in terms of angular frequencies. To plot the coefficient graph, master curve data of G″ and frequency were used.

Figure 17 and 18 show that G′/ω and η′=G′′/ω are plotted in terms of angular frequencies. Sepehr *et al.*[98] have studied the rheological and mechanical performance of PS with organoclay. The study used the dynamic elasticity coefficient (ψ=G′/ω^2) which is related to the structural information in the melt. The graphs of ψ= G′/ω^2 vs. ω are similar to η′ vs. ω and the plot of $\psi\omega$=G′/ω vs. ω also shows evidence of nanofiber effects in the blends. Both Figure 17 and 18 describe that the shapes of the graph from the blends of PS-*b*-PI/PS are not changed. However, higher fiber content shows slope changes from 0 to -1 at low frequencies. The Doi and Edwards model[102] result in an expression for G′ and G″ with frequency (ω) and relaxation time (λ), where at low frequencies, a slope of 1 for G′/ω vs. ω and zero slope for G″/ω vs. ω can be expected using a homopolymer. The blends with nanofibers show a change in the slopes at low frequency ranges whereas the slopes remain relatively the same in the blends with the PS-*b*-PI copolymer. These results suggest the presence of a critical concentration for changing structural information where the nanofibers start to interact and perhaps form a certain structural shape such as continuous domain.

The Cox-Merz relationship[109] is used to obtain the shear strain dependence of viscosity from the dynamic viscosity data:

$$\eta(\dot{\gamma})\big|_{\dot{\gamma}=\omega} = \left|\eta^*(\omega)\right| = \sqrt{\eta'^2(\omega) + \eta''^2(\omega)} \tag{2}$$

For further analysis, various generalized Newtonian models involving shear viscosity terms can be used. The cross-Williamson model[110] was used to find zero-shear viscosity and relaxation time of the blends, a three-parameter model for polymer melts, which describes the experimental results well for neat PS well. The Cross-Williamson model is given by

$$\eta = \frac{\eta_0}{1 + \left|\lambda\dot{\gamma}\right|^{1-n}} \tag{3}$$

where $\eta_0 = \lim_{\dot{\gamma}\to 0}\eta(\dot{\gamma})$ is the zero shear rate viscosity, λ is the characteristic time of the blends, and n is the power-law exponent. The Cross-Williamson model typically demonstrates longer transitions from the zero shear to the shear thinning behavior[111].

Table 5
Calculated parameters from the three-parameter Cross-Williamson model using blends of nanofiber with PS.

Parameters	PS	0.5 wt%	1.0 wt%	2.0 wt%	5.0 wt%	10.0 wt%
η_0 (Pa.s)	36,300	75,780	87,800	84,100	100,300	149,400
λ (sec)	1.262	2.309	2.59	2.424	2.914	4.836
n	0.2678	0.2539	0.2554	0.2582	0.2627	0.2763

Table 6
Calculated parameters from the three-parameter Cross-Williamson model using blends of PS-*b*-PI with PS.

Parameters	PS	0.5 wt%	1.0 wt%	2.0 wt%	5.0 wt%	10.0 wt%
η_0 (Pa.s)	36,300	41,340	44,040	53,090	74,560	60,170
λ (sec)	1.262	1.378	1.373	1.763	2.534	2.477
n	0.2678	0.2864	0.2710	0.2701	0.2632	0.2748

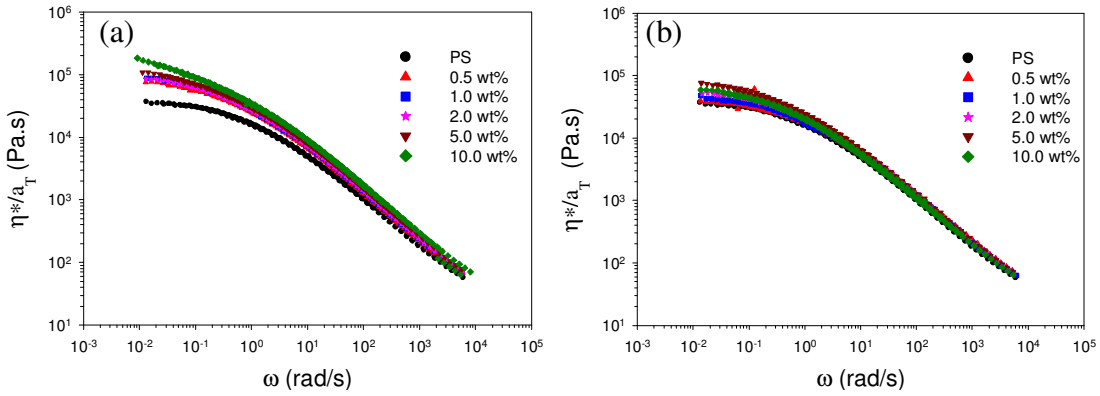

Figure 19 Master curves of complex viscosity of blend samples (a) nanofiber blends with PS and (b) PS-*b*-PI blends with PS.

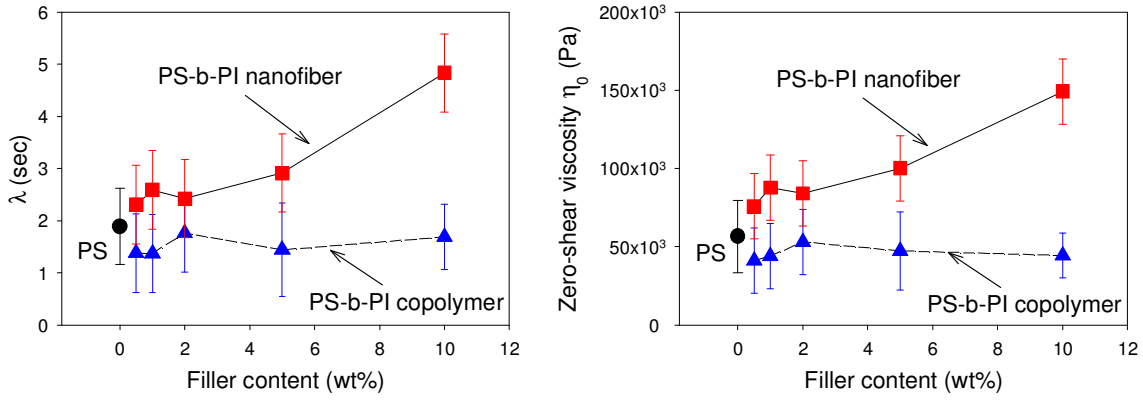

Figure 20. Relaxation time and zero shear viscosity vs. filler content resulting from model fitting data. Solid line with triangle and dashed line with rectangular indicate PS-*b*-PI nanofiber and copolymer, respectively.

The model parameters fitted using experimental data are listed in Table 5 and Table 6 (all R^2 values ≥ 0.997). The relaxation time increased as the amount of nanofiber was increased. In the case of copolymer blends, the relaxation time also increased but it remained the same beyond 5 wt% filler loading. The zero shear viscosity vs. filler content data also showed similar results as shown in Figure 20. The larger relaxation time is likely due to the excellent interaction between the matrix and the shell of the nanofibers and due to the crosslinked nanofiber structure of the core. The relaxation time of the nanofiber blends is increased with increasing filler content. However, the uncrosslinked block copolymers caused an increase in the relaxation time of PS up to 5 wt%. Since the total volume fraction of PS was increased, the copolymer formed spheres of copolymer domains in the PS matrix[20]. Thus, the relaxation time did not increase after 5wt% of copolymer.

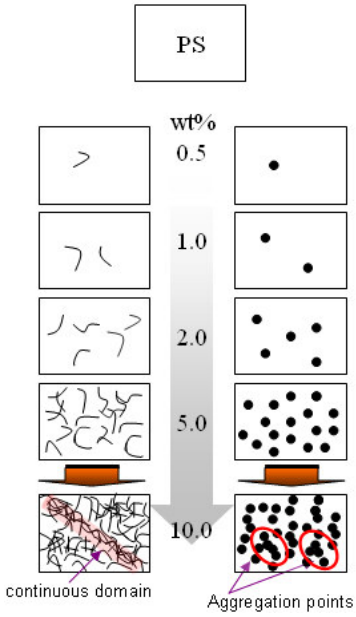

Figure 21. Schematic illustration of blend models for blends of polystyrene with nanofiber and uncrosslinked PS-PI copolymer.

Based on SEM images, model fitting, and rheological data, the blend model shown in Figure 21 is suggested. In the case of nanofiber blends, the rheological data suggests a structural change between 5 wt% and 10 wt% where the nanofibers form a continuous or entanglement domain in the matrix. In general, the critical volume fraction for percolation thresholds of conducting materials are typically measured by electrical conductivities and then compared to simulated results. Celzard *et al.*[112] studied the percolation threshold for composites using graphite flakes and carbon fibers. The study was analyzed by an empirical excluded volume method, showing that the percolation threshold can be estimated for rods.

$$1-\exp\left(-\frac{1.4V}{<V_e>}\right) \le \phi_c \le 1-\exp\left(-\frac{2.8V}{<V_e>}\right) \quad (1)$$

where ϕ_c is the critical volume fraction, V is the volume of the fiber, and $<V_e>$ is the exclude volume of the fiber. The values of 1.4 and 2.8 are applied as lower and upper limits by assuming that PS-*b*-PI nanofibers are randomly oriented and infinitely thin rods[112]. The calculated critical volume fraction of PS-*b*-PI nanofiber blends is between $0.027 \le \phi_c \le 0.053$ which agrees with these results within acceptable error ranges. Another model, suggested and demonstrated by Bug *et al.*[113] and Zheng *et al.*[114] – a simulation of a dimensional percolation threshold by nanorod dispersions in terms of shearing effect – results in a value of 0.035 also of similar order of magnitude as Celzard's model[112]. These calculations suggest that the transition that occurred at around 5 vol% is due to a percolation transition.

For the uncrosslinked PS-*b*-PI copolymer, the relaxation time and zero-shear viscosity increased up to 5 wt% of the value and no significant changes were observed with increasing the content of uncrosslinked PS-*b*-PI. According to Hashimoto *et al.*[17], the blends of PS-*b*-PI copolymer with PS are not mixed well when the molecular weight of PS is higher than the molecular weight of PS which is a part of the block copolymer. Since long molecules are very difficult to diffuse into small molecules, the sphere formed block copolymers could be aggregated with each other after 5 wt% of the content. Therefore, the proposed scheme suggests the differences of behavior of the crosslinked and uncrosslinked block copolymers in the matrix in terms of zero-shear viscosity and relaxation time which is shown in Figure 21.

Our results highlight the effect of geometry in polymer blends as indicated by the significant difference between cylindrical and spherical geometries in the blends. Comparison with percolation models suggest that these elastomeric nanofibers can be modeled as rigid rods at least at their current aspect ratio. Since the behavior can be expected to differ significantly at higher lengths, the effect of aspect ratio can be studied systematically be varying the preparation conditions. The use of crosslinked block copolymers to explore the effect of other geometries is also reported using elastomeric inclusions such as nanosheets.

4.3. Conclusion

The blends of crosslinked and uncrosslinked PS-*b*-PI copolymer with pure PS were investigated with varying filler content. The cold vulcanization process was used to prepare the nanofibers. The storage and loss moduli (G′ and G″) from rheology were

increased with increasing the nanofiber contents, but decreased with increasing the copolymer content. The dynamic elasticity coefficient was used to explain the structural changes of blends using master curves. The three-parameter Cross-Williamson model was employed to predict the rheological values: zero shear viscosity, relaxation time, and power-law index. The calculated values showed that the relaxation time of the matrix was increased with nanofiber contents but decreased with increasing copolymer contents. The cylindrical morphology of the PS-*b*-PI copolymer could be preserved in the blends because of the crosslinks in the minority block of isoprene. The differences in morphology led to the difference in mechanical and rheological properties between the two blends.

The calculated critical volume fraction of nanofiber blends and indirect evidence from the experimental results suggest a structural change between 5 and 10 wt% of nanofiber content where the nanofibers reach a percolation threshold. This blend study presented the critical concentration of block copolymer nanofibers. This information provides a better understanding of other crosslinked structures that can be derived from crosslinked block copolymers such as spheres or sheets and their effects on the mechanical properties of blends.

CHAPTER 5

VISCOELASTIC PROPERTIES OF BLENDS OF POLYSTYRENE AND CROSSLINKED POLYSTYRENE-POLYISOPRENE NANOSHEET

5.1. Introduction

Polymer blends and nanocomposites have had much attention for the last several decades in research and industry[68, 115, 116] in various applications such as optical[117, 118], biomedical[119], electrical[120-122], and as reinforces[26, 28, 123, 124]. Many studies have been carried out in order to understand their morphologies[125] and mechanical behavior[81, 126]. Polymer blends have been studied for their toughening mechanism using elastomer modified epoxy as exemplified in recent reviews and articles discussed in chapter 2. In addition, many studies involving inorganic nanoparticles such as CNT, clay, and $CaCO_3$ with various morphologies in polymer nanocomposites have been performed[28, 29, 82].

In this chapter, the influences of morphology in elastomeric nano-morphology are investigated. Elastomeric PS-PI nanosheets were prepared and characterized and the rheological behavior of elastomeric nanofiber and nanosheet blends was studied. Using rheological behavior, the critical volume fraction was investigated through a three parameter Cross-Williamson model and percolation threshold theory. The moduli increased with increasing crosslinked nanosheet loading, and also the critical volume fraction of the nanosheet blends was found and compared with nanofiber blends.

5.2. Result and Discussion

5.2.1. Characterization of nanofibers and nanosheets

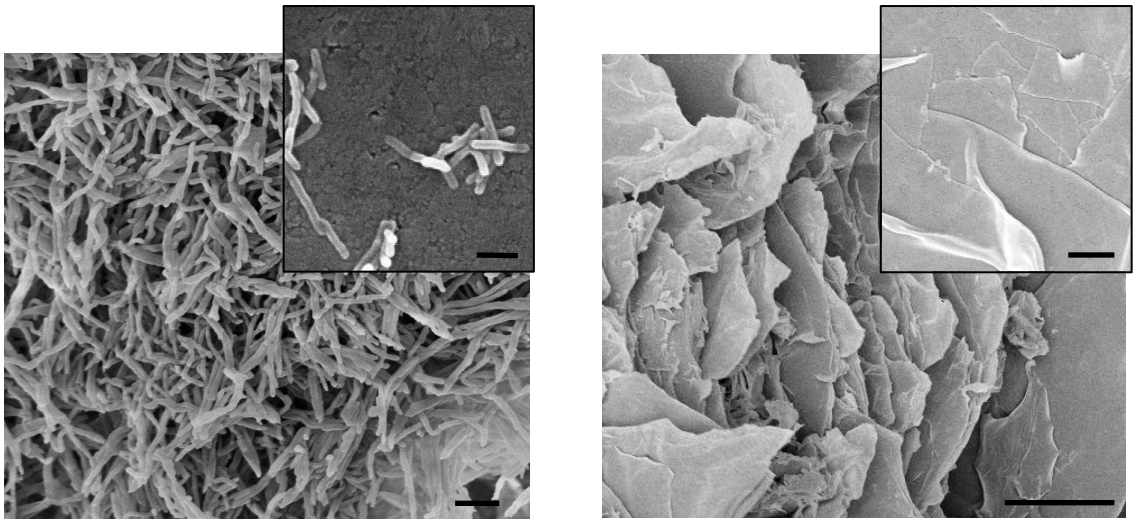

Figure 22. SEM image of nanofiber and nanosheet morphology in bulk state. The inserted images are shown as single nanofiber and nanosheet on silicon wafer. The scale bars in (a) indicate 300 nm and 100 nm and 10 μm and 1 μm.

Nanofibers and nanosheets were synthesized by cold vulcanization using self-assembly of PS-b-PI copolymer. Cylindrical and lamellar morphology of PS-b-PI were used as a form of fiber and sheet. In general, if PS and PI maintained a volume fraction 77 and 23, respectively, it forms a cylindrical morphology having a PS shell and PI core[89]. When S_2Cl_2 crosslinking agent is applied to the cylinder morphology of PS-b-PI sample, the double bond of polyisoprene starts to make a linkage between back bone chains by generating sulfur bridges. Thus, the crosslinked core can maintain the cylindrical morphology as a fiber. In the case of nanosheets, the same process is applied and the only difference is the volume fraction of PS and PI as 57 and 43. As can be seen

in Figure 22, the nanofiber and nanosheet morphologies are clearly confirmed as bulk and individual nanofillers are shown from inserted images. The diameter of each nanofiber is ca. 40 nm and the thickness of each nanosheet is ca. 70 nm[127]. The diameter and thickness of the nanofiller resulting from vulcanization of the block copolymer strongly depends on the molecular weight of PS-b-PI copolymer[57]. The crosslinking density was confirmed using FT-IR and DSC[128].

5.2.2 Rheology Studies

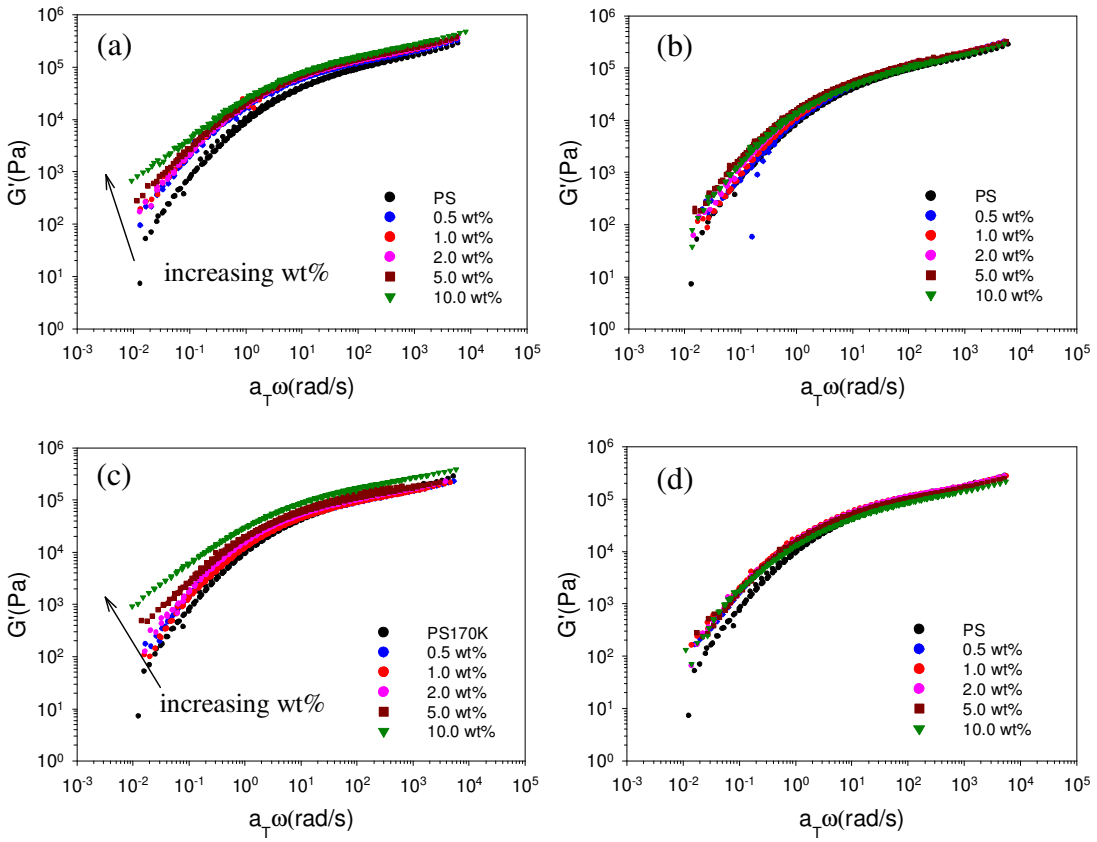

Figure 23. Master curve of storage modulus of (a) PS/nanofiber, (b) PS/SI23, (c) PS/nanosheet, and (d) PS/SI43 blends with varying weight fraction of fillers. The Reference temperature is 180 °C.

The rheological results at 180 ^{o}C show that the moduli increase with increasing nanofiber or nanosheet loading compared with neat PS and SI23 or SI43 blends. In order to study a wider of frequencies, a master curve was used.

The master curves of the blends are shown in Figure 23. The storage modulus vs. frequency is plotted for the two nanofiller blends and two uncrosslinked blends (PS/SI23 and PS/SI43). The graphs show that the storage modulus of nanofiber and nanosheet blends increase with increasing in nanofiller content whereas modulus of PS/SI23 and PS/SI43 blends do not have any significant increase with increasing SI23 or SI43 content. The difference is caused by the effect of crosslinking. Nanofibers or nanosheets maintain their structures in the blends because of the crosslinking isoprene. However, SI23 and SI43 are not able to sustain their own morphology such as cylinder or lamellar when blended with neat PS because the total volume fraction of PS increase. In Figure 23 (a) and (c), the 10 wt% nanosheet blends have higher modulus value than 10 wt% nanofiber blends. The reason is that the nanosheets are more effective at preventing the mobility of neat PS because of the different aspect ratios of nanofibers and nanosheets based on the measured average length and thickness from SEM images. This result shows that the shape or geometry of the elastomeric nanofillers is important factor in the blends and composites.

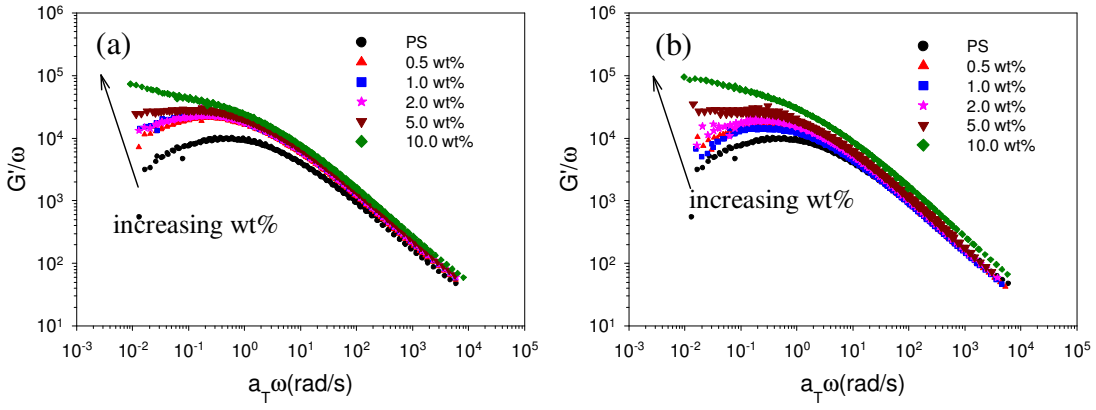

Figure 24 G'/ω versus angular frequencies was plotted using master curve. (a) nanofiber/PS blends and (b) nanosheet/PS blends in terms of nanofiller loading.

G'/ω and $\eta'(G''/\omega)$ versus angular frequency are presented in Figure 24. According to Sepehr et al.[98], the dynamic elasticity coefficient is expressed as $\psi = G'/\omega^2$ and the plot of $G'/\omega = \psi\omega$ versus ω gives the information of the melt in terms of structural change. In addition, the plot of $\psi = G'/\omega^2$ versus ω shows very similar results to $\eta'(G''/\omega)$ versus ω . Nanofiber and nanosheet blends from both Figure 24 (a) and (b) indicate that there are three dimensional structure changes between 2 wt% and 10 wt%. In the case of the nanosheet blends, the graphs show similar results with the nanofiber blends. The slope variation at the low frequency range suggests a new structure such as continuous domain or aggregation start to form around 2 wt%, 5 wt% and can be clearly distinguished based on the slope change at low frequencies. From the graphs, the nanosheet blends have a larger change than the nanofiber blends in terms of the slope at low frequency ranges and the variation appears more gradual than the nanofiber blends. This suggests that the structural change did not take effect until 2 wt% and then the nanofibers may generate continuous structure. However, in the case of the nanosheets,

the filler started to affect the structural change from low nanosheet contents because of the morphology of the fillers.

In order to investigate the effect of relaxation, the Cole-Cole plot is used. The long relaxation behavior also can be seen in the Cole-Cole plot by comparing the radius in graph.

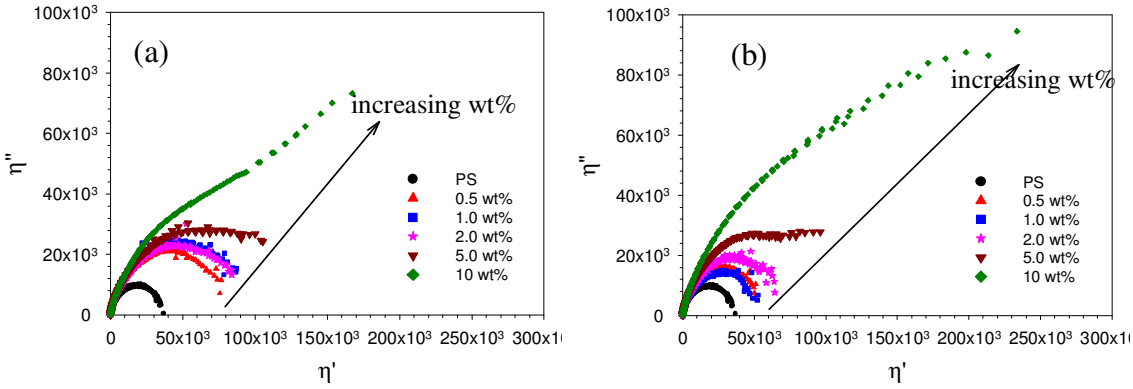

Figure 25. Cole-Cole plot (η″ vs. η′) of blends of neat PS with (a) PS/nanofiber and (b) PS/nanosheet using master curve.

The calculated Cole-Cole plot consists of the imaginary part and real part of the frequency dependent shear modulus[129], directly indicating stress relaxation time by the changing radius of plotted data. In Figure 25, the Cole-Cole plots are shown using various nanofiller loading. As can be seen in the figure, the radius of each sample increase with increasing filler loading. In the plot of nanofiber blends, the radius increases dramatically at 0.5 wt% and then slowly increases until 2 wt%. In between 2 and 5 wt%, the radius increases dramatically again. This suggests that small loadings of nanofibers can affect the relaxation time in neat PS and that there is a structural change between 2 and 5 wt%. However, in the case of the nanosheet blends, the radius increases gradually until 2 wt% and then dramatically increases at 5 wt%. This indicates that the

nanosheets are less effective than nanofiber due to the morphology. The Cole-Cole plot shows more clearly that the relaxation time increases with increasing nanofiller loading.

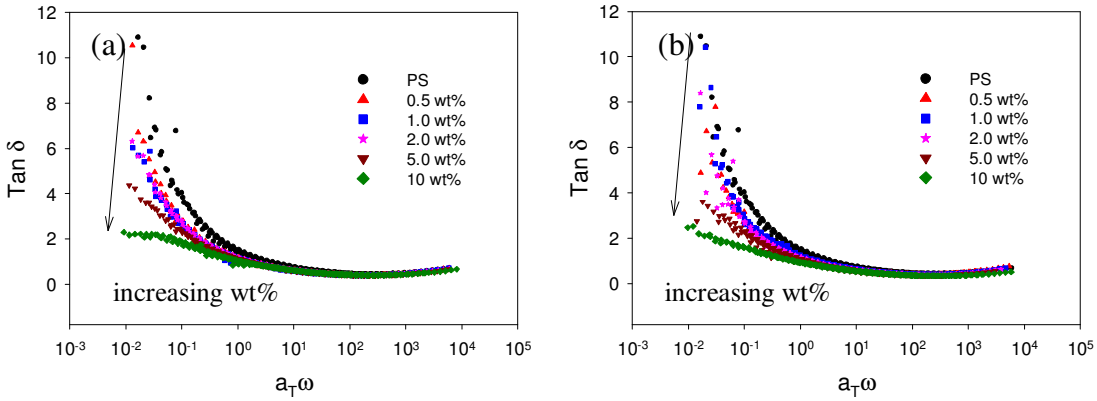

Figure 26. tan δ plot of (a) PS/nanofiber and (b) PS/nanosheet blends in terms of angular frequencies with varying nanofiller loading.

The tan δ provides another method to present the relaxation process[130, 131]. Tan δ is defined as a ratio of the loss modulus and storage modulus. From the Doi and Edwards model[102] loss and storage moduli are expressed by an equation which is a combination of relaxation time and angular frequency. Thus, tan δ can be expressed by

$$Tan\,\delta = \frac{G''}{G'} = \sum_p \frac{1}{p}\frac{\omega\tau_p}{1+(\omega\tau_p)^2} \Big/ \sum_p \frac{1}{p}\frac{(\omega\tau_p)^2}{1+(\omega\tau_p)^2} \tag{5}$$

where τ is relaxation time and ω is angular frequency. When $\omega \to 0$, this leads to a proportionality between tan δ and ω^{-1}. And thus a log – log plot of tan δ vs. ω^{-1} should yield a slope of -1 at low ω.

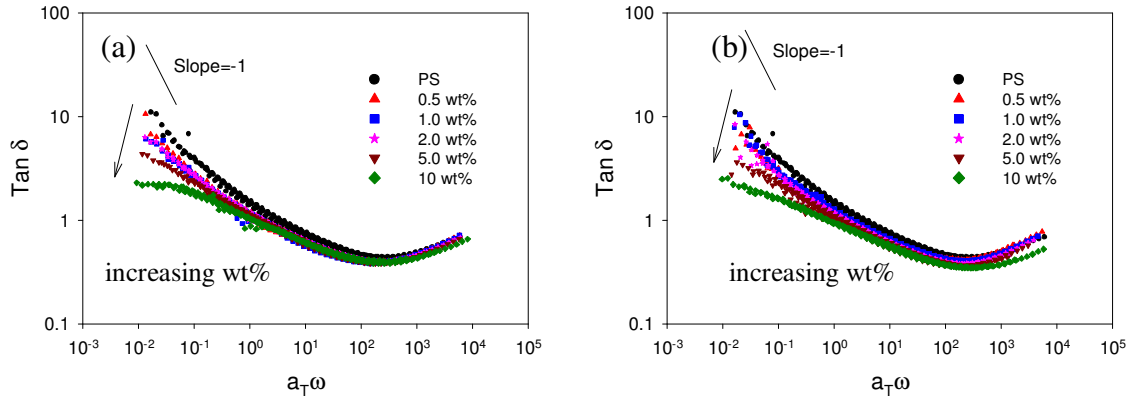

Figure 27. Logarithm of tan δ plot of (a) PS/nanofiber and (b) PS/nanosheet blends in terms of angular frequencies with varying nanofiller loading.

Table 7 . Slope results of logarithm tan δ plot with varying nanofiller loading. Slope of neat PS is -0.54

Wt % of filler	0.5	1	2	5	10
Nanofiber (Slope)	-0.57	-0.44	-0.43	-0.30	-0.09
Nanosheet (Slope)	-0.48	-0.64	-0.46	-0.26	-0.19

Tan δ vs. angular frequency taking logarithm curves are plotted in Figure 27. According to Han *et al.*[100], they found the relationship between log G′ and log G″ as a slope of 2 using the Doi-Edwards tube model. In some cases, however, the slope is less than 2 because of two reasons: one is that sufficiently low frequency has not been reached for the terminal region and another is the polydispersity is higher than 1. In this case, the relationship between log (tan δ) and log ω yield a slope of -1 using the Doi-Edwards tube model was found. The slope of neat PS is -0.54 which is different to the slope of -1 at low frequency region because of the above-mentioned reasons. As can be seen in Figure 27 and Table 7, the slope increases with increasing filler loading. For comparison with nanofiber and nanosheet blends, the slope of nanofiber blends increases

rapidly which means that nanofibers can be more effective in increasing relaxation time. According to these results, nanofibers are more influential than nanosheets because the fiber morphology makes nanofibers disperse better in the neat PS during blending. However, the nanosheets have a larger width and length compared with length of nanofibers and the flexible nanosheets form easily folded or bended structures. So, the slope for nanosheet blends is lower than the slope for nanofiber blends.

The Cox-Merz relation[109] is used to obtain the shear strain dependence of viscosity from the dynamic viscosity data:

$$\eta(\dot{\gamma})\big|_{\dot{\gamma}=\omega} = \left|\eta^*(\omega)\right| = \sqrt{\eta'^2(\omega) + \eta''^2(\omega)}\,. \tag{6}$$

Various generalized Newtonian models use shear viscosity terms in order to analyze the viscoelastic properties of polymer blends and nanocomposites. The suggested model equation, the Cross-Williamson model[110], involves the terms which are zero-shear viscosity and relaxation time and this study used this three-parameter model for melt behavior of polymer blends. This model has good agreement with the experimental results and calculated data compared with the other three parameter models. The model is given by

$$\eta = \frac{\eta_0}{1 + \left|\lambda\dot{\gamma}\right|^{1-n}}, \tag{7}$$

where $\eta_0 = \lim_{\dot{\gamma}\to 0}\eta(\dot{\gamma})$ is the zero shear rate viscosity, λ is the characteristic time of the blends, and n is the power-law exponent.

Table 8. Calculated results using the Cross-Williamson three parameter model for zero-shear viscosity, relaxation time, and power-law exponent with neat PS, nanofiber blends, nanosheet blends with varying nanofiller loading.

Parameters	PS	Nanofiber blends					Nanosheet blends				
		0.5	1.0	2.0	5.0	10.0	0.5	1.0	2.0	5.0	10.0
η_0 (Pa.s)	36,300	75,780	87,800	84,100	100300	149400	53540	50270	64430	89090	197400
λ (sec)	1.262	2.309	2.59	2.424	2.914	4.836	1.823	1.740	1.929	2.587	5.489
n	0.2678	0.2539	0.2554	0.2582	0.2627	0.2763	0.2382	0.2423	0.2322	0.2327	0.2513

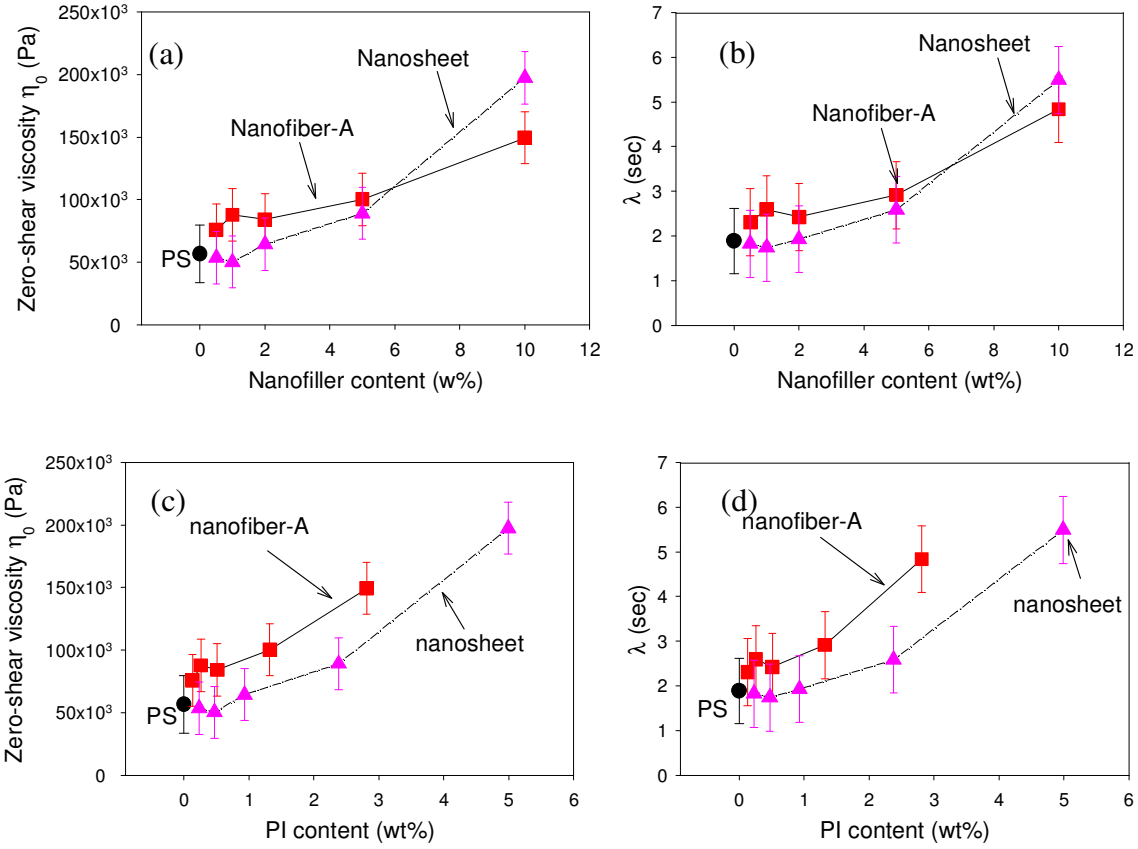

Figure 28. Zero shear viscosity (a) and Relaxation time (b) vs. filler content plotted by fitting data. (c) and (d) are plotted using PI content. Solid line with triangle and dashed line with rectangles indicate PS/nanofiber and PS/nanosheet blends, respectively.

5.2.3. Percolation threshold studies

Based on the calculation using the Cross-Williamson three parameter model, the zero-shear viscosity and relaxation time values are obtained. Figure 28 (a) and (b) were plotted using the values in terms of nanofiller content for nanofiber and nanosheet blends. Below 5 – 6 wt%, the values of nanosheet blends are lower than that of nanofiber blends. However, after 6 wt% the increasing rate of nanosheet blends is higher than nanofiber blends. For comparison with nanofibers and nanosheets in terms of crosslinkable PI content, zero-shear viscosity and relaxation time vs. PI content were plotted as shown in Figure 28 (c) and (d). The values keep increasing without any crossing point which means that the values are proportionally increased to PI content. At the same content of PI, the value of nanofibers is higher than the value of nanosheets because nanofibers have good dispersion. In order to study theoretically, the percolation threshold using critical volume fraction is explored:

$$1-\exp\left(-\frac{1.4V}{<V_e>}\right) \le \phi_c \le 1-\exp\left(-\frac{2.8V}{<V_e>}\right) \quad (8)$$

Generally, the critical volume fraction in blends or composites can be calculated by electrical conductivities using conducting nanofillers to study percolation thresholds. Researchers have compared these experimental results to simulated results. In the previous results, chapter 4[132], the critical concentration of nanofibers in the blends is calculated using equation (8)[112] and found to have a value between $0.027 \le \phi_c \le 0.053$.

According to Balberg[133], critical concentration is related to the total excluded volume, $\langle V_{ex} \rangle$. Volume of a disk $\langle V_e \rangle$ in three dimensions can be expressed as

$$\phi_c = 1 - \exp\left(- \frac{\langle V_{ex} \rangle V}{\langle V_e \rangle} \right) = 1 - \exp\left(- N_c V \right) \tag{9}$$

where N_c is the critical number of objects per unit volume. The case of a thin disk which has a radius and is randomly dispersed in a matrix has been studied by Charlaix, Guyon, and Rivier[134]:

$$\langle V_e \rangle = 4\pi r^3 \int_0^{\theta} \sin^2 \beta d\beta \tag{10}$$

where β is the angle between the planes of two disks and θ is the angle of the greatest disorientation of the disks. In the randomly oriented disk, $\theta = \pi / 2$ was used. Based on equations (9) and (10), Celzard *et al*.[112] have derived the following equation,

$$1 - \exp\left(- \frac{1.8t}{\pi r} \right) \le \phi_c \le 1 - \exp\left(- \frac{2.8t}{\pi r} \right) \tag{11}$$

where t is the thickness of the disks. $\langle V_{ex} \rangle$ of an infinitely thin disk is known to be 1.8 and, for a sphere, 2.8. In this case, the nanosheets have a random shaped sheet not a regular shaped disk, so the nanosheets are disk shape having radius r and the thickness is

70 nm are assumed. Also the structural change starts from 2 wt% of nanosheet loading. These parameters are used to calculate the critical concentration in terms of disk radius.

Based on the assumption, the radius of nanosheets is around 2 – 3 μm for the disk by calculating critical concentration in terms of the radius of nanosheets; however, there is only a range of radius of nanosheets because the nanosheet shapes are quite random and irregular shape as shown in Figure 22 (b).

Thus, the range of critical concentration is between $0.013 \leq \phi_c \leq 0.031$. This value is slightly overlapped with the critical concentration of nanofiber blends ($0.027 \leq \phi_c \leq 0.053$). The rheological result also presents similar data in terms of structural function due to the overlapped critical concentration shown in Figure 24.

5.3. Conclusion

This blend study presented and compared empirical and theoretical results of elastomeric nanoparticles in terms of particle shape factor. The shapes of nanofiber and nanosheet fillers were formed by self-assembly of PS-PI block copolymers and prepared using a cold crosslinking process. Rheological behavior of nanofiber and nanosheet blends was investigated and compared in the melt state in terms of varying frequencies and temperatures. The master curves of two blends indicated that the moduli of nanofiller blends increased with increasing the nanofiller content whereas the moduli of the block copolymer blends (PS/SI23 and PS/SI43) did not have any significant changes. In order to study the information of structural changes, dynamic elasticity coefficient was used to

estimate the onset of structural changes in the blends such as continuous domain or aggregation. The three parameter Cross-Williamson model was used to find zero-shear viscosity and relaxation time. The theoretical values were calculated by the percolation threshold equation assuming the elastomeric nanoparticles as rod and disk shape. The calculation indicated that the range of the percolation threshold of nanofibers in the blends was between $0.027 \leq \phi_c \leq 0.053$ and the value of nanosheets was $0.013 \leq \phi_c \leq 0.031$. Nanofibers prevent more effectively the motion of matrix PS than nanosheets because of high surface area and good dispersion of the nanofibers. This information will provide the initial approach for the studies of blends or nanocomposites using the elastomeric nanoparticles.

CHAPTER 6

THE EFFECT OF CROSSLINKED ELASTOMERIC NANOPARTICLE SHAPES ON DYNAMIC MECHANICAL PROPERTIES OF BLENDS

6.1. Introduction

Mechanical and rheological behaviors of blends of polymers and nanoparticles have been explored and investigated in the last 40 years and the collected results and data are used for finding structure-property relationship in the blends[135, 136]. Polymer blends generate outstanding physical properties in electrical[137], rheological[138], and mechanical[30] applications resulting from the behavior of nanoparticles in the polymer matrix. One of the issues is to understand the shape effect of nanoparticles in blends in order to improve their physical properties.

Dynamic studies of polymer blends or composites can be performed by dynamic mechanical analysis. The data are collected during deformation of blends or composites as a function of temperature, frequencies, or amplitude in order to understand the various factors such as geometry or the interfacial effect in blends or composites.

The purpose of this chapter is to understand the shape effect in blends using elastomeric nanoparticles, which are nanofibers and nanosheets, in terms of thermo-mechanical properties. The nanoparticles, which have nanosize diameter or thickness may affect the behavior of blends and delay the relaxation time of the matrix polymer.

This is the first empirical study in blends using elastomeric nanofiber and nanosheet shaped nanofillers.

6.2. Results

6.2.1. Characterization of nanoparticles and blends

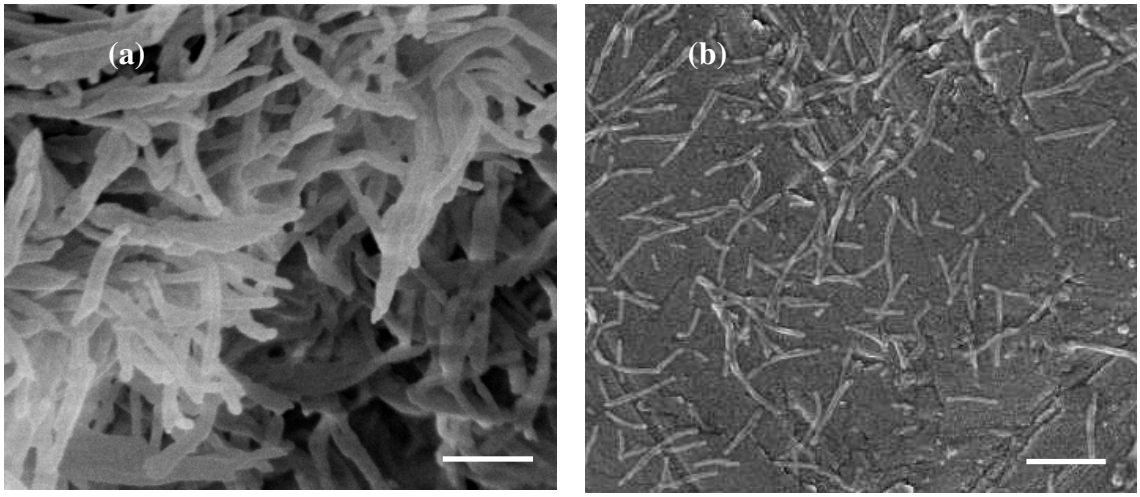

Figure 29. SEM images of nanofiber resulting from cold vulcanization of SI23. (a) is bulk sample of nanofiber and (b) is individual nanofiber. The scale bars indicate 300 nm and 1 μm, respectively.

The nanofiber and nanosheet morphologies were characterized and imaged using SEM. Figure 29 (a) and (b) show bulk and individual nanofiber images, respectively. The diameters of nanofibers are 30 - 50 nm and the average length of nanofibers is around 750 nm. The length distribution of the nanofibers was studied using controlled sonication time by Liu[89] and the nanofibers synthesized in this thesis have a narrow length distribution profile described in chapter 4[132]. Nanofiber morphology is generated using the cold vulcanization process as can be seen in Figure 29.

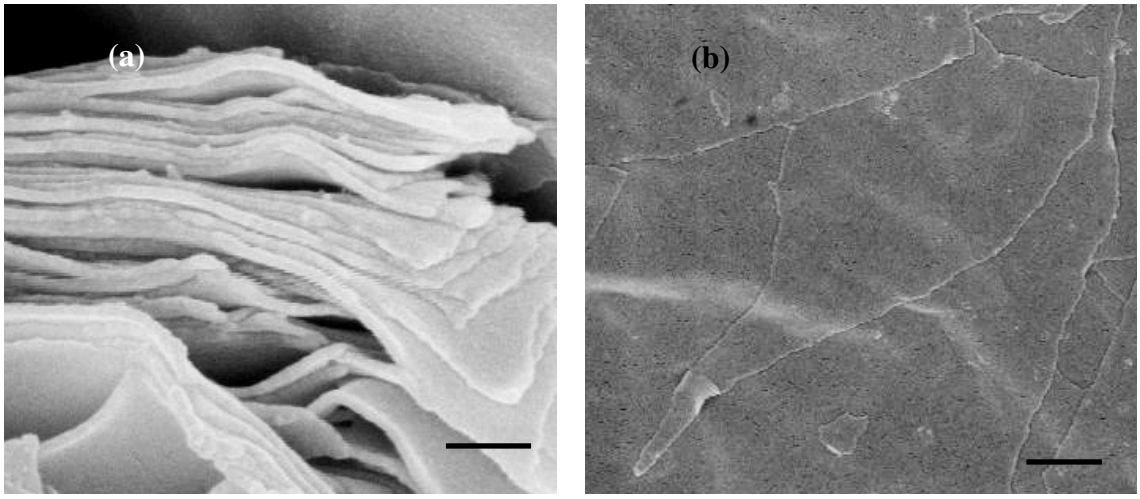

Figure 30. SEM images of (a) stacked nanosheet from cold vulcanization of SI43 and (b) shows the separated nanosheet individually. The scale bars indicate 300 nm and 1 μm, respectively.

The nanosheet morphologies were also imaged and characterized by SEM. As shown Figure 30 (a), nanosheets are stacked and the thickness of the nanofibers is confirmed to be 70 nm. Since molecular weight of SI43 which has lamellar morphology is larger than cylindrical SI23, the thickness of nanosheets is somewhat larger than nanofiber diameter which is 35 nm[132]. Figure 30 (b) indicates that the synthesized nanosheets can be separated from stacked sample of nanosheets and individual nanosheets can be obtained. The nanosheets have a regular thickness but they have various widths and lengths. According to Figure 30 (a) and (b), the morphology of nanosheets is successfully synthesized using cold vulcanization and their morphology also was characterized using SEM.

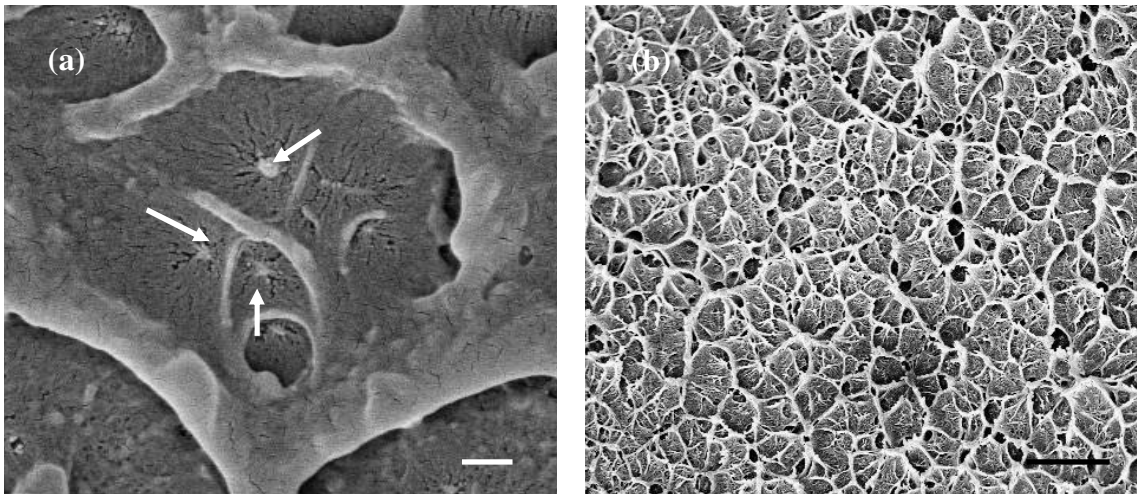

Figure 31. SEM images of blends of neat PS and nanofiber. (a) shows the fracture surface of DMA sample having 0.5 wt% filler loading. The arrow indicates the broken nanofiber in the blends. (b) shows the fracture surface of DMA sample having 10 wt% filler loading. The scale bars indicate 300 nm and 2 um, respectively.

The characterization of nanofibers in the blends was carried out using SEM of fracture surfaces of DMA samples to understand nanofibers behavior in thermo-mechanical tests. In Figure 31, fracture surfaces of 0.5 wt% and 10 wt% loaded nanofiber blends are shown. As can be seen in Figure 31 (a), arrows indicate the broken nanofibers resulting from fracture. Since the molecular weight of SI23 is about ten times lower than the molecular weight of matrix PS, the matrix is much tougher than the nanofibers. In addition, the crosslinked isoprene part also makes the nanofiber brittle. These effects confirm that the nanofibers are broken first followed by the matrix, resulting in the cell-like shapes surrounding broken nanofibers. The number of cell structures increase with increasing nanofiber loading due to good dispersion of the nanofibers as shown in Figure 31 (b).

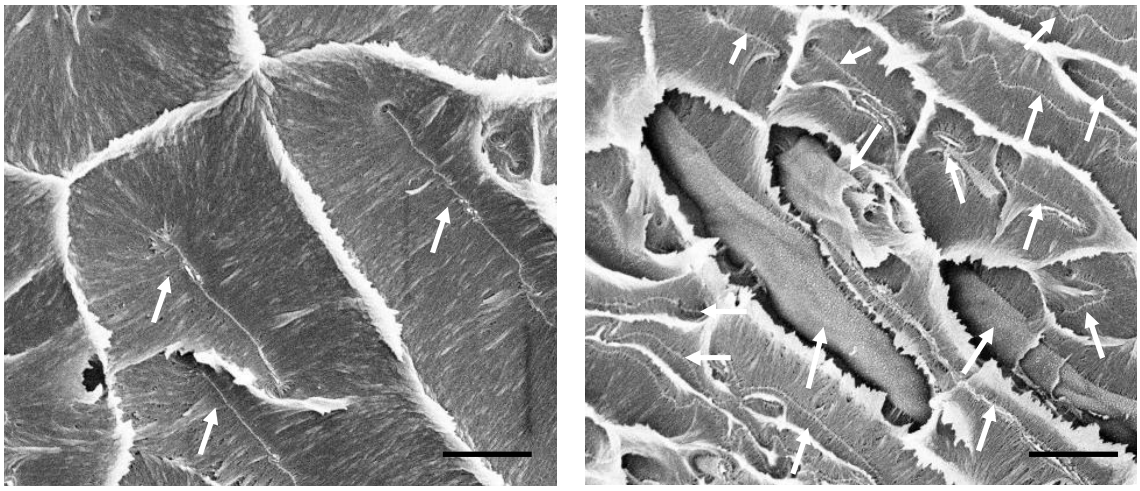

Figure 32. SEM images of blends of neat PS and nanosheet from fractured DMA samples. (a) is 1.0 wt% filler loaded nanosheet blend. The arrows point out broken nanosheet by fracture in the blend. (b) is fracture surface of blend having 10.0 wt% nanosheet loading. The arrows also indicate the nanosheet and the center of the image shows rolled up nanosheet in the blend. The scale bar indicates 2um.

The SEM images of the fracture surfaces of 1 and 10 wt% nanosheet blend samples are shown in Figure 32. The nanosheet morphologies are clearly indicated by the arrows in Figure 32 (a) and (b). Most nanosheets are located parallel to the compression direction because of their high aspect ratio. As described in the SEM image of nanofiber blends, the molecular weight of SI43 is also around ten times lower than the matrix PS. Thus, the images show that the nanosheets are located in the center of cell-like structures resulting from fractured matrix PS. The reason is that nanosheets are broken first and then the matrix during the fracture. At higher nanosheet loading in the blends, the rolled up nanosheets can be detected but most of their shapes and locations are similar to lower nanosheet blends. The number of cell-like structures increase with increasing nanosheet loading as described in nanofiber blends.

6.2.2. Dynamic mechanical analysis studies

Dynamic mechanical measurement is a very useful and sensitive technique to analyze and interpret the viscoelastic properties of materials. The properties of polymer blends, such as structure, crystallinity, crosslinking density, and glass transition temperature, can be explained by dynamic mechanical properties in terms of storage modulus (G′), loss modulus (G″), and loss factor (tan δ)[126]. In nanocomposites and blends, the nanoparticle effects resulting from varying mobility of the surrounding polymer chains can be understood by DMA[139].

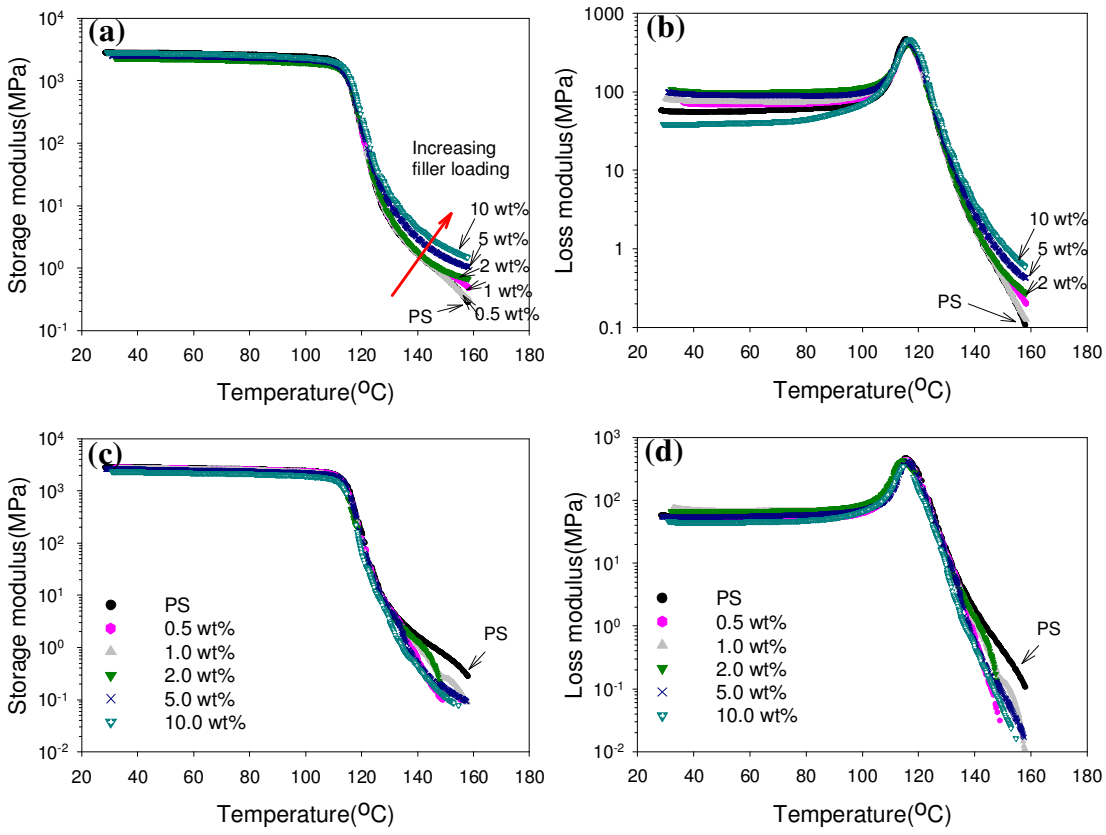

Figure 33. Dynamic mechanical behavior of blends of neat PS/nanofiber and neat PS/SI23 as a function of temperature (a) storage and (b) loss modulus of PS/nanofiber blends. (c) and (d) show storage and loss modulus of PS/SI23 blends, respectively.

In order to understand the effect of nanofibers and nanosheets on the viscoelastic properties of polymer matrix, DMA measurement is used. Figure 33 (a) and (b) shows the DMA results of blends of neat PS and nanofibers with varying nanofiber contents. The storage modulus of nanofiber blends shows an increase above glass transition temperature with increasing nanofiber contents shown in Figure 33 (a). The same behavior is also seen in loss modulus results in Figure 33 (b). To compare the nanofiber effects on the matrix, the blends of PS and SI23 was also prepared as shown in Figure 33 (c) and (d). The storage modulus values show very similar behavior to the storage modulus of traditional crosslinked polymers. Thus, the increasing storage modulus values are closely related to crosslinked nanofiber loading. The nanofibers in the PS matrix can affect the mobility of PS matrix resulting in increased relaxation time. However, when SI23 blends were tested, the modulus values are similar to neat PS and some values are even lower than neat PS as shown in Figure 33 (c) and (d).

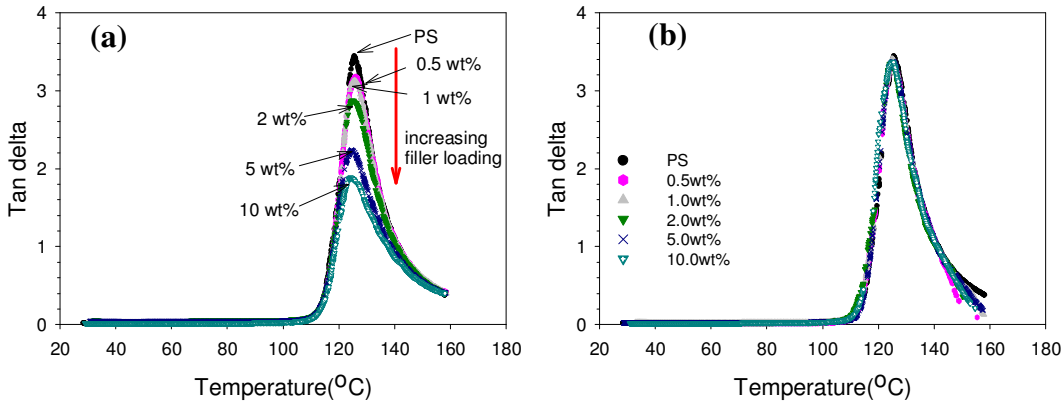

Figure 34. Tan δ curve as a function of temperature for blends of (a) PS/nanofiber and (b) PS/SI23. Tan δ of PS/nanofiber blends decreases with increasing nanofiber loading whereas no changes in PS/SI23 blends.

In general, polymers dissipate a large amount of energy through viscous behavior during the glass transition given by the ratio of loss and storage modulus, also known as tan δ in the DMA experiment[139]. The peak height or area of tan δ is closely related to the mobility of polymer chains[140]. Figure 34 (a) and (b) show tan δ data for nanofiber and SI23 blends, individually. The difference between Figure 34 (a) and (b) is that the tan δ value decreases with increasing nanofiber contents whereas no change was seen in SI23 blends. In other words, the relative storage modulus increases with increasing nanofiber contents. This means that the stiffness of the blends increases with increasing nanofiber loading. However, there are no changes in the blends of PS with SI23. One reason is that SI23 morphology can be changed from cylinder to sphere due to total volume fraction of PS. Another reason is that crosslinked PS has a higher modulus than uncrosslinked PI.

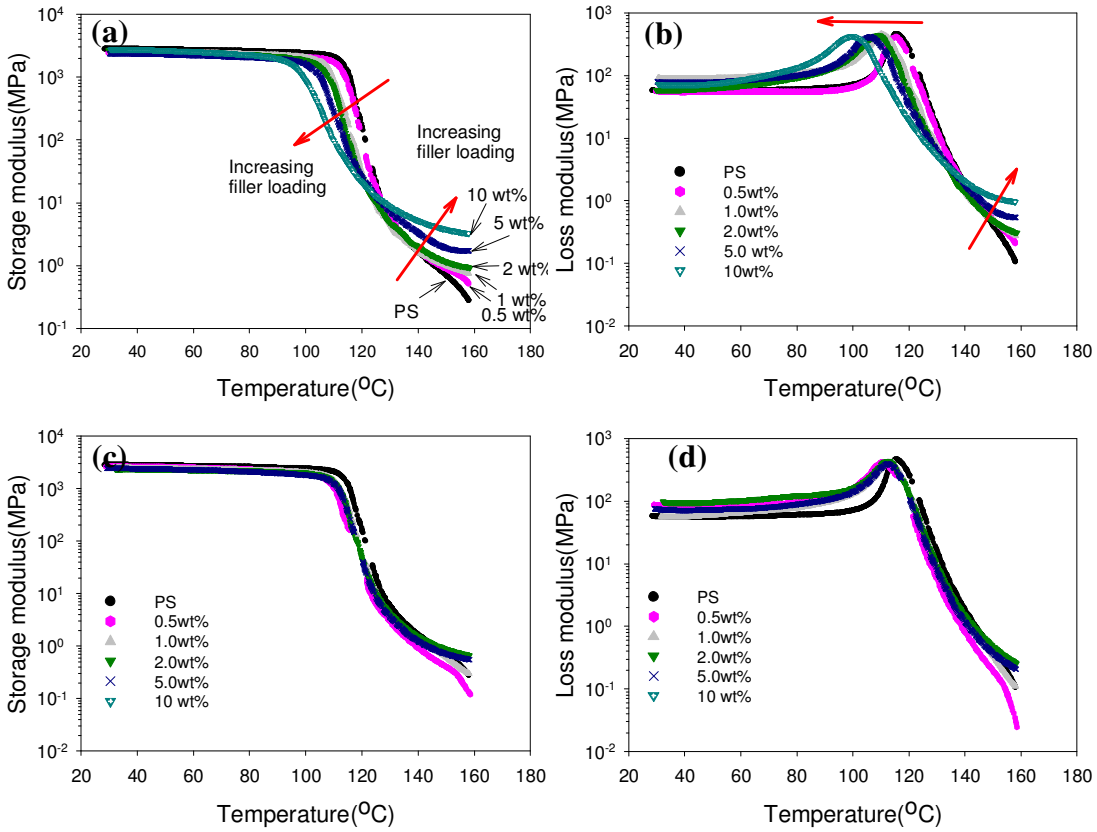

Figure 35. Dynamic mechanical behavior of blends of neat PS/nanosheet and neat PS/SI43 as a function of temperature (a) storage and (b) loss modulus of PS/nanosheet blends. (c) and (d) show storage and loss modulus of PS/SI43 blends, respectively.

Figure 35 shows the storage and loss modulus versus temperature curves for blends of PS with nanosheet and SI43 blends having a range from 0.5 to 10 wt% filler loading. The nanosheet blends (Figure 35 (a) and (b)) indicates that the moduli increase with increasing filler loading above 125 °C, which is the T_g by Tan δ of neat PS. However, above 90 °C, the moduli decrease with increasing nanosheet loading until around 125 °C, which is the T_g by tan δ of neat PS. This means that the nanosheet morphologies may affect the moduli drop between the temperatures. Specific details will be discussed in the next section. In the case of SI43 blends, the graph is very similar to the plot of SI23 because uncrosslinked isoprene cannot influence the relaxation behavior of the PS matrix

as shown in Figure 35 (c) and (d). In addition, when SI23 and SI 43 are blended with neat PS, the driving force to reduce the surface tension prevents it from maintaining the cylindrical morphology.

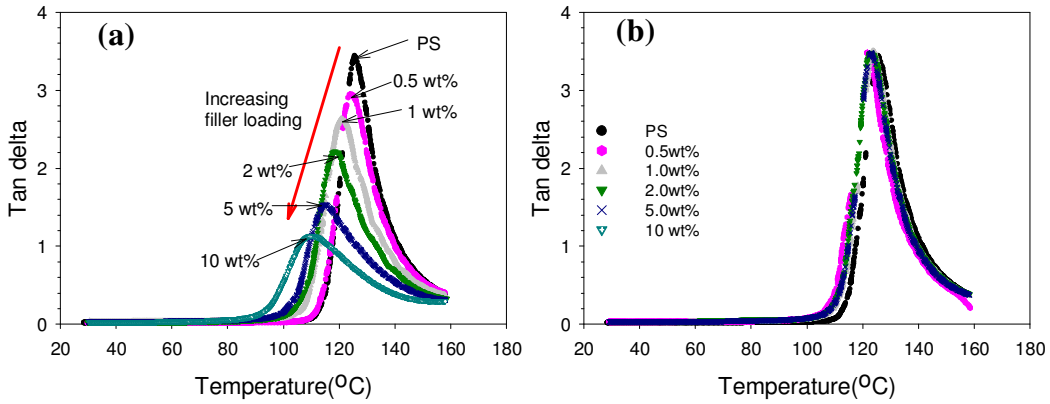

Figure 36. Tan δ curve as a function of temperature for blends of (a) PS/nanosheet and (b) PS/SI43. Tan δ and T_g temperature of PS/nanosheet blends decreases with increasing nanosheet loading whereas there is no significant changes in PS/SI43 blends.

In Figure 36, tan δ curves of nanosheet and SI43 blends with filler loading from 0.5 to 10 wt% are shown. The difference between the blends of PS/nanosheet is that tan δ values decrease with increasing nanosheet contents and also T_g shifts to lower temperatures as shown in Figure 36 (a) and (b), whereas no variation in tan δ and T_g is observed for SI43 blends, as shown in Figure 36 (b).

6.3. Discussion

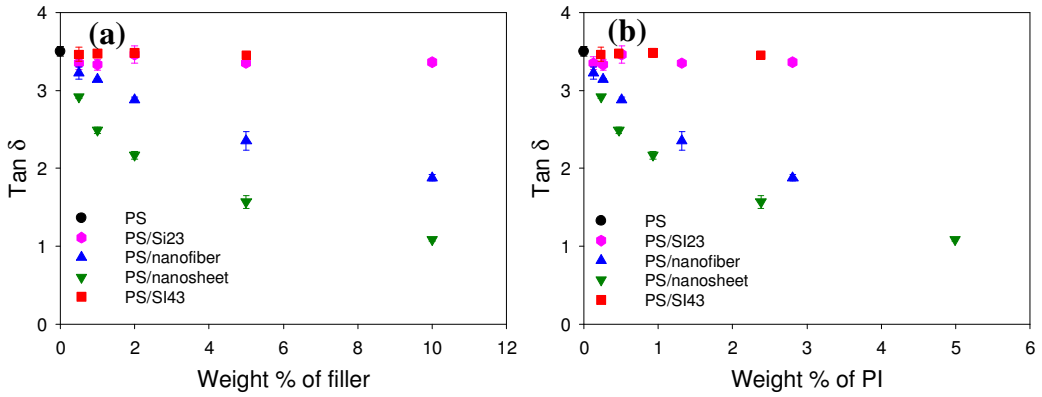

Figure 37. Tan δ at peak center versus filler loading plots in terms of nanofiller loading (a) and in terms of polyisoprene loading (b) for various blend samples: PS, PS/SI23, PS/nanofiber, PS/SI43, and PS/nanosheet.

Tan δ results indicate that the peak values decrease with increasing nanofiber or nanosheet loading. This means that the blend sample becomes stiffer because of crosslinked nanofillers. Nanofillers which have fiber and sheet morphology were compared. In order to investigate the effect of crosslinking and morphology, tan δ peak versus filler loading and tan δ peak versus PI loading were plotted in Figure 37. The tan δ peak decreases with increasing filler loading, and nanosheet blends have lower tan δ peaks than nanofibers due to higher volume fractions of crosslinked PI. Thus, PI content is directly related to the value of the tan δ peak resulting from increasing the stiffness of blends. Thus, the PI contents are calculated and compared as shown in Figure 37 (b) in order to investigate the effect of PI content. When sheet and fiber blends having similar weight fraction of the PI are compared, the tan δ peak of sheet blends is lower than the tan δ peak of fiber. This suggests that not only PI loading but also the morphology can affect the variation of the tan δ peak. In addition, the morphology or shape of nanofiller is more influential than crosslinking in terms of tan δ peak in elastomeric nanoparticles.

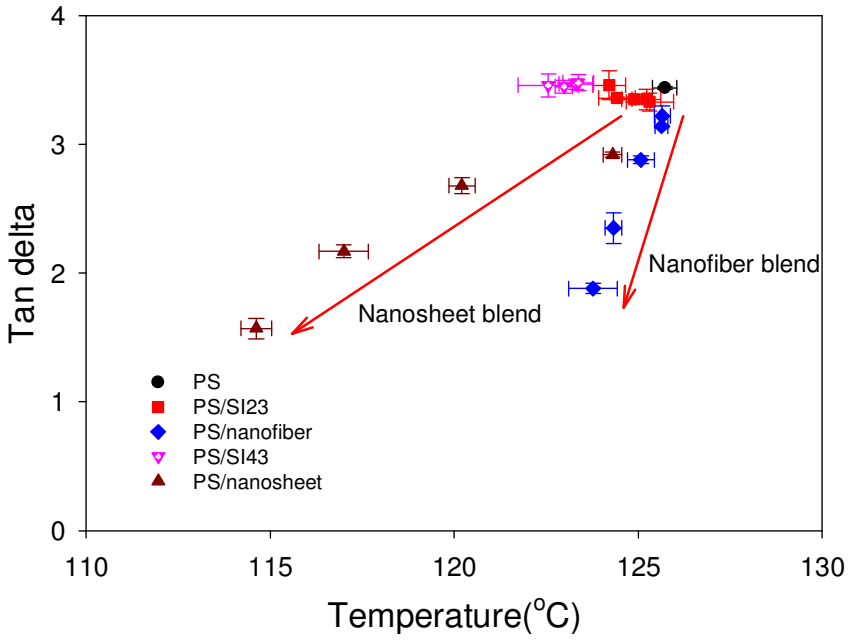

Figure 38. Tan δ vs. temperature of tan δ peak plot using blend samples with different filler loadings.

DMA results of blends were described in Section 6.2. In Figure 38, tan δ peak vs. T_g is plotted using DMA results from the blends. The tan δ and T_g peaks decrease with increasing nanofiber or nanosheet loading. T_g peak variation of nanosheet blends is much larger than that of nanofiber blends. This indicates that the morphology of the elastomeric fillers such as cylinder and lamellar can affect the variation of T_g. This significant T_g drop – up to 10°C in the 10 wt% blends – cannot be explained by the difference in the T_g values of homo PS (104°C by DSC) and the much shorter PS brush on the nanosheets (98-99°C by DSC). Thus, a likelier explanation for the decrease in T_g is the effect of higher free volume in the nanosheet blends, caused by the high surface area of nanosheets and the possibility of folding or rolling-up. In the work of Chen et al. on porous PS[141], higher free volume generated by CO_2 can shift the T_g of PS to lower temperatures (up to 75 °C). Zhang and coworkers[142] studied the relationship between glass transition and free volume of high impact PS (HIPS)/TiO_2 nanoparticles. They found that good

dispersion led to high surface area, which provides free volume between PS and TiO_2 particles and caused the T_g of PS to shift to lower temperatures (85 ^oC at 1.0 wt% of TiO_2). In the case of nanosheet blends, although the nanosheets can be dispersed individually, the nanosheets are able to fold or roll up because the width and length is much higher than the thickness. This creates a situation similar to the porous PS or to the HIPS/TiO2 composites where the matrix and particles have poor interactions. Thus the increase in free volume in the blends can shift the T_g to lower values.

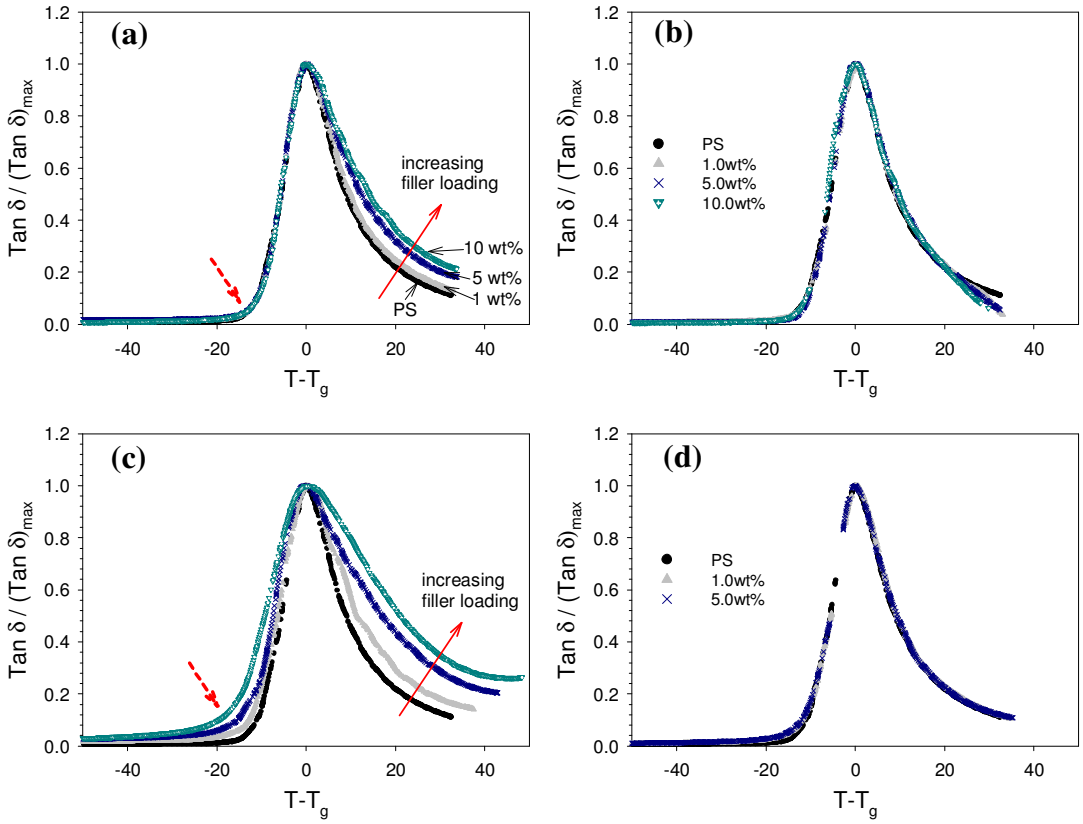

Figure 39. The normalized plots of Tan δ / (Tan δ)$_{max}$ vs. T - T_g for blends of (a) nanofiber, (b) SI23, (c) nanosheet, and (d) SI43 with neat PS with 1, 5, and 10 wt% filler loading.

In Figure 39, normalized tan δ values are plotted in terms of T - T_g in order to investigate crosslinking and nanofiller shape effects. Figure 39 (a) shows that the

normalized tan δ increases with increasing nanofiber loading above 0. This means that the stiffness of the sample increases with increasing crosslinking nanofiller loading because the mobility of homo PS chain is prevented by the nanofibers. This tendency can also be observed for nanosheet blends as seen in Figure 39 (c). Thus, in this plot, the crosslinking effect can be confirmed by the increasing of normalized tan δ. The morphology effect in elastomeric nanofiller blends is also shown in this normalized plot. In the region from -30 to -10 of the $T - T_g$ axis, the normalized tan δ value increases with increasing nanosheet loading whereas there is no increase in the nanofiber blends. The one difference between nanofiber and nanosheet blends is nanofiller shape. In the blends, nanofibers can be dispersed well without any entanglement. This indicates that nanofiber blends do not have any free volume resulting from entanglement between fillers. However, in the case of nanosheet blends, nanosheets can fold and bend by itself resulting in generated free volume. This free volume is not occupied by homo PS because of the R_g of matrix PS[143]. Thus, this free volume in the blends can affect the glass transition temperature of nanosheet blends sample, resulting in an increase in normalized tan δ in the plot.

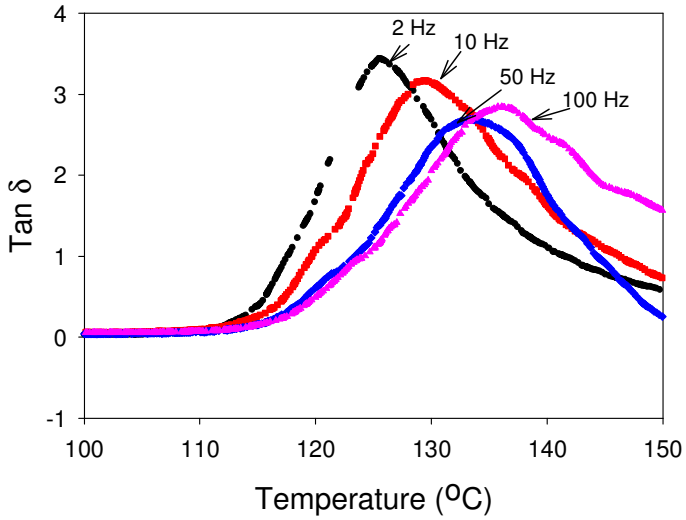

Figure 40. The effect of frequency on DMA results of neat PS.

In order to investigate the activation energy of two nanofiller shapes, various frequencies were applied: 2, 10, 50, and 100 Hz. In Figure 40, the glass transition temperature of tan δ of neat PS is shown. The temperature at the tan δ peak resulting from chain relaxation increases with increasing frequency from 2 to 100 Hz. The relationship between variation of T_g and the frequency is expressed by an Arrhenius equation[144]:

$$f = f_0 \exp \frac{-E_a}{RT} \tag{12}$$

where f is the frequency in the test, f_0 is a constant, R and E_a are the gas constant and the activation energy in the equation.

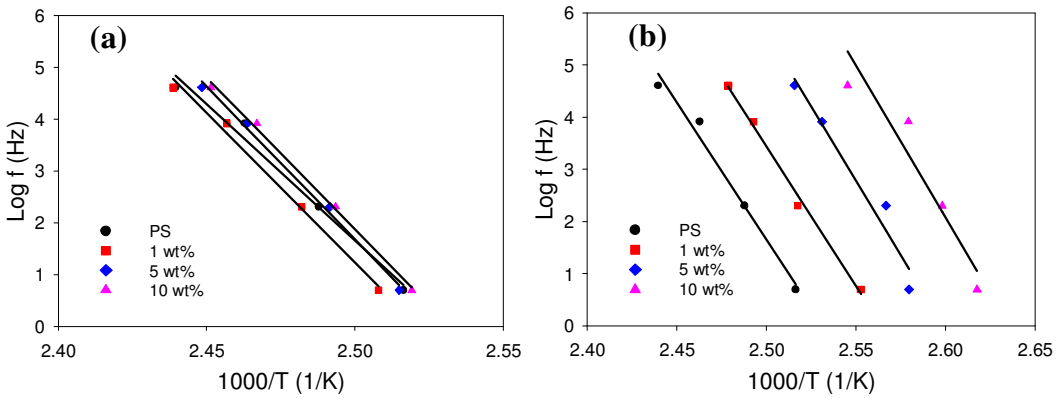

Figure 41. The logarithm of frequency values versus inverse temperature for nanofiber (a) and nanosheet (b) blends with various filler loading. R^2 values of nanofiber blends are higher than 0.99 and nanosheet blends are higher than 0.92.

Table 9. The activation energy (kcal/mol) of blends of PS with nanofiber and nanosheet with various filler loading calculated by Arrhenius Equation[144].

Sample(wt%) PS/nanofiber	Activation Energy Ea(KJ/mole)	Sample(wt%) PS/nanosheet	Activation Energy Ea(KJ/mole)
99/1	106.7	99/1	114.6
95/5	112.9	95/5	117.1
90/10	115.6	90/10	115.8

According to the equation (12), the plot between 1/T and logarithmic frequency should have a first order dependence. As shown in Figure 41, all points follow a linear line within an acceptable error range. The list of activation energies of each blends are listed in Table 9. The activation energies of both blends increase with increasing filler loading. This means that the filler has an interaction with neat PS resulting in delayed relaxation process. However, this result did not show the significant differences of two nanofillers in terms of the activation energy effect. The reason is that the differences are

too close to distinguish in solid state. To investigate the issues of activation energy, the rheological properties need to be studied in various temperature ranges.

6.4. Conclusion

In summary, the crosslinked elastomeric nanofibers and nanosheets are able to increase the storage and loss modulus in the terminal region. The values increase with increasing nanofiber filler loading and especially in the case of nanosheets, the values increase with increasing nanosheet loading above the T_g of neat PS but the opposite result occurs from 90 ^oC to 125^oC (T_g of neat PS). Nanofibers in the blends disperse well without any aggregation but the nanosheets are able to fold and bend due to the ratio between width or length and thickness. Thus, the free volume resulting from its morphology increases the free motion of the PS chain in the PS block of nanosheets. Plotting tan δ vs. filler loading or PI content demonstrates that the morphology is more effective in providing free volume than crosslinked filler loading in elastomeric nanofiller blends. The viscoelastic behavior of the blends below T_g is only affected by nanosheets and not by the nanofibers, likely because the nanosheets produce higher free volume compared to the nanofibers. However, this induced free volume effect is inoperative above T_g where the PS matrix has higher mobility, causing the viscoelastic properties to depend mainly on the filler loading and not on their morphology. Further studies of the effect of the free volume will provide to understand the behavior of elastomeric nanoparticles in blends or nanocomposites.

CHAPTER 7

EFFECTS OF CROSSLINKING DENSITY ON DYNAMIC MECHANICAL PROPERTIES

7.1. Introduction

There are a number of studies which focused on carbon filler[27, 123] and inorganic nanoparticles[27, 29, 145], that have considered the effect of morphology of fillers. For example, graphite, CNT, and graphene represent spherical, cylindrical, and sheet morphologies[82, 146, 147]; $CaCO_3$, metal nanowire, and clay also have been used as inorganic particles with these three different morphologies[29, 145, 148]. However, the studies of cylindrical and sheet morphology of elastomeric nanoparticles have not been investigated and analyzed more specifically in the literature. Most of the studies have been dealing with spherical shaped particles[31, 149] because of the surface tension and phase separation properties of elastomeric nanoparticles. The objective of this chapter is to understand the effect of geometry of elastomeric nanoparticles resulting from crosslinking density.

In this chapter, polystyrene-polyisoprene block copolymer was used in order to generate nanofiber morphology, and the mechanical properties of blends were investigated using DMA. In comparison with fully crosslinked nanofiber blends, three other blends are studied and discussed: fully crosslinked nanofiber and partially crosslinked sample having multi-junction points, and uncrosslinked PS-PI block copolymer blends.

7.2. Results

7.2.1. Cold vulcanization and crosslinking density control

A cold vulcanization process was accomplished by using a S_2Cl_2 sulfur compound at room temperature. Figure 42 shows the schematic illustration of preparation of FCF and FCM using the cold vulcanization process. Two different morphologies existed in the cylindrical ordering of PS-b-PI bulk film. Since it is possible to have a junction between cylinder morphologies when the bulk has defects, two crosslinked PS-b-PI structures are expected. One is the well ordered cylinders and the other is the cylinders having junction points. When the crosslinking reaction was applied, the former formed FCF and the latter formed FCM samples as shown in Figure 42 (a) and (b).

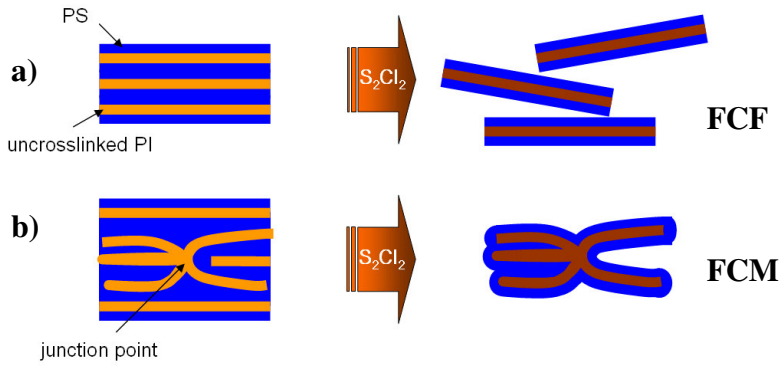

Figure 42. Schematic illustration of cold vulcanization process using PS-*b*-PI copolymer. (a) and (b) show well ordered single and multi-junction point in PS-*b*-PI bulk. FCF and FCM indicate fully crosslinked nanofiber and fully crosslinked multi-junction, respectively.

Sonication and centrifugation were used to separate between FCF and FCM. The mixture of FCF and FCM swelled in THF was first sonicated for 12 hrs and then centrifugation using 3000 rpm. Final products were obtained by precipitation in methanol then labeled as FCF and FCM. PCM which was exposed to 3 wt% S_2Cl_2 solution for 24

hrs was prepared in order to investigate the crosslinking density effect. For comparison with the samples, UBC was also prepared.

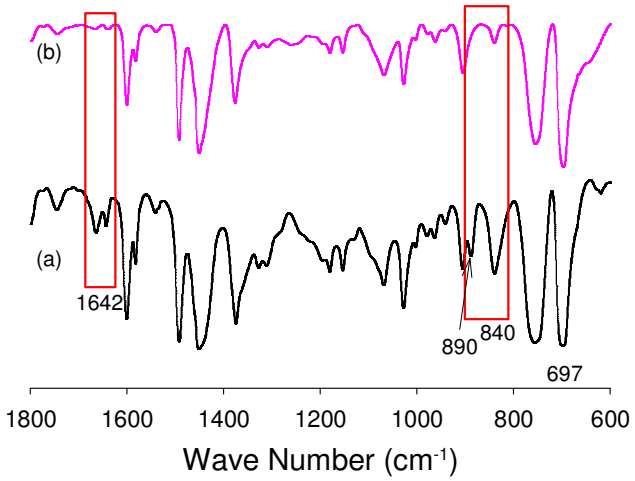

Figure 43. FT-IR spectra of uncrosslinked PS-b-PI (a) and crosslinked PS-b-PI with 100 wt% S_2Cl_2 using 168 hr crosslinking time (b).

The crosslinking reaction was studied using the intensity change of the double bond peaks at 1642, 890, 840 cm^{-1} as shown in Figure 43. The relative intensities of characteristic peaks decrease with the increasing crosslinking time which indicates that their crosslinking density is increasing. The standard peak of mono-substituted phenyl ring (697 cm^{-1}) was used as a reference in order to obtain a quantitative analysis[107].

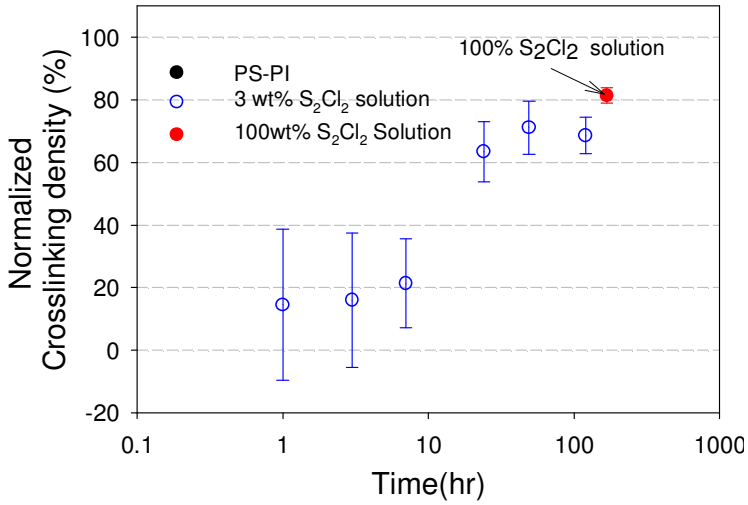

Figure 44. Normalized crosslinking density plotted as a function of crosslinking time. Filled block circle indicates uncrosslinked PS-b-PI. Hollow blue circles and filled red circle indicate crosslinked PS-b-PI using 3wt% and 100wt% S_2Cl_2, respectively.

Figure 44 shows a graph of normalized crosslinking density versus crosslinking time. The hollow circles show the PS-b-PI sample using 3wt% S_2Cl_2 in hexane varying crosslinking time from 1 to 120 hours. The crosslinking density increases dramatically up to 24 hours but increases slowly after 24 hours due to saturation of vulcanization. In order to compare the effect of crosslinking density for the blends, the samples crosslinked for 24 and 168 hrs using 3wt% and 100 % S_2Cl_2 were chosen. Morphological effect of the fiber was also investigated by FCF, FCM, and PCM.

7.2.2. Morphologies of crosslinked samples

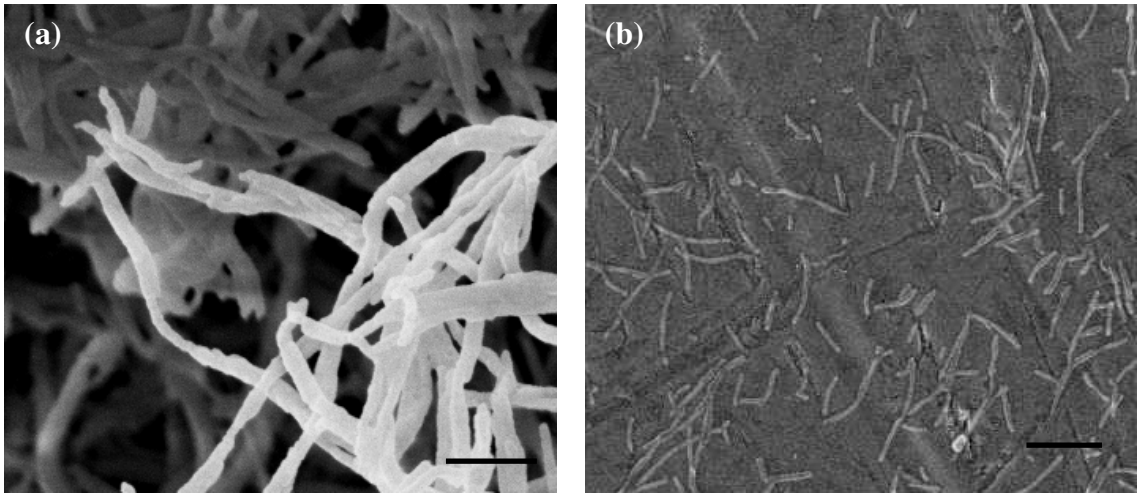

Figure 45. SEM images of single nanofibers from bulk sample (a) and individual nanofibers (b). The bars indicate 300 nm and 1 μm, respectively.

Figure 45 (a) and (b) show SEM images of bulk and individual single FCF samples, respectively. The bulk nanofibers were obtained from yellowish powder on the filter paper and imaged using SEM. The individually distributed nanofiber sample was prepared using diluted THF solution and sprayed on the SEM holder using a syringe. The SEM images indicate that the diameter of nanofibers is in the range of 30 – 50 nm and the length of single nanofiber is around 1 μm. In addition, the nanofibers can be separated by FCF without any entanglement. The length distribution of FCF on the SEM microscope was measured to have an average of 750 nm. Based on these results, sonication was conducted for 12 hrs in order to produce a narrow length distribution profile and obtained ~ 750 nm length of the single fiber as well.

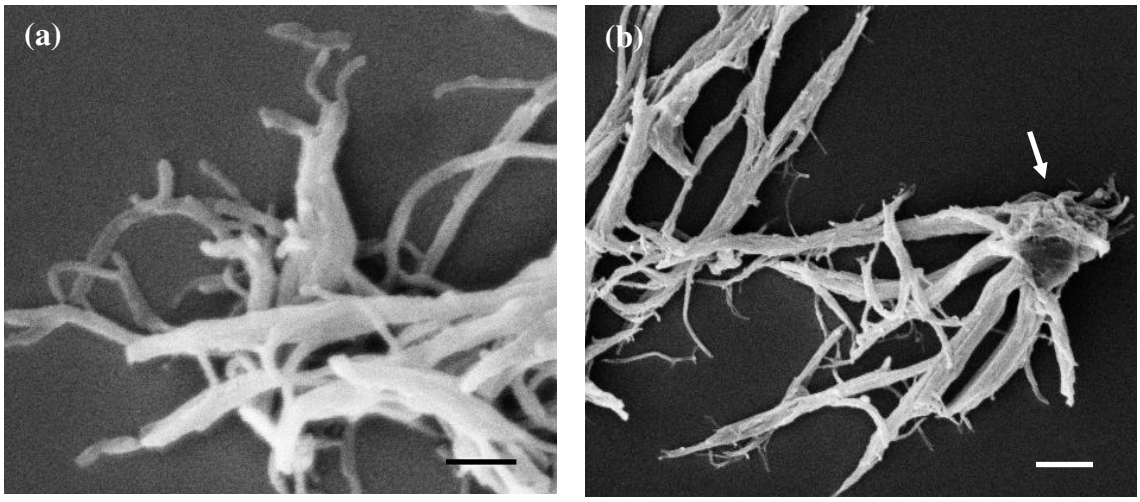

Figure 46. SEM images of fully crosslinked multi-junction samples (FCM). The white arrow is pointing out large and bulk junction of the sample. The bars indicate 300 nm and 1 μm, respectively.

In the bulk state, although the annealing temperature and time are controlled, block copolymer in which the volume ratio of styrene to isoprene is maintained at 70:30 forms a mixture of ordered cylinders and cylinders having multi-junction points. The former and latter have the morphology of single and multi-junction nanofiber, respectively. Figure 46 (a) and (b) shows SEM images of FCM samples which have been separated from the mixture of FCF and FCM using sonication and centrifugation. The average size of FCM is around 5 μm, depending on the number of junctions. The diameter of the nanofibers is in the range of 40 nm to several hundred nanometers. Two or more single nanofibers were combined by junction points resulting in large and bulky morphologies indicated by the arrow in Figure 46 (b).

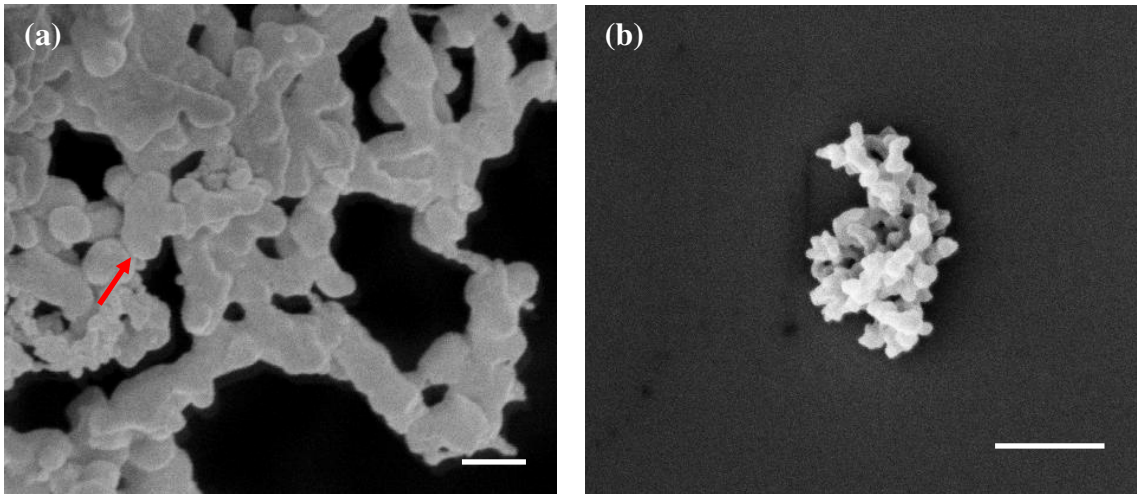

Figure 47. SEM images of partially crosslinked multi-junctioned sample (PCM) for 24 hr crosslinking time 3-Dimentional complicated morphology. The arrow in (a) shows one of the junction points in bulk samples. The bars indicate 300 nm and 1 μm, respectively.

In the case of the 24 hour crosslinked sample, the structure has a three-dimensional entangled structure rather than nanofiber morphology. The reason is that when the PS-b-PI copolymer was exposed to S_2Cl_2, the crosslinking reaction was not complete, leaving crosslinkable double bonds in the PI. Thus, when the swelling process was performed with vigorous stirring in THF, the double bonds reacted with other double bonds in neighboring fibers in the solution. The SEM images show the junction points as shown in Figure 47. The size of PCM ranges from 1 μm to 200 nm.

7.2.3. Crosslinking density and morphology effect in blends

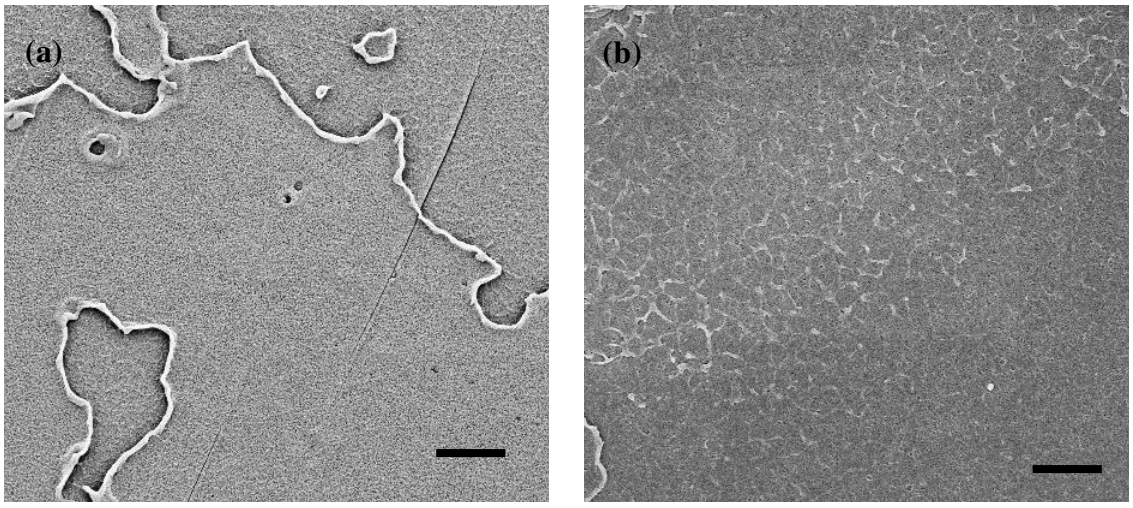

Figure 48. SEM images of fracture surface of DMA sample for neat PS and UBC/PS blends. The scale bars indicate 1 μm.

SEM images were taken from fracture surfaces obtained from tensile testing in order to investigate the filler effect in blends. Figure 48 shows SEM images of neat PS and 10 wt% UBC blends. As can be seen in Figure 48 (a), the fracture surface of neat PS is very smooth. A similar image is shown in 10 wt% UBC blends (Figure 48 (b)).

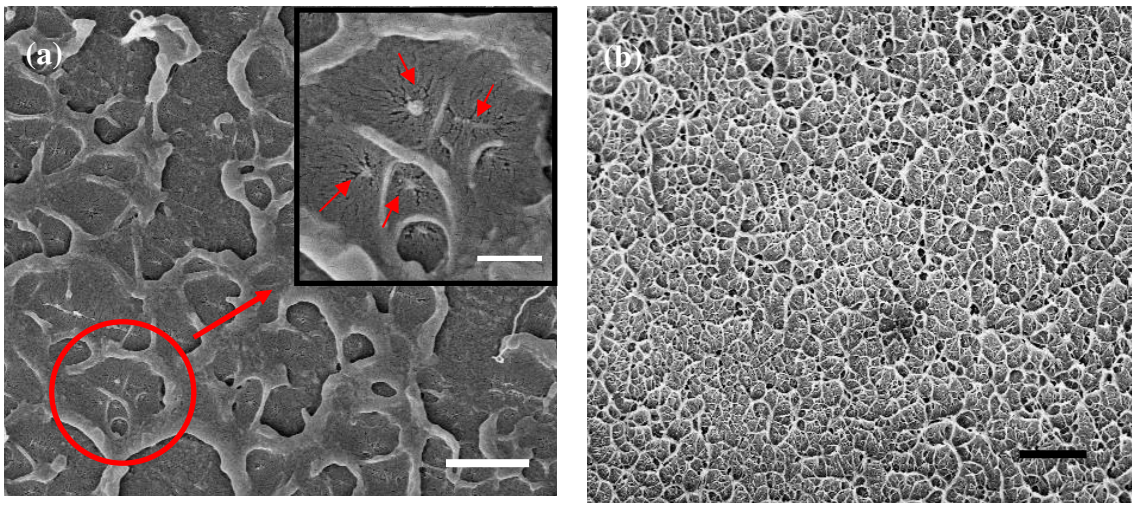

Figure 49. SEM images of cutting surface for FCF/PS blends. (a) and (b)shows 0.5 wt% and 10 wt% filler loaded sample, respectively. The insert shows a higher magnification image for single fibers. The scale bars in (a) indicate 2 μm and 500 nm for inserted image, respectively. The scale bar in (b) indicates 3 μm.

Figure 49 (a) is an SEM image of fracture surface of FCF blends with 0.5 wt% and 10wt% filler loading, respectively. In the high resolution SEM image in Figure 49 (a), the red arrows indicate the broken fibers. With increasing FCF loading, the number of separated cell-like structures increases as shown in Figure 49 (b) and empty holes can be observed. Figure 49 (a) and (b) indicate that the surface roughness increases with increasing fiber loading and cell number also increase. The individual cell was generated from individual fibers when the fracture occurred.

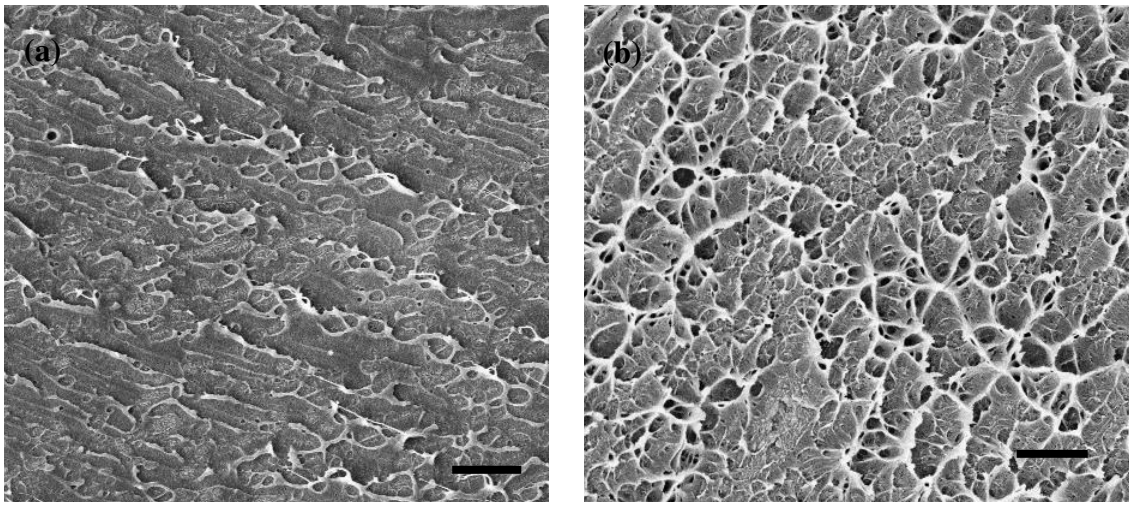

Figure 50. SEM images of cutting surfaces for (a) PCM/PS and (b) FCM/PS blends. (a) and (b) show 5 wt% and 10 wt% filler loaded sample, respectively. The scale bar in (a) and (b) indicate 3 μm.

Higher crosslinking densities can make fiber brittle because of its effects on chain mobility[150]. The crosslinking density was controlled using dilution of S_2Cl_2 solution with hexane such as 3 wt% and 100 wt% as described in the experimental section.

The geometric factor using FCF and FCM blends is also investigated. In the fracture surface of FCM blends, there are no big differences except the size and number of cell. The cell size in FCM blends is larger than in FCF blend due to the filler size

difference between FCF and FCM. In addition, the number of cells in FCF blends is higher than in FCM blends, as can be seen in Figure 50 (b).

7.2.4. Dynamic Mechanical Analysis (DMA) studies

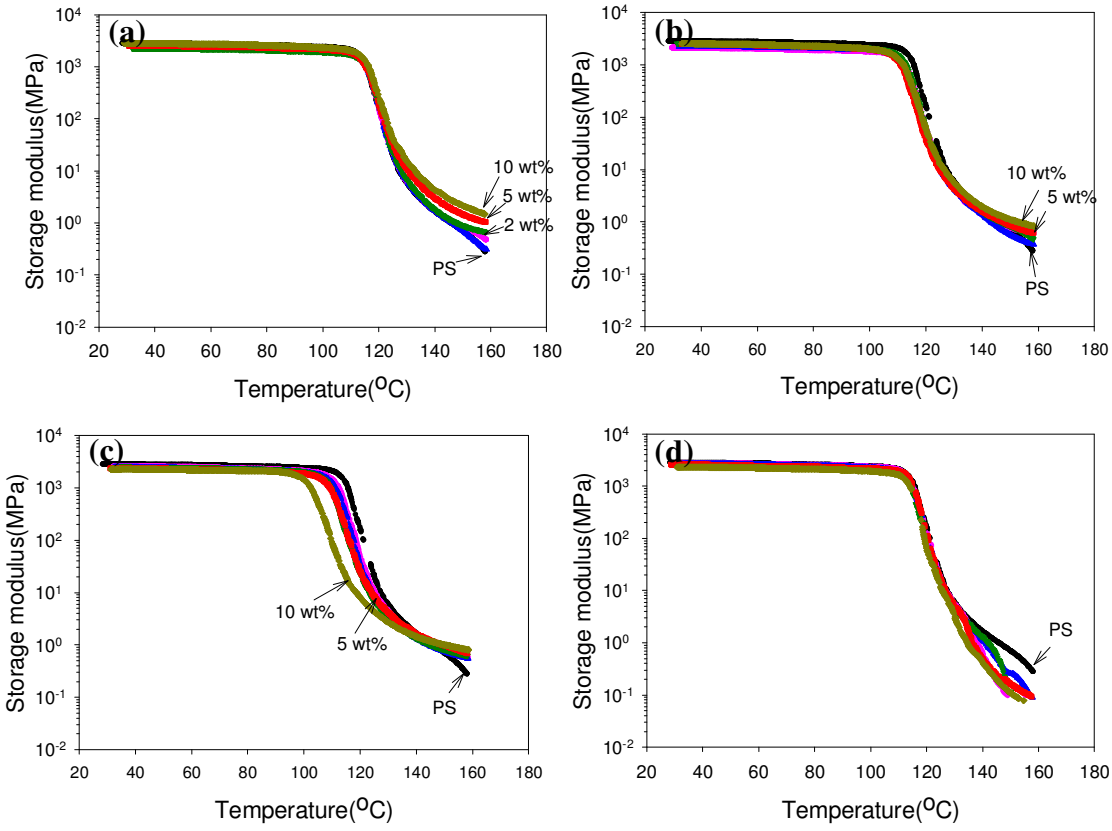

Figure 51. Storage modulus vs. temperature graphs of FCF, PCM, FCM, and UBC with 0, 0.5, 1, 2, 5, and 10 wt%. (a), (b), and (c) show that G′ are increase with increasing filler loading wt% but (d) shows lower values than neat PS. Interesting results are shown in (c). G′ is decreasing with increasing filler loading wt% from 90 °C to 125 °c which is T_g of neat PS. (●: PS, ⬢: 0.5, ▲: 1.0, ▼: 2.0, ■: 5.0, ◆: 10.0)

Figure 51 shows the storage modulus vs. temperature curves for blends of FCF, PCM, FCM, and UBC with neat polystyrene. The storage moduli at low temperature have similar values with varying filler loading. Above the T_g of neat polystyrene (125 °C), the storage moduli of all blends increase with increasing filler loading except UBC blends. This tendency appeared in all samples that were exposed to crosslinking reagent, but the

PCM and FCM blends have lower storage modulus values than neat PS up to the T_g of neat PS. In the FCM blends, the differences are shown in the range between 100 ^oC and 125 ^oC. It shows the opposite effect above T_g of neat PS on PCM and FCM blends. The crosslinking effect is shown in the storage modulus after T_g of neat PS. Below T_g of neat PS, the storage modulus decreases with increasing loading of FCM filler.

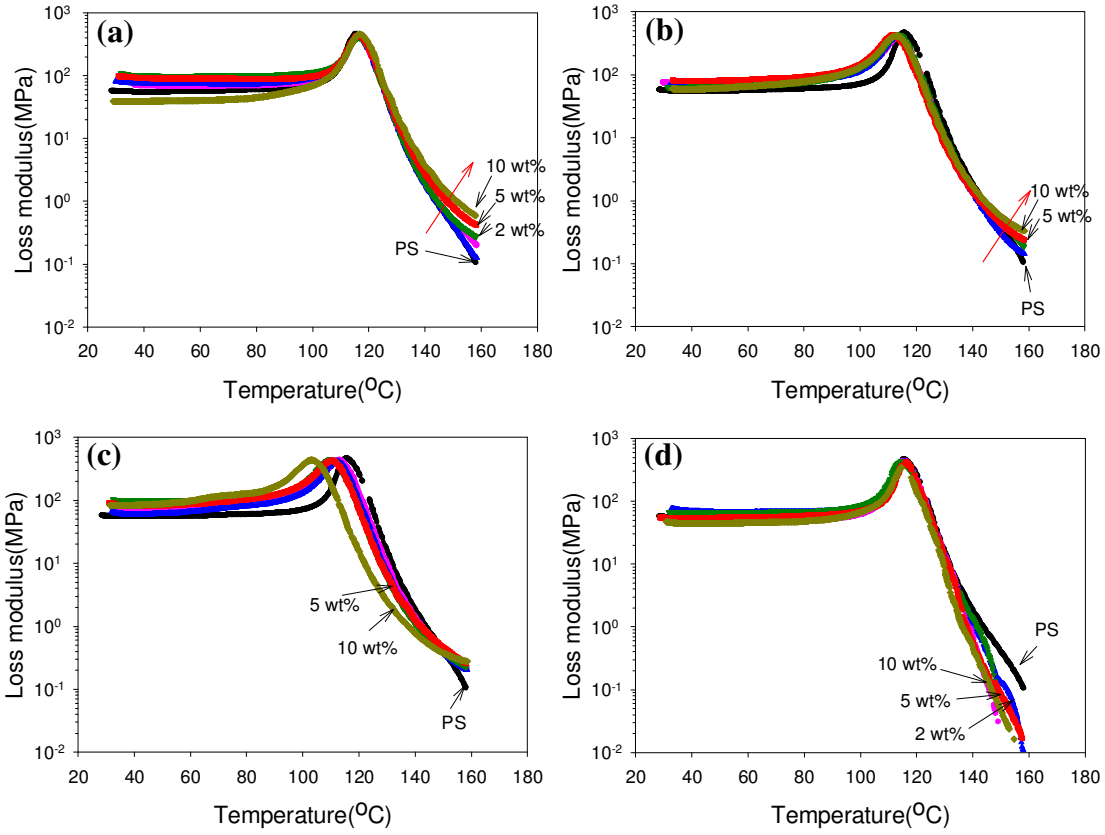

Figure 52. Loss modulus vs. Temperature curves for blends of (a)FCF, (b)PCM, (c)FCM, and (d)UBC with neat PS. G″ increased with increasing filler loading. However, the values are lower than neat PS in the case of blends of uncrosslinked PS-b-PI with neat PS. (●: PS, ●: 0.5, ▲: 1.0, ▼: 2.0, ■: 5.0, ◆: 10.0)

The loss modulus plots are shown in Figure 52 for FCF, PCM, FCM, and UBC blends. Each curve exhibits a similar trend compared with storage modulus curves for the blends. The curves for blends which were crosslinked increase with increasing filler

loading except UBC blends. The results where the modulus values decrease with increasing FCM loading are also shown on FCM blends. The glass transition temperature is shifted to lower temperatures with increasing FCM loading.

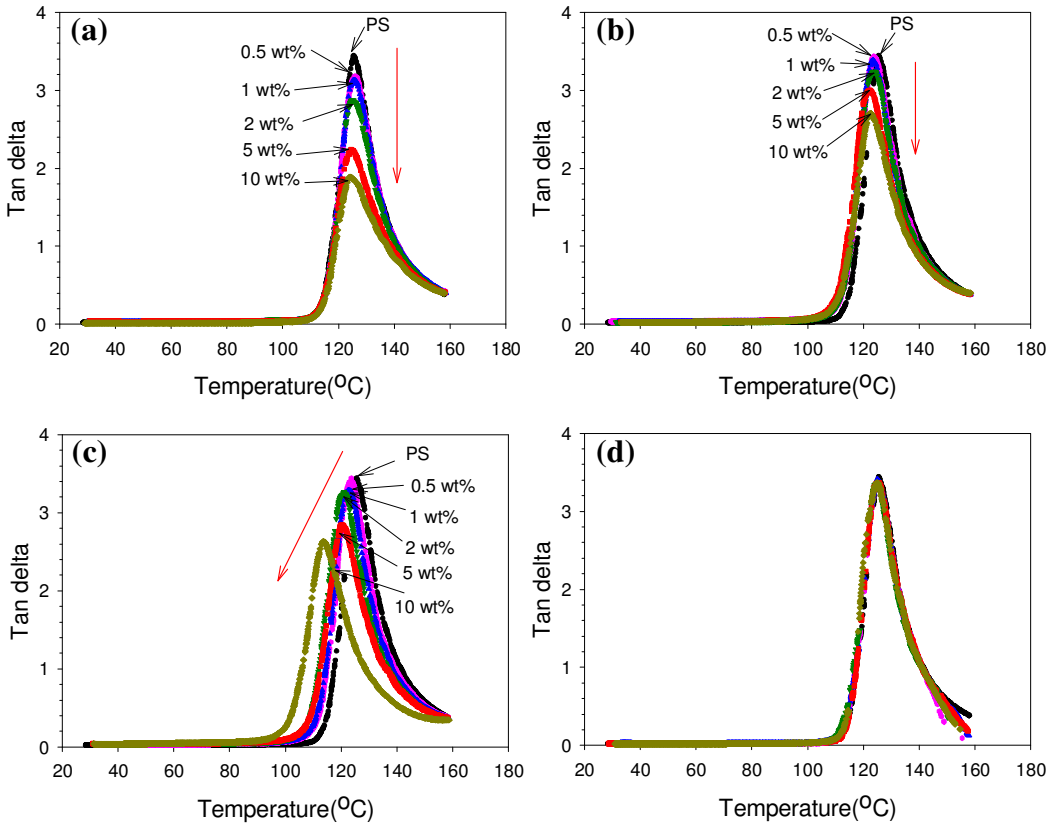

Figure 53. Variation of tan δ values against temperature for (a)FCF/PS, (b)PCM/PS, (c)FCM/PS, and (d)UBC/PS blends. (a) Tan δ of FCF/PS blends decreases with increasing filler loading. (b) and (c) show that with increasing filler loading tan δ values and temperature are decreasing. (●: PS, ●: 0.5, ▲: 1.0, ▼: 2.0,■: 5.0,◆: 10.0)

In Figure 53, the calculated loss factor (tan δ) which consists of the ratio between loss modulus and storage modulus, are shown. Maximum values of loss factor indicate the glass transition temperature (T_g of tan δ) which is very sensitive to detect the changes of the glass transition of blends. As can be seen from tan δ curves in Figure 53 (a), the value of tan δ decreases with increasing FCF loading due to crosslinked FCF without any

changing of temperature. In comparison with FCF blends, the value of tan δ and temperature in UBC blends are similar with neat PS (Figure 53 (d)). The differences in the tan δ graph are shown in PCM and FCM blends, Figure 53 (a) and (c), which have crosslinking density and morphological factors. The only difference is the morphologies in this case: FCF and FCM. The tan δ vs. temperature curves show that in the FCM blends the tan δ value decreases and T_g of tan δ also decreases with increasing filler loading. The tan δ plot of PCM blends, which has low crosslinking density, has proven that crosslinking density can affect the tan δ value as shown in Figure 53 (b).

7.3. Discussion

The physical properties of blends or nanocomposites are very closely related to filler/filler and filler/matrix interactions. Also, researchers who have studied blends or nanocomposites consider surface geometries of fillers and their morphologies due to their strong influence on the physical properties of the system. Those factors can affect the physical properties of blends or nanocomposites using very small variation. The nanoparticles as reinforcement in polymer matrix contribute the variation of the viscoelastic properties because of their good mechanical properties.

Uncrosslinked PS-b-PI could not sustain their morphology because absence of sulfur bonds between polyisoprene blocks. Thus, the fracture surface of UBC blends shows smooth surface in SEM images as shown in Figure 48. Since matrix PS has higher molecular weight than PS-b-PI, the interaction between molecules of neat PS is higher than FCF due to molecular weight. Hashimoto et al[17]. reported a separation between PS and PS-b-PI in blends when PS has much higher molecular weight than PS block in

PS-b-PI. There was no aggregation of fiber in FCF blends as can be seen in SEM images of Figure 45 (b). However, the entanglement between molecules of neat PS is much higher than the interaction between PS block in PS-b-PI and neat PS because of molecular weight. Figure 50 (a) shows an SEM image obtained from PCM blends. The morphology of fracture surfaces in PCM blends indicates that there were nanofibers. However the cell structures are not observed in compared with FCF blends (Figure 50 (b)). This means that the filler size and distribution are different.

Moduli of all blends increased with increasing filler loading except UCB blends. This suggests that the relaxation time is increased because crosslinked nanofiller prevents the chain mobility of matrix PS. Since the morphology of PS-b-PI in PS-b-PI/PS blends is determined by the total volume fraction of PS, UCM blends could have a spherical morphology of PS-b-PI. In FCM blends, the moduli decrease with increasing FCM loading and T_g of tan δ shifts to low temperature as shown in Figure 51 (c) and Figure 53 (c). This observation could be explained by the free volume effect. The small molecular weight of PS block could have a plasticizing effect due to oligomeric short chains[151]. In addition, matrix PS could not cover all surface of FCM such as junction point and inside of junction because R_g of the neat PS is around 11 nm[152]. Therefore, the major factor for decreasing of the tan δ value and T_g are crosslinking density and multi-junctioned architectures.

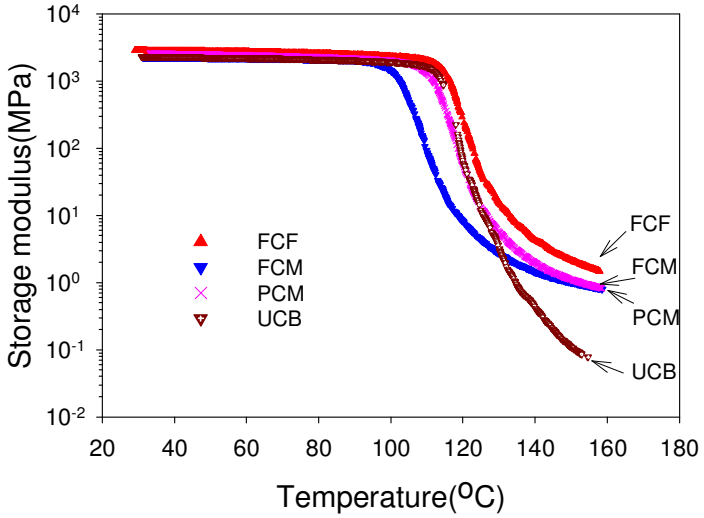

Figure 54. Storage modulus of 10 wt% filler loading of FCF, FCM, PCM, and UBC blends. At the terminal region the moduli show the crosslinked filler effects as an order of fully (FCF and FCM), partially (PCM– crosslinking time for 24hr) and uncrosslinked (UBC) blends. There are different modulus values between FCF and FCM because of filler dispersion properties.

In this study, the shape of filler was controlled and the crosslinking density effect was investigated as well. Dynamic mechanical analysis of samples (FCF and FCM) with the same crosslinking density shows that both filler loading and the filler morphology affect the viscoelastic properties. Storage modulus of blends of PS/FCF and PS/FCM are compared in Figure 54. The values of the blends that have the same weight percent of FCF and FCM loading show that the storage modulus of FCM, which has complicated filler morphology (FCM and PCM), is lower than FCF. The reason is that FCF can disperse well in the matrix but the multi-junction fillers (FCM and PCM) can generate free volumes at junction points.

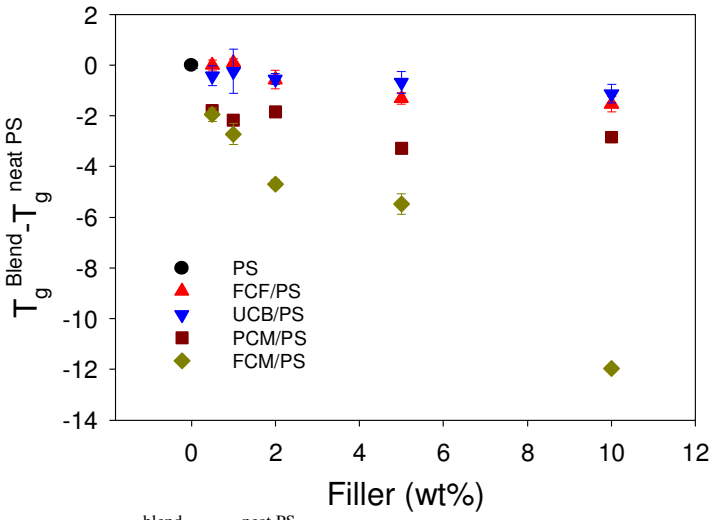

Figure 55. Normalized plot of $T_{g,}^{\ blend} - T_{g,}^{\ neat\ PS}$ vs. filler loading for blends of FCF, UBC, PCM, and FCM with neat PS.

Figure 55 shows the filler loading dependence of $T_{g,}^{\ blend} - T_{g,}^{\ neat\ PS}$ for various blends: FCF, PCM, FCM, and UBC with neat PS. These normalized T_g values are obtained from the peak position of tan δ curve. This plot shows that the T_g of all blends decreases with increasing filler loading. The largest decrease is observed from FCM blends. PCM blends have T_g values in between FCF and FCM blends. Comparing FCF with UBC blends there are only very small differences in terms of T_g. It means that the fiber morphology does not affect any T_g changes but is only related to the variation of tan δ values due to crosslinking effect. Also, T_g of FCM blends with complicated filler structures decreased with increasing FCM. In the case of single fiber architecture, single fiber loading leads to a small decrease in T_g. However, if fiber architecture is more complicated, the morphological effect could lead to a large decrease in T_g. Based on these observations there are two possible factors for changing T_g, one is free volume in between multi-junction and another is short molecular length of PS block compared with matrix PS. One of the questions is whether the crosslinking density could affect the T_g

changing with increasing filler loading. The plot also shows the T_g result of PCM blends. So the conclusion of this result is that crosslinking density is a minor cause for variation of T_g in blends.

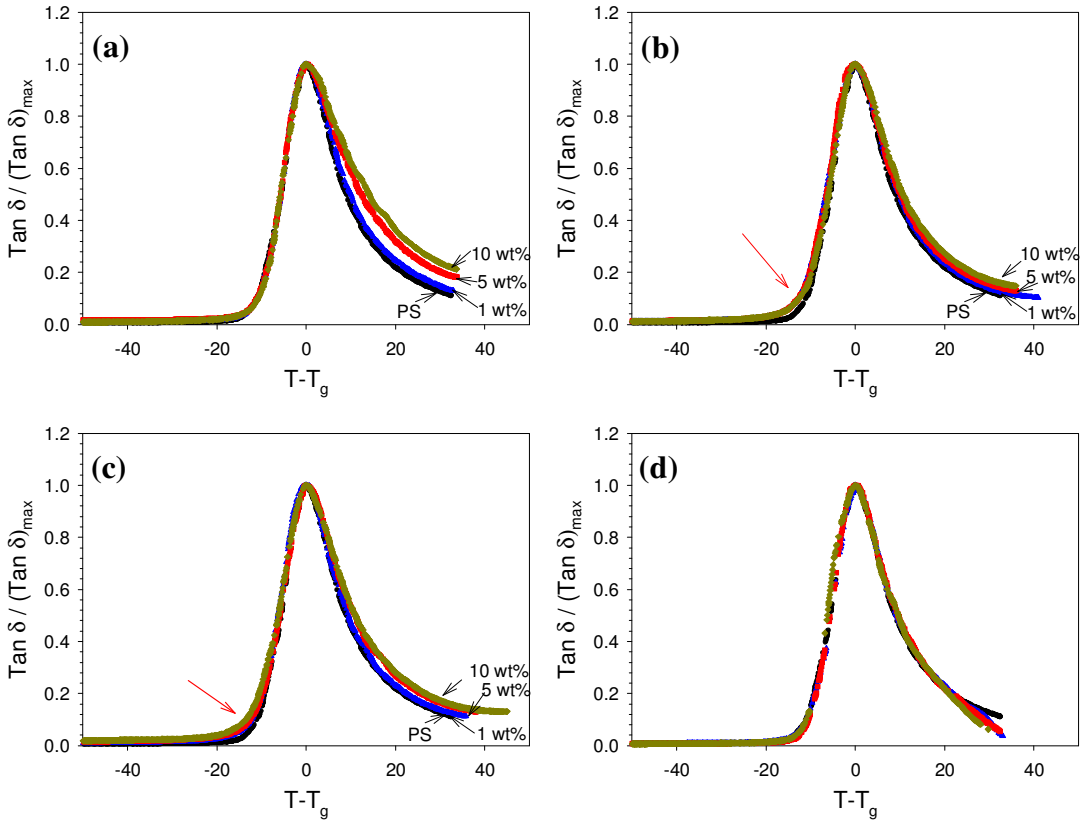

Figure 56. The normalized plots of Tan δ / (Tan δ)$_{max}$ vs. T - T_g for blends of (a) FCF, (b) PCM, (c) FCM, and (d) UBC with neat PS at 1, 5, and 10 wt% filler loading. (●: PS, ▲: 1.0, ■: 5.0, ◆: 10.0)

The normalized plots which are tan δ / (tan δ)$_{max}$ versus T – T_g are shown in Figure 56, where tan δ and (tan δ)$_{max}$ represent the value of the loss tangent at any temperature and the corresponding maximum temperature. Comparing Figure 56 (a) with (b), there is an effect resulting from crosslinked filler loading in the positive values in the T - T_g axis. The normalized value of tan δ increases with increasing the amount of crosslinked filler and the gap between FCF blends also increases with increasing temperature. However, in

the case of UBC blends, there are no significant changes as shown in Figure 56 (d). Different morphology can induce quite different physical properties such as viscoelasticity, glass transition temperature, and mechanical properties even in the same material. As can be seen in Figure 46, FCM has multi-junction morphology. The structural difference between FCF and FCM was shown in Figure 56 (a) and (c). The increased result from crosslinking is smaller than FCF. This assumption can be supported by Figure 56 (b) which is PCM having multi-junction points (Figure 47). It means that in the FCF filler the filler can disperse well in the PS matrix. The filler (FCM and PCM), however, cannot disperse in the matrix because it forms aggregated morphologies. Thus, the amount of crosslinked filler and morphology affects the value of tan δ / $(\tan \delta)_{max}$ in the normalized graph.

Another observation is the increase at -15 of T - T_g identified by the arrow in these normalized plots. Figure 56 (a) FCF and (d) UBC have similar values with neat PS by varying FCF and UBC loading, but only Figure 56 (b) FCM and (c) PCM having multi-junction point show this increase. As discussed in section 7.3., one of the purposes is to study the crosslinking density of block copolymer having cylindrical morphology in the blends. The result and difference in the morphology suggest that the T_g drop of PCM and FCM blends could be explained by the effect of using free volume and its plasticizing effect.

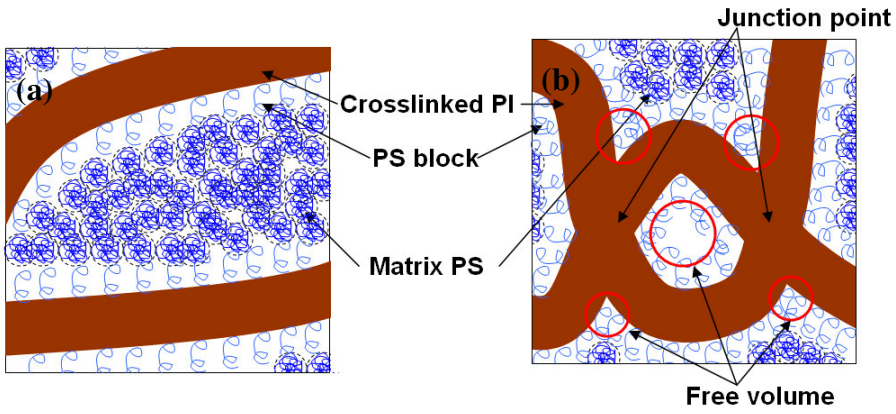

Figure 57. Conceptual diagram of (a) a blend of FCF with neat PS. Fully crosslinked fiber (FCF) is blended with neat PS. The PS cover the all surface area of FCF, (b) a blend of fully crosslinked multi-junction sample (FCM) with neat PS. Free volume can be generated in cross junction point and junction inside. Lined circle indicates R_g of neat homo PS (~11 nm)

Based on the molecular weight of homo polystyrene, R_g of homo polystyrene used here is in the range of 11 nm. In the calculation, the average value of the statistical segment length was used as 6.8 Å, as found by Ballard[152]. It means that in the FCF blends the homo polystyrene can access the nanofiber surface and interact with the PS block. However, in the case of FCM, neat PS is difficult to reach the junction inside and the size of cross junction points is smaller than R_g of neat PS. It indicates that there are free volumes which affect the T_g of blends. The models of FCF and FCM blends are shown in Figure 57 and the differences of the models can be found in terms of free volume.

7.4. Conclusion

Fiber morphology was separated using centrifugation and sonication time from bulk block copolymer film and controlled crosslinking density was used as well. The fiber blends were investigated by dynamic mechanical analysis in terms of morphological

effect and crosslinking density. The main factor for causing tan δ to decrease was crosslinking density, and the T_g shifting toward lower temperature was explained by morphological effect. The blends of neat PS and FCF observed no T_g shift only detected decreasing tan δ by increasing FCF loading. However, the blends of neat PS and FCM showed tan δ decreasing as well as T_g shifted to lower temperatures. PCM blends having 24 hr crosslinking time showed no tan δ decrease and small down shifting of T_g. Thus, the crosslinking density can affect the tan δ values of the blends and also the filler morphology can influence the variation of T_g of matrix. The elastomeric nanoparticles which have multi-junctions can provide free volumes which are limited to access of matrix PS because of their complicate morphologies. The study of free volumes in blend of elastomeric nanoparticles will be very useful in the study of blends and nanocomposites of organic nanoparticles.

CHAPTER 8

THE EFFECT OF CROSSLINKED CORE SIZE ON IN HOMOGENEOUS BLENDS

8.1. Introduction

Because of their structural specificity, nanofibers have various advantages such as a high aspect ratio, small pore size, and large surface area. Hence, research in making nanofibers has increased in science and engineering fields. They have used in a wide range of applications including textiles, composites, membranes/filters, and tissue engineering.

In chapter 2, the blends of A type homopolymer and AB type diblock copolymer was briefly introduced. There are a variety of possibilities of morphologies in the blends in terms of relative chain length, alpha, which related to molecular weight of homopolymer and block copolymer. The studies of these binary blends were conducted by Hashimoto[17-21, 57] and Winey[23, 58, 59] in terms of block copolymer and homopolymer mixture.

In this chapter, morphology was changed from lamellar to cylinder by adding neat polystyrene in polystyrene-b-polyisoprene copolymer. The cold vulcanization process was applied to generate nanofiber morphologies. This chapter also focuses on the influence of the elastomeric polyisoprene size in nanofiber blends with neat polystyrene in terms of rheological properties.

8.2. Results and Discussion

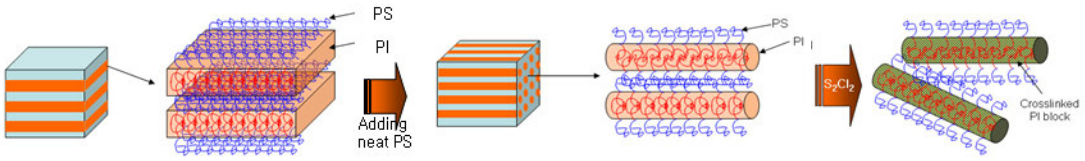

Figure 58. Schematic illustration of generating nanofiber-B from PS-b-PI copolymer having lamellar morphology by adding additional neat PS.

Figure 58 illustrates schematic illustration of preparing nanofiber-B resulting from PS-b-PI copolymer having 50 and 50 volume fraction. By adding neat PS before crosslinking, the morphology of bulk PS-b-PI copolymer can be changed from lamellar to cylindrical. This means that nanofiber-A (FCF) and B have the same morphology and that a similar molecular weight of each PS on block copolymer can lead to a similar size of shell, but four times difference of PI molecular weight can lead to two times differences in the core diameter of each PI. The effect of the elastomeric part can be investigated and studied.

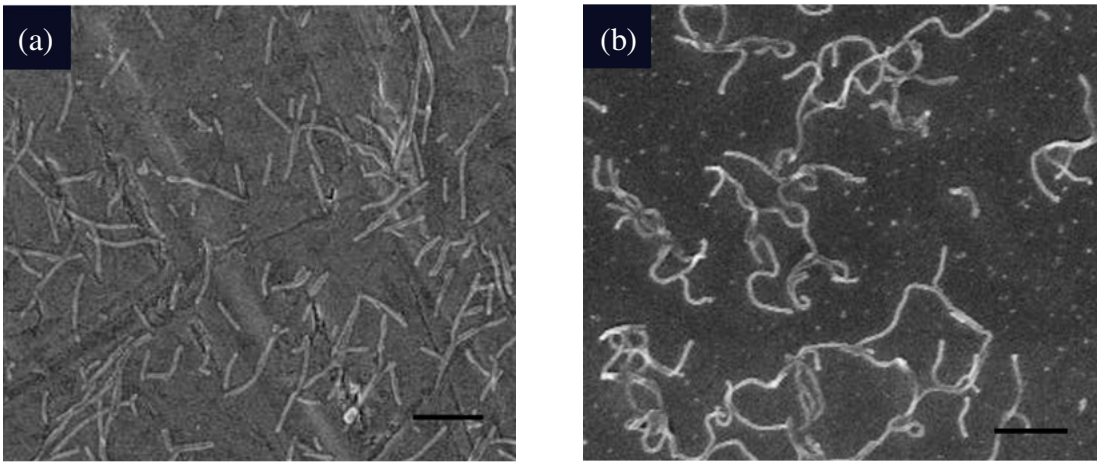

Figure 59. SEM images of nanofiber-A (a) and nanofiber-B (b). The bars indicate 1 μm, respectively.

The morphologies of nanofiber-A and B were confirmed by SEM as shown in Figure 59 (a) and (b). Figure 59 (a) shows the individual nanofiber morphology of nanofiber-A and the diameter was measured as 40 nm. In order to determine the length of nanofibers, the swelled nanofibers were sprayed on the SEM holder. The average length of nanofiber-A was 750 nm measured by manually using SEM images.

In Figure 59 (b), the SEM images of nanofiber-B show that it was successfully generated from lamellar morphology of PS-PI block copolymer by adding additional PS. The diameter of nanofiber-B was approximately 70 nm. The length was around 2-3 μm. Nanofiber-B, which has higher PI content, appears more flexible and curled than nanofiber-A.

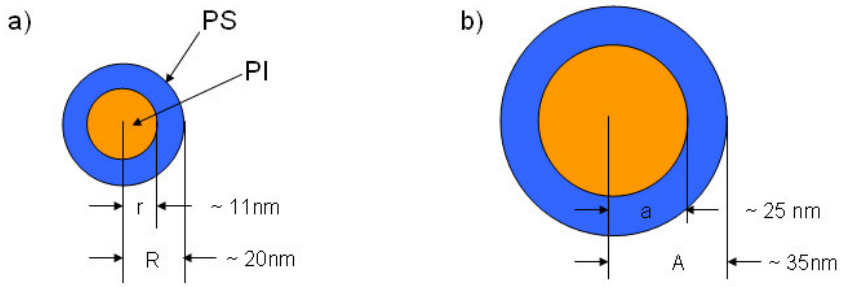

Figure 60. Schematic illustration of the cross section of nanofiber-A (a) and nanofiber-B (b). Yellow core area and blue shell area indicate polyisoprene, which is crosslinked, and polystyrene, respectively. R and r indicate the diameter of core and total of nanofiber-A. A and a indicate the diameter of core and total of nanofiber-B. The corona diameter was calculated by the ratio of molecular weight of PS and PI block.

Figure 60 shows a schematic illustration of comparable size of PI and PS for nanofiber-A and nanofiber-B based on a calculation using measured diameter of each fiber from SEM images. Based on the ratio of block size and sample geometrical relationships, the following core/shell ratios are expected.

$$r = \sqrt{\frac{3}{10}}R \quad \text{and} \quad a = \sqrt{\frac{1}{2}}A \tag{13}$$

where, R and r is diameter of nanofiber-A and PI core, respectively and A and a is diameter of nanofiber-A and PI core. As observed in SEM images in Figure 59**,** nanofiber-B is more flexible than nanofiber-A. These results suggest that nanofiber-A is more glassy than nanofiber-B because of the amount of PI as well as crosslinking density. In the case of nanofiber-B, the nanofiber was synthesized by a blend of lamellar morphology of PS-PI block copolymer and neat PS. The PS-PI block copolymer was covered with neat PS so that the crosslinking density can be lower than bulk of cylindrical PS-PI block copolymer at the same crosslinking time. In addition, the related amount of PS and PI is 7:3 and 5:5 for nanofiber-A and nanofiber-B, respectively. Therefore, the glassy nanofiber-A can be broken into short fibers when a sonicator was used but flexible nanofiber-B can maintain their length. In order to prove flexibility and its affect in blends, the rheological properties were measured.

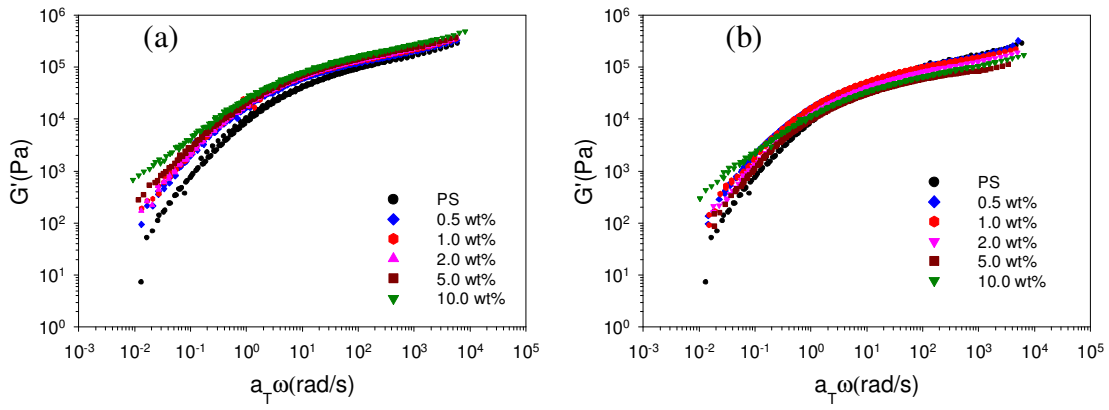

Figure 61. Master curve of storage modulus of (a) nanofiber-A/PS, (b) nanofiber-B/PS with varying weight fraction of fillers. The reference temperature is 180 ^{o}C.

The rheological properties were investigated in order to understand the behavior of nanofibers in the melt state. The master curves of the blends are shown in Figure 61 using the shift factor resulting from WLF equation[108]. Storage modulus of nanofiber-A/PS blends increasing with increasing nanofiber contents. However, Figure 61 (b) shows the storage modulus of nanofiber-B/PS blends increasing only in the 10 wt% nanofiber loading and the value is slightly lower than nanofiber-A blends. The dispersion of nanofiber-A in the PS matrix is much greater than nanofiber-B and the motion of matrix PS chain is more delayed in the blends of nanofiber-A.

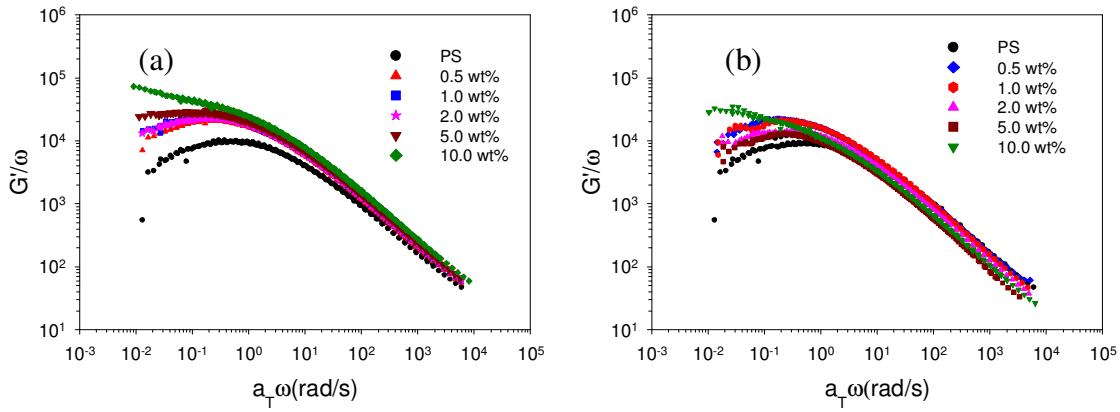

Figure 62. G'/ω versus angular frequencies was plotted using master curve. (a) nanofiber-A/PS blends and (b) nanofiber-B/PS blends in terms of nanofiber loading.

In order to study the structural information of nanofibers, the dynamic elasticity coefficient was used and G′/ω versus frequency was plotted. The slope of neat polymer is +1 in the lower frequency region but if there are some effects in the material, the slope will change. The slope of the nanofiber-A blends in the lower frequency region is decreasing. However, in the case of nanofiber-B blends, there are similar slopes until 5 wt% and on increase at 10 wt% as shown in Figure 62 (a) and (b). These results suggest that nanofiber-A in the blends can influence the mobility of neat PS even small amount

but nanofiber-B only can affect after 5 wt% loading. The reason is the differences in dispersion, hardness, and length of each nanofiber.

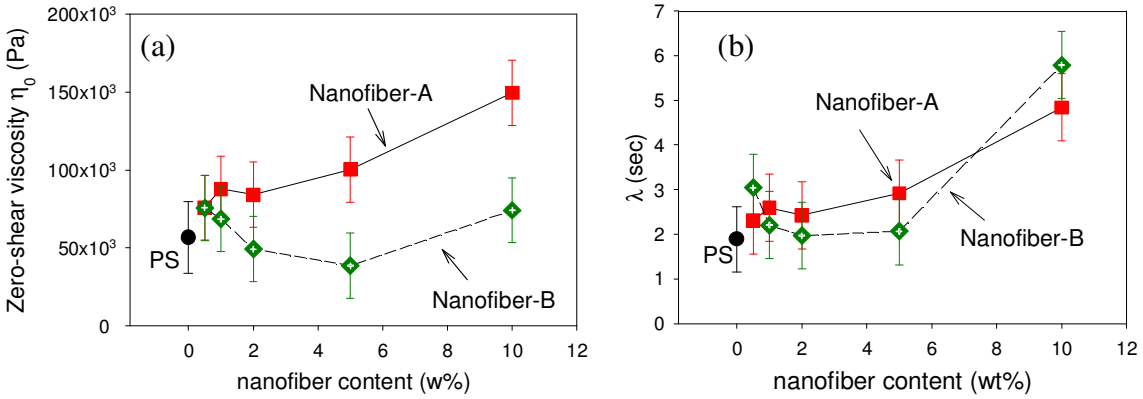

Figure 63. Zero shear viscosity (a) and Relaxation time (b) vs. nanofiber content plotted by model fitting data.

The value of zero-shear viscosities and relaxation times resulting from the three parameter Cross-Williamson model is obtained in order to investigate the effect of crosslinked PI size and content. The zero-shear viscosity values of nanofiber-B/PS blends are similar to those of nanofiber-A/PS blends at 0.5 wt% nanofiber loading but lower above the 0.5 wt% loading because of an increased amount of PI content. This suggests that the flexibility from PI is the critical factor in zero-shear viscosity. However, in the case of relaxation time data, the nanofiber-B/PS blend has a similar value to the nanofiber-A/PS blend. This indicates that the morphology of nanofiller in the blend can increase the relaxation time with increasing nanofiber contents.

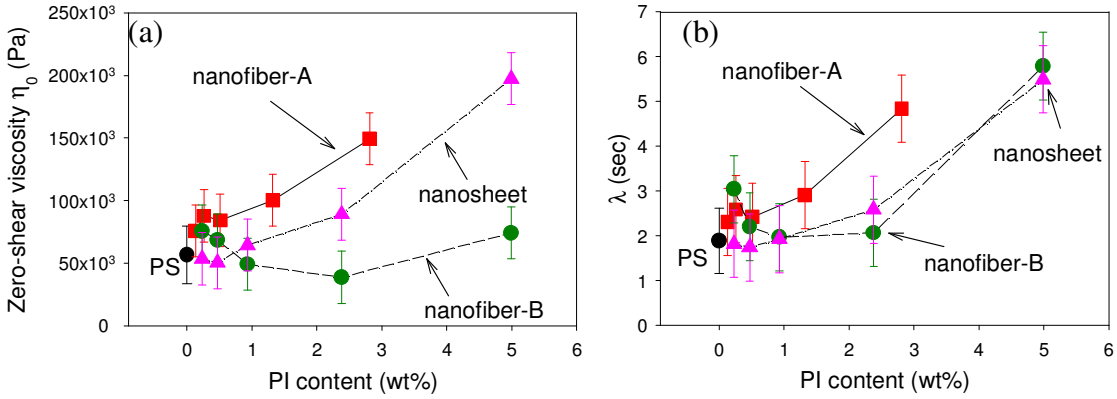

Figure 64. Zero-shear viscosity (a) and relaxation time (b) of nanofiber-A, nanofiber-B, and nanosheet vs. PI content are plotted. Solid line with rectangular, dashed line with triangle, and dash-dot-dot line with circle indicate PS/nanofiber-A, PS/nanofiber-B, and PS/nanosheet blend, respectively.

In order to investigate the effect of PI and PS block content, the zero-shear viscosity and relaxation time of the blends are plotted as a function of PI content. As discussed on the previous page, the PI content is more effective than morphology of nanofibers in terms of zero-shear viscosity. However, Figure 64 (a) shows that nanofiber-A has the highest value and the nanosheet is higher than nanofiber-B even though they have same PI content. This means that there are other factors such as PS block content or surface area. In the case of relaxation time, below 1wt% of PI loading, nanofiber-A, nanofiber-B, and nanosheet show very similar trend; however, above 1 wt% of PI content nanofiber-B and nanosheet show comparable results. This suggests that, at high PI loading, the values of nanofiber-A are higher than nanofiber-B and nanosheet that show a similar trend. The reason is that PS and PI composition in nanofiber-B and nanosheet are the same but the composition of PS is higher than that of PI in nanofiber-A. Also, the morphologies of nanofillers affect the relaxation time of the blends.

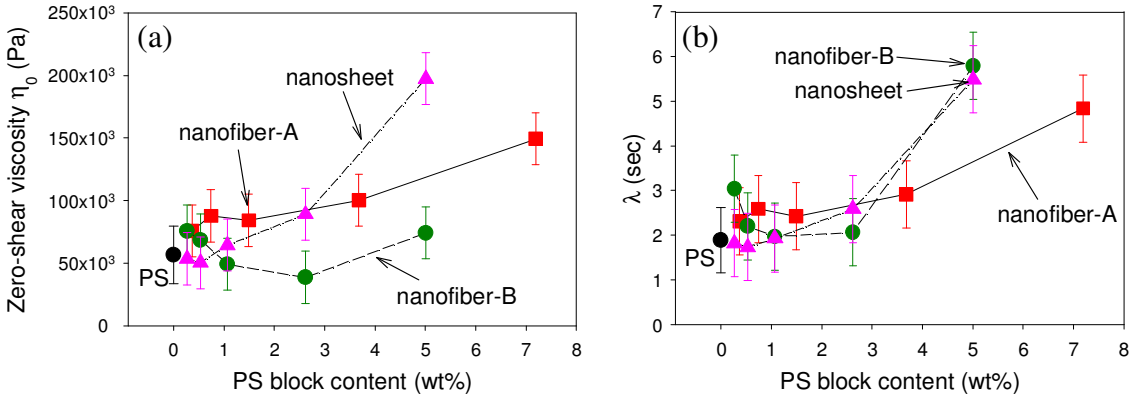

Figure 65. Zero-shear viscosity (a) and relaxation time (b) of nanofiber-A, nanofiber-B, and nanosheet vs. PS content in PS-b-PI copolymer are plotted. Solid line with rectangular, dashed line with triangle, and dash-dot line with circle indicate PS/nanofiber-A, PS/nanofiber-B, and PS/nanosheet blend, respectively.

In order to investigate PS block effect on the nanoparticles, the PS block content of nanofiber-A, nanofiber-B, and nanosheet blends is plotted. Figure 65 (a) shows zero-shear viscosity values as a function of PS block content. As can be seen, nanosheet has the highest value and nanofiber-A has a higher value than nanofiber-B. This result also indicate that PS block content is not a major factor because the zero-shear viscosity values of nanosheet and nanofiber-B are completely different even though they have the same PS block content. In the case of relaxation time, nanosheet and nanofiber-B have similar values. Thus, morphologies of nanofillers influence the relaxation time in the elastomeric nanoparticle blends because relaxation time is a result of local chain interactions between nanoparticles and matrix polymer.

In the zero-shear viscosity of the blends, the surface area of nanoparticle can be one major factor because zero-shear viscosity is affected by overall interactions from nanoparticles and matrix polymer. Specific surface area of nanoparticles can be calculated by the ratio of surface area and mass. A calculated result indicates that the specific surface area of nanofiber-A > nanosheet > nanofiber-B based on diameter and

thickness of the nanoparticles. The values of zero-shear viscosity as a function of PI content are well matched with calculated surface areas of the nanoparticles. Thus, zero-shear viscosity is closely related to PI content and surface area in elastomeric nanoparticle blends.

8.3. Conclusion

Two nanofiber samples were successfully prepared and characterized. Nanofiber-B was more flexible than nanofiber-A because of the composition of elastomeric core PI size. The storage modulus of nanofiber-A/PS blends increased with increasing filler loading but only increased at the 10 wt% filler loading in the case of nanofiber-B/PS blends. More glassy nanofiber-A is able to affect the motion of the matrix PS with even small loadings but nanofiber-B prevents the PS motion above certain weight percent because of core PI size and crosslinking density. The zero-shear viscosity and relaxation time data were obtained from the three parameter Cross-Williamson model. The results of zero-shear viscosity indicate that the values are influenced by specific surface area and PI contents. The reason is that zero-shear viscosity is affected by the mobility of the overall chain in the blends. Thus, the surface area is a major factor for varying zero-shear viscosity. In these elastomeric nanoparticle blends, the PS block can move freely but the motion of crosslinked PI is limited. So, the PI content is also closely related to zero-shear viscosity. The effect of morphology is observed from relaxation time data. The values of relaxation time of nanofiber-B and nanosheet are very similar in varying PS and PI content. This means that PS and PI block contents are a minor factor for influencing their relaxation time. The reason is that relaxation time is a result of local chain motion resulting from the interaction between the PS brush and matrix PS. Thus, the morphology

of nanoparticles is a major factor for the relaxation time in the elastomeric nanoparticle blends. The information of viscoelastic properties regarding morphologies in elastomeric nanoparticles will provide a fundamental understanding for future studies of organic nanoparticles which have various morphologies.

CHAPTER 9

CONCLUSIONS AND RECOMMENDATIONS FOR FUTURE WORKS

9.1. Conclusion

In this thesis, blends of homopolymer and elastomeric block copolymer nanoparticles were investigated. Elastomeric block copolymer nanoparticles were first self-assembled by the thermodynamic property of PS-PI diblock copolymer and then synthesized by a cold vulcanization process in order to maintain specific morphology particularly, cylinder and lamellar as a form of fiber and sheet. In nanofiber blends, the moduli from rheology increased with increasing nanofiber content. The dynamic elasticity coefficient was used to explain the morphological change with increasing nanofiber content. Calculated critical volume fraction suggests that nanofibers reach a percolation threshold between 5 and 10 wt% of nanofiber loading. This range of values is consistent with that obtained from dynamic elasticity coefficient measurements.

In the case of nanosheet blends, the calculated critical volume fraction in the nanosheet blends ($0.013 \le \phi_c \le 0.0310$) was lower than that in the nanofiber blends ($.027 \le \phi_c \le 0.053$). Since the percolation threshold is proportional to the aspect ratio of the nanoparticle, nanosheets have a lower value of critical volume fraction than nanofibers. But, the rheological values and SEM images show that the critical values are in between 5 and 10 wt%.

Dynamic mechanical properties were also investigated using nanofiber and nanosheet blends. Both elastomeric nanofibers and nanosheets increased the storage and loss modulus in terminal region. Since these crosslinked morphologies prevent the motion of neat PS in matrix, the relaxation time was increased. However, the values decreased with increasing nanosheet loading. This result can be explained by the presence of folded nanosheet. Nanofiber dispersed well without any aggregation in blends but the nanosheet, which has good flexibility, can roll or fold and touch because of their large aspect ratio. So, trapped polystyrene inside the nanosheets did not affect matrix neat polystyrene which has higher molecular weight than trapped polystyrene. This low molecular weight of polystyrene can act as plasticizers. This result was also investigated using a normalized tan δ plot.

The effect of crosslinking density in elastomeric nanoparticle is also one important issue to understand morphology and toughness. In order to investigate the influence of crosslinking density, four samples were prepared as a function of crosslinking time. The results show that the storage modulus decreases and tan δ shifts to lower temperature and can be observed from only fully crosslinked and partially crosslinked multi-junctioned samples. Multi-junctions in nanoparticles provide free volume where there is no influence of neat polystyrene so there is only the motion of polystyrene in the nanoparticles. Thus, the crosslinking density of elastomeric nanoparticles can affect the elasticity of blends and the nanoparticle morphology also affects the T_g shifts.

The study of elastomeric polyisoprene size was also conducted using PS-PI cylindrical morphology (nanofiber-A) and PS-PI lamellar morphology by modification to the cylinder (nanofiber-B). Generated nanofiber resulting from the blend of

homopolystyrene and nanofiber-B has twice the PI diameter than nanofiber-A. The SEM image shows that nanofiber-B is more flexible than nanofiber-A. Since nanofiber-B was generated from the blend of homopolymer and lamellar morphology of PS-b-PI, the crosslinking density can be lower than nanofiber-A. In addition, two times larger PI diameter also can affect the flexibility of the nanofiber. This property is observed directly in rheology results. The modulus values of nanofiber-A blends are higher than the blends of nanofiber-B with increasing nanofiber content. This suggests that the glassy nanofiber-A more effectively prevent the motion of neat polystyrene than flexible nanofiber-B. In addition, the polyisoprene content and surface area can have a huge affect on zero-shear viscosity because zero-shear viscosity is affected by the mobility of the overall chain in the blends. The rheological results also show that the morphologies of elastomeric nanoparticles play a role on the relaxation time which is affected by local chain motion.

This thesis has shown that crosslinking of block copolymer is a facile method to generate elastomeric nano-morphologies such as nanofibers and nanosheets. Furthermore, the viscoelastic and rheological properties of homopolymer can be tuned with the addition of these nanoparticles. In this system, morphology affects viscoelastic properties as well as rheological properties, likely because of aspect ratio and surface area. Moreover, the core PI size is also an important factor to influence the properties because PI provides elasticity in blends. These studies of blends of elastomeric nanoparticles will be of fundamental value in understanding polymer blends and nanocomposites of organic nanoparticles.

9.2 Recommendations for future works

9.2.1. Block copolymer nanoparticles

The importance of polymer blends and composites has been explored in the last several decades for various applications in terms of mechanical[27, 123, 145], electrical[120, 121], and optical properties[117]. Although there are differences in the details of blend and composite theory containing the use of organic and inorganic nanoparticles as fillers or modifiers, some basic concepts of structure-property relationships apply to both systems[29, 153]. In addition, the basic concepts involve important parameters such as interaction between matrix-filler and the effect of filler roughness or shape[124]. There are various approaches to accomplish the shape control using inorganic nanoparticles. However, only a few theoretical studies have been conducted on the study of generation of organic nanoparticle especially block copolymer nanoparticles. In this thesis, the generation of elastomeric nanofiber and nanosheet was successfully reproduced. In addition, mechanical and rheological studies were also performed. In this thesis, I mainly focused on the study of nanofibers such as crosslinking density and PI size effect but study of nanosheet also has many fascinating opportunities. In addition, the shape changes of elastomeric nanoparticle during rheological studies are also interesting in terms of mechanical processing comparing with hard or glassy inorganic nanoparticles. The blends of homopolymer and block copolymer or two block copolymer enable one to achieve various tailored blend morphologies by controlling the blend ratio and composition factor[32]. This means that the generation of various elastomeric or other block copolymer nanoparticles can be possible so that the particles can be used in mechanical, electrical, and biomedical applications.

9.2.2. Electrospinning

Polymer fibers have been used in a variety of applications ranging from textiles to composite fillers[154, 155]. Fibers have been prepared by melt, wet/dry and gel spinning methods. Traditionally, nanofibers have been prepared by melt[156], wet/dry[157] and gel[158] spinning methods. However, recently, several methods such as electrospinning[159] and phase separation processing[89] have been introduced to generate nano-sized fiber. The fiber diameter is typically tens to hundreds of nanometer scale whereas lengths vary from less than a micron to millimeters[160]. Because of their structural specificity, nanofibers have various advantages such as high aspect ratios, small pore size, and large surface areas. Their applications have wide ranges including textile[154], composite[155], membrane/filter[161], and tissue engineering[162].

In chapter 8, the nanofiber resulting from the blends of polystyrene and lamellar morphology of PS-b-PI was generated. However, the length effect in blends cannot be investigated because of the difficulty of long range ordering in block copolymer. As a future study, electrospinning in homopolymer and block copolymer will provide longer nanofiber lengths and than the study of blends in terms of the effect of nanofiber length will suggest fascinating results as well as blends of elastomeric nanoparticle effect in electrospinning as shown in appendix B can be an attractive research area.

APPENDIX A

TEM MICROGRAPH OF NANOFIBER AND NANOSHEET

Figure A.1 and A.2 show TEM micrograph of nanofiber and nanosheet. The diameter of nanofiber is ca. 40 nm. Figure A.2 shows flexible individual nanosheet

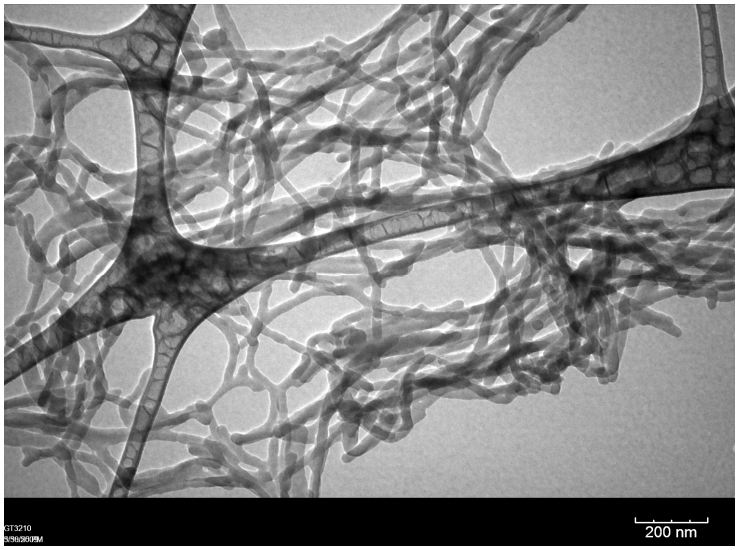

Figure A.1 TEM micrograph of nanofibers resulting from cold vulcanization using cylindrical morphology of PS-b-PI copolymer. The diameter of each nanofiber is around 40 nm and the length is 700 nm.

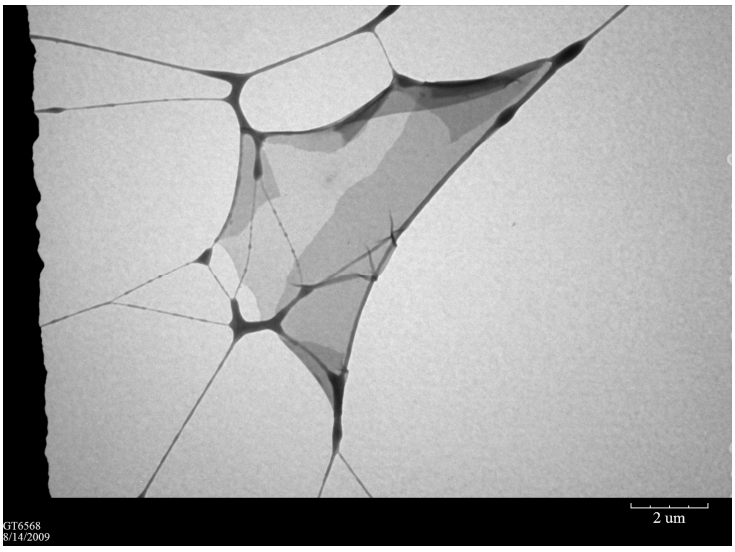

Figure A.2 TEM micrograph of nanosheets resulting from cold vulcanization using lamellar morphology of PS-b-PI copolymer.

APPENDIX B

SEM MICROGRAPHS OF ELECTROSPUN BLENDS OF POLYSTYRENE AND NANOFIBER

Figure B.1 and B.2 show electrospun blends of PS/nanofiber and PS/nanosheet by increasing nanofiber and nanosheet loading. Number of beads is decreasing with increasing the nanoparticle loading as well as shape of beads is changed.

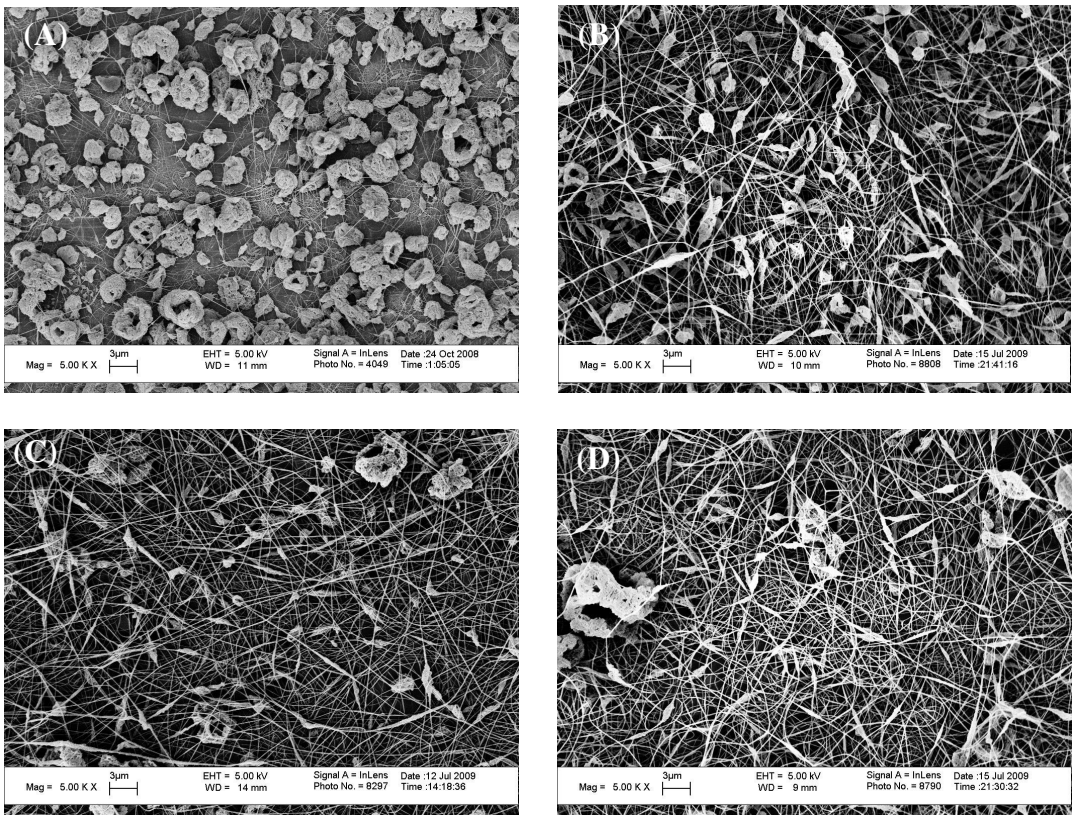

Figure B.1 SEM micrographs of electrospun blends of neat PS and nanofibers with varying weight percent of nanofiber (0 wt%, 5wt% 10 wt% 15 wt%).

Table B.1. Blend compositions of PS and nanofiber as well as electrospinning condition

	PS	nanofiber	Electrospun conditions
(a)	100 %	0 %	- Concentration: 3 wt%
(b)	95 %	5 %	- Solvent: THF/DMF mixture (50:50)
(c)	90 %	10 %	- Operating voltage: 20 KV
(d)	85 %	15 %	- Distance: 10 cm

APPENDIX C

SEM MICROGRAPHS OF ELECTROSPUN BLENDS OF POLYSTYRENE AND NANOSHEET

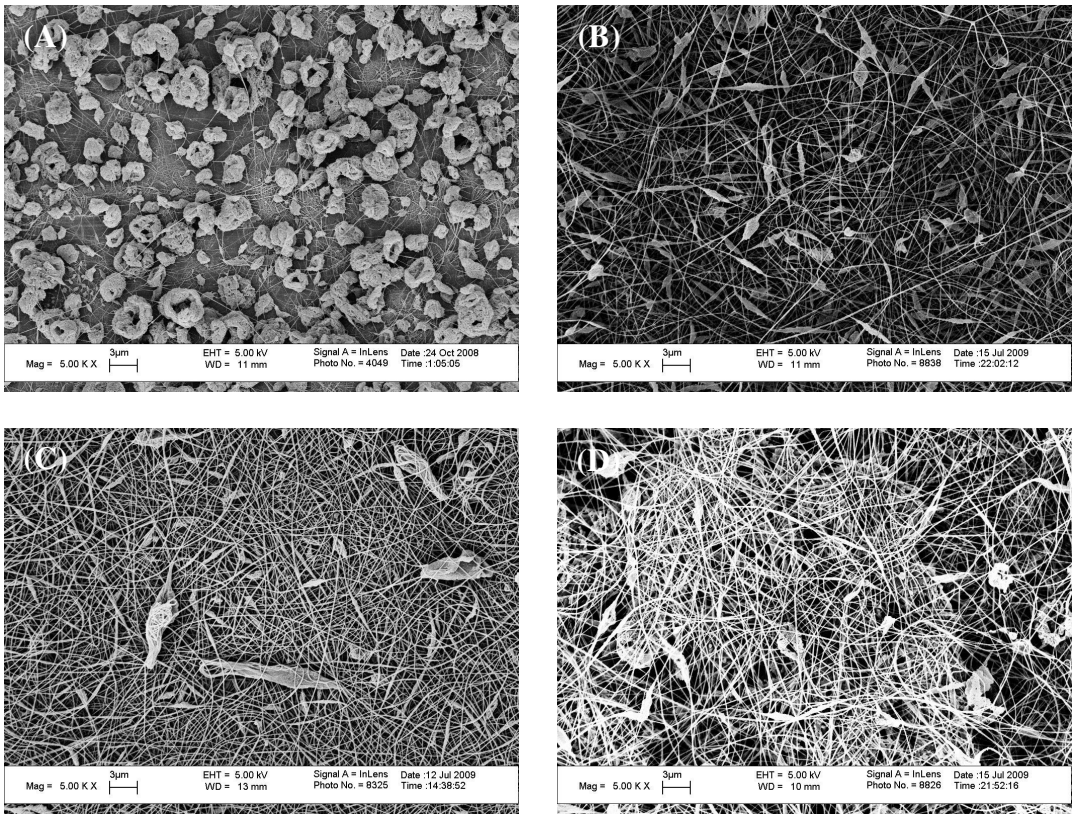

Figure C.1 SEM micrographs of electrospun blends of neat PS and nanofibers with varying weight percent of nanofiber (0 wt%, 5wt% 10 wt% 15 wt%).

Table C.1. Blend compositions of PS and nanosheet as well as electrospinning condition

	PS	nanosheet	Electrospinning conditions
(a)	100 %	0 %	- Concentration: 3 wt%
(b)	95 %	5 %	- Solvent: THF/DMF mixture (50:50)
(c)	90 %	10 %	- Operating voltage: 20 KV
(d)	85 %	15 %	- Distance: 10 cm

REFERENCES

[1] A. V. Ruzette and L. Leibler, "Block copolymers in tomorrow's plastics," *Nature Materials,* vol. 4, pp. 19-31, Jan 2005.

[2] Y. S. Thio, J. X. Wu, and F. S. Bates, "Epoxy toughening using low molecular weight poly(hexylene oxide)-poly(ethylene oxide) diblock copolymers," *Macromolecules,* vol. 39, pp. 7187-7189, Oct 2006.

[3] R. Adhikari, G. H. Michler, S. Henning, R. Godehardt, T. A. Huy, S. Goerlitz, and K. Knoll, "Morphology and micromechanical deformation behavior of styrene-butadiene block copolymers. Iv. Structure-property correlation in binary block copolymer blends," *Journal of Applied Polymer Science,* vol. 92, pp. 1219-1230, Apr 2004.

[4] M. Denac, V. Musil, and I. Smit, "Structure and mechanical properties of talc-filled blends of polypropylene and styrenic block copolymers," *Journal of Polymer Science Part B-Polymer Physics,* vol. 42, pp. 1255-1264, Apr 2004.

[5] C. C. Honeker and E. L. Thomas, "Impact of morphological orientation in determining mechanical properties in triblock copolymer systems," *Chemistry of Materials,* vol. 8, pp. 1702-1714, Aug 1996.

[6] C. D. Han, J. Kim, J. K. Kim, and S. G. Chu, "Viscoelastic behavior of mixtures of a block copolymer and a homopolymer," *Macromolecules,* vol. 22, pp. 3443-3451, Aug 1989.

[7] M. Thunga, B. K. Satapathy, U. Staudinger, R. Weidisch, M. Abdel-Goad, A. Janke, and K. Knoll, "Dynamic mechanical and rheological properties of binary s-(s/b)-s triblock copolymer blends," *Journal of Polymer Science Part B-Polymer Physics,* vol. 46, pp. 329-343, Feb 2008.

[8] M. Thunga, U. Staudinger, B. K. Satapathy, R. Weidisch, M. Abdel-Goad, A. Janke, and K. Knoll, "Influence of molecular architecture of s-s/b-s triblock copolymers on rheological properties," *Journal of Polymer Science Part B-Polymer Physics,* vol. 44, pp. 2776-2788, Oct 2006.

[9] N. Nishiyama and K. Kataoka, "Nanostructured devices based on block copolymer assemblies for drug delivery: Designing structures for enhanced drug

function," in *Polymer therapeutics ii: Polymers as drugs, conjugates and gene delivery systems*. vol. 193, 2006, pp. 67-101.

[10] A. Harada and K. Kataoka, "Supramolecular assemblies of block copolymers in aqueous media as nanocontainers relevant to biological applications," *Progress in Polymer Science,* vol. 31, pp. 949-982, Nov 2006.

[11] E. Waris, N. Ashammakhi, M. Lehtimaki, R. M. Tulamo, P. Tormala, M. Kellomaki, and Y. T. Konttinen, "Long-term bone tissue reaction to polyethylene oxide/polybutylene terephthalate copolymer (polyactive (r)) in metacarpophalangeal joint reconstruction," *Biomaterials,* vol. 29, pp. 2509-2515, Jun 2008.

[12] R. Duncan, "The dawning era of polymer therapeutics," *Nature Reviews Drug Discovery,* vol. 2, pp. 347-360, May 2003.

[13] H. Bonnemann and R. M. Richards, "Nanoscopic metal particles - synthetic methods and potential applications," *European Journal of Inorganic Chemistry,* pp. 2455-2480, Oct 2001.

[14] R. Glass, M. Moller, and J. P. Spatz, "Block copolymer micelle nanolithography," *Nanotechnology,* vol. 14, pp. 1153-1160, Oct 2003.

[15] F. S. Bates, "Polymer-polymer phase-behavior," *Science,* vol. 251, pp. 898-905, Feb 1991.

[16] T. L. Morkved, B. R. Chapman, F. S. Bates, T. P. Lodge, P. Stepanek, and K. Almdal, "Dynamics of ternary polymer blends: Disordered, ordered and bicontinuous microemulsion phases," *Faraday Discussions,* pp. 335-350, 1999.

[17] T. Hashimoto, H. Tanaka, and H. Hasegawa, "Ordered structure in mixtures of a block copolymer and homopolymers .2. Effects of molecular-weights of homopolymers," *Macromolecules,* vol. 23, pp. 4378-4386, Oct 1990.

[18] S. Koizumi, H. Hasegawa, and T. Hashimoto, "Ordered structure of block polymer homopolymer mixtures .4. Vesicle formation and macrophase separation," *Makromolekulare Chemie-Macromolecular Symposia,* vol. 62, pp. 75-91, Sep 1992.

[19] S. Koizumi, H. Hasegawa, and T. Hashimoto, "Ordered structures of block copolymer/homopolymer mixtures .5. Interplay of macrophase and microphase transitions," *Macromolecules,* vol. 27, pp. 6532-6540, Oct 1994.

[20] H. Tanaka, H. Hasegawa, and T. Hashimoto, "Ordered structure in mixtures of a block copolymer and homopolymers .1. Solubilization of low-molecular-weight homopolymers," *Macromolecules,* vol. 24, pp. 240-251, Jan 1991.

[21] H. Tanaka and T. Hashimoto, "Ordered structures of block polymer homopolymer mixtures .3. Temperature-dependence," *Macromolecules,* vol. 24, pp. 5713-5720, Sep 1991.

[22] D. J. Kinning, K. I. Winey, and E. L. Thomas, "Structural transitions from spherical to nonspherical micelles in blends of poly(styrene butadiene) diblock copolymer and polystyrene homopolymers," *Macromolecules,* vol. 21, pp. 3502-3506, Dec 1988.

[23] K. R. Shull and K. I. Winey, "Homopolymer distributions in lamellar copolymer homopolymer blends," *Macromolecules,* vol. 25, pp. 2637-2644, May 1992.

[24] K. I. Winey, E. L. Thomas, and L. J. Fetters, "The ordered bicontinuous double-diamond morphology in diblock copolymer homopolymer blends," *Macromolecules,* vol. 25, pp. 422-428, Jan 1992.

[25] S. T. Knauert, J. F. Douglas, and F. W. Starr, "The effect of nanoparticle shape on polymer-nanocomposite rheology and tensile strength," *Journal of Polymer Science Part B-Polymer Physics,* vol. 45, pp. 1882-1897, Jul 2007.

[26] K. Y. Lee and L. A. Goettler, "Structure-property relationships in polymer blend nanocomposites," 2004, pp. 1103-1111.

[27] M. Cadek, J. N. Coleman, V. Barron, K. Hedicke, and W. J. Blau, "Morphological and mechanical properties of carbon-nanotube-reinforced semicrystalline and amorphous polymer composites," *Applied Physics Letters,* vol. 81, pp. 5123-5125, Dec 2002.

[28] T. Lan and T. J. Pinnavaia, "Clay-reinforced epoxy nanocomposites," *Chemistry of Materials,* vol. 6, pp. 2216-2219, Dec 1994.

[29] Y. S. Thio, A. S. Argon, R. E. Cohen, and M. Weinberg, "Toughening of isotactic polypropylene with caco3 particles," *Polymer,* vol. 43, pp. 3661-3674, Jun 2002.

[30] Y. J. Li, Y. Kadowaki, T. Inoue, K. Nakayama, and H. Shimizu, "A novel thermoplastic elastomer by reaction-induced phase decomposition from a miscible polymer blend," *Macromolecules,* vol. 39, pp. 4195-4201, Jun 2006.

[31] R. Asaletha, M. G. Kumaran, and S. Thomas, "Thermoplastic elastomers from blends of polystyrene and natural rubber: Morphology and mechanical properties," *European Polymer Journal,* vol. 35, pp. 253-271, Feb 1999.

[32] I. W. Hamley, *The physics of block copolymers*: Oxford Science Publications, 1998.

[33] I. Goodman, *Developments in block copolymers* vol. 1. London: Applied Science, 1982.

[34] I. Goodman, *Developments in block copolymers* vol. 2. London: Elsevier Applied Science, 1985.

[35] G. Riess, G. Hurtrez, and P. Bahadur, *In encyclopedia of polymer science and engineering (block copolymers)* vol. 2, 1985.

[36] I. R. Schmolka, "Polyoxamers in the pharmaceutical industry," in *In polymers for controlled durg delivery*, P. J. Tarcha, Ed. Boston: CRC Press, 1991.

[37] V. M. Nace, "Polyoxyalkylene block copolymers," in *Nonionic surfactants* New York: Marcel Dekker, 1996.

[38] P. I. Flory, "Thermodynamics of high polymer solutions," *Journal of Chemical Physics,* vol. 10, pp. 51-61, Jan 1942.

[39] M. L. Huggins, "Theory of solutions of high polymers," *Journal of the American Chemical Society,* vol. 64, pp. 1712-1719, Jul-Dec 1942.

[40] L. Leibler, "Theory of microphase separation in block co-polymers," *Macromolecules,* vol. 13, pp. 1602-1617, 1980.

[41] A. K. Khandpur, S. Forster, F. S. Bates, I. W. Hamley, A. J. Ryan, W. Bras, K. Almdal, and K. Mortensen, "Polyisoprene-polystyrene diblock copolymer phase diagram near the order-disorder transition," *Macromolecules,* vol. 28, pp. 8796-8806, Dec 1995.

[42] E. Helfand, "Block copolymer theory .3. Statistical-mechanics of microdomain structure," *Macromolecules,* vol. 8, pp. 552-556, 1975.

[43] E. Helfand, "Block copolymers, polymer-polymer interfaces, and theory of inhomogeneous polymers," *Accounts of Chemical Research,* vol. 8, pp. 295-299, 1975.

[44] E. Helfand and Z. R. Wasserman, "Block copolymer theory .4. Narrow interphase approximation," *Macromolecules,* vol. 9, pp. 879-888, 1976.

[45] E. Helfand and Z. R. Wasserman, "Statistical thermodynamics of micro-domain structures in block copolymer systems," *Polymer Engineering and Science,* vol. 17, pp. 582-586, 1977.

[46] E. Helfand and Z. R. Wasserman, "Block copolymer theory .5. Spherical domains," *Macromolecules,* vol. 11, pp. 960-966, 1978.

[47] E. Helfand and Z. R. Wasserman, "Block co-polymer theory .6. Cylindrical domains," *Macromolecules,* vol. 13, pp. 994-998, 1980.

[48] M. W. Matsen and F. S. Bates, "Unifying weak- and strong-segregation block copolymer theories," *Macromolecules,* vol. 29, pp. 1091-1098, Feb 1996.

[49] Y. Rabin and J. F. Marko, "Microphase separation in charged diblock copolymers - the weak segregation limit," *Macromolecules,* vol. 24, pp. 2134-2136, Apr 1991.

[50] J. D. Vavasour and M. D. Whitmore, "Self-consistent mean field-theory of the microphases of diblock copolymers," *Macromolecules,* vol. 25, pp. 5477-5486, Sep 1992.

[51] P. G. D. Gennes, "Theory of x-ray scattering by liquid macromolecules with heavy atom labels," *Journal De Physique,* vol. 31, pp. 235-&, 1970.

[52] M. W. Matsen and M. Schick, "Microphase separation in starblock copolymer melts," *Macromolecules,* vol. 27, pp. 6761-6767, Nov 1994.

[53] M. W. Matsen and M. Schick, "Stable and unstable phases of a linear multiblock copolymer melt," *Macromolecules,* vol. 27, pp. 7157-7163, Nov 1994.

[54] E. F. Edwards, "The statistical mechanics of polymers with excluded volume," *Proc. Phys. Soc.,* vol. 85, p. 613, 1965.

[55] K. M. Hong and J. Noolandi, "Theory of inhomogeneous multicomponent polymer systems," *Macromolecules,* vol. 14, p. 727, 1981.

[56] T. Ohta and K. Kawasaki, "Equilibrium morphology of block copolymer melts " *Macromolecules,* vol. 19, p. 2621, 1986.

[57] T. Hashimoto, M. Shibayama, and H. Kawai, "Domain-boundary structure of styrene-isoprene block co-polymer films cast from solution .4. Molecular-weight dependence of lamellar microdomains," *Macromolecules,* vol. 13, pp. 1237-1247, 1980.

[58] K. I. Winey, E. L. Thomas, and L. J. Fetters, "Swelling a lamellar diblock copolymer with homopolymer - influences of homopolymer concentration and molecular-weight," *Macromolecules,* vol. 24, pp. 6182-6188, Nov 1991.

[59] K. I. Winey, E. L. Thomas, and L. J. Fetters, "Isothermal morphology diagrams for binary blends of diblock copolymer and homopolymer," *Macromolecules,* vol. 25, pp. 2645-2650, May 1992.

[60] M. W. Matsen, "Phase-behavior of block-copolymer homopolymer blends," *Macromolecules,* vol. 28, pp. 5765-5773, Aug 1995.

[61] M. W. Matsen, "Stabilizing new morphologies by blending homopolymer with block-copolymer," *Physical Review Letters,* vol. 74, pp. 4225-4228, May 1995.

[62] M. W. Matsen, "Immiscibility of large and small symmetrical diblock copolymers," *Journal of Chemical Physics,* vol. 103, pp. 3268-3271, Aug 1995.

[63] I. W. Hamley, *Developments in block copolymer science and technology*. New York: JOHN WILEY AND SONS, 2004.

[64] R. L. Lescanec, L. J. Fetters, and E. L. Thomas, "Assessing homopolymer distribution in abc triblock copolymer/homopolymer blends through a transition in interfacial geometry," *Macromolecules,* vol. 31, pp. 1680-1685, Mar 1998.

[65] I. Kimishima, H. Jinnai, and T. Hashimoto, "Control of self-assembled structures in binary mixtures of a-b diblock copolymer and a-c diblock copolymer by changing the interaction between b and c block chains," *Macromolecules,* vol. 32, pp. 2585-2596, Apr 1999.

[66] L. Kane, D. A. Norman, S. A. White, M. W. Matsen, M. M. Satkowski, S. D. Smith, and R. J. Spontak, "Molecular, nanostructural and mechanical characteristics of lamellar triblock copolymer blends: Effects of molecular weight and constraint," *Macromolecular Rapid Communications,* vol. 22, pp. 281-296, Mar 2001.

[67] J. Abetz, "Encyclopedia of polymer science and technology," in *Encyclopedia of Polymer Science and Technology*, 3 ed. vol. 1, J. I. Kroschwitz, Ed. New Jersey: John Wiley & Sons, 2003, pp. 482-523.

[68] M. R. Bockstaller, R. A. Mickiewicz, and E. L. Thomas, "Block copolymer nanocomposites: Perspectives for tailored functional materials," *Advanced Materials,* vol. 17, pp. 1331-1349, Jun 2005.

[69] A. Okada, M. Kawasumi, T. Kurauchi, and O. Kamigaito, "Synthesis and characterization of a nylon 6-clay hybrid," *Abstracts of Papers of the American Chemical Society,* vol. 194, pp. 10-MACR, Aug 1987.

[70] A. Usuki, Y. Kojima, M. Kawasumi, A. Okada, Y. Fukushima, T. Kurauchi, and O. Kamigaito, "Synthesis of nylon 6-clay hybrid," *Journal of Materials Research,* vol. 8, pp. 1179-1184, May 1993.

[71] G. H. Fredrickson and J. Bicerano, "Barrier properties of oriented disk composites," *Journal of Chemical Physics,* vol. 110, pp. 2181-2188, Jan 1999.

[72] P. J. Hine, H. R. Lusti, and A. A. Gusev, "Numerical simulation of the effects of volume fraction, aspect ratio and fibre length distribution on the elastic and

thermoelastic properties of short fibre composites," *Composites Science and Technology,* vol. 62, pp. 1445-1453, 2002.

[73] A. Gusev, H. R. Lusti, and P. J. Hine, "Stiffness and thermal expansion of short fiber composites with fully aligned fibers," *Advanced Engineering Materials,* vol. 4, pp. 927-931, Dec 2002.

[74] T. D. Fornes, J. W. Baur, Y. Sabba, and E. L. Thomas, "Morphology and properties of melt-spun polycarbonate fibers containing single- and multi-wall carbon nanotubes," *Polymer,* vol. 47, pp. 1704-1714, Feb 2006.

[75] E. Lahiff, R. Leahy, J. N. Coleman, and W. J. Blau, "Physical properties of novel free-standing polymer-nanotube thin films," *Carbon,* vol. 44, pp. 1525-1529, Jul 2006.

[76] S. R. C. Vivekchand, U. Ramamurty, and C. N. R. Rao, "Mechanical properties of inorganic nanowire reinforced polymer-matrix composites," *Nanotechnology,* vol. 17, pp. S344-S350, Jun 2006.

[77] M. Franco, I. Mondragon, and C. B. Bucknall, "Blends of epoxy resin with amine-terminated polyoxypropylene elastomer: Morphology and properties," *Journal of Applied Polymer Science,* vol. 72, pp. 427-434, Apr 1999.

[78] O. K. Muratoglu, A. S. Argon, R. E. Cohen, and M. Weinberg, "Toughening mechanism of rubber-modified polyamides," *Polymer,* vol. 36, pp. 921-930, Mar 1995.

[79] D. Mangaraj, "Elastomer blends," *Rubber Chemistry and Technology,* vol. 75, pp. 365-427, Jul-Aug 2002.

[80] R. S. Rajeev and S. K. De, "Thermoplastic elastomers based on waste rubber and plastics," *Rubber Chemistry and Technology,* vol. 77, pp. 569-578, Jul-Aug 2004.

[81] A. F. Yee and R. A. Pearson, "Toughening mechanisms in elastomer-modified epoxies .1. Mechanical studies," *Journal of Materials Science,* vol. 21, pp. 2462-2474, Jul 1986.

[82] S. Kumar, M. A. Alam, and J. Y. Murthy, "Effect of percolation on thermal transport in nanotube composites," *Applied Physics Letters,* vol. 90, Mar 2007.

[83] M. Akiba and A. S. Hashim, "Vulcanization and crosslinking in elastomers," *Progress in Polymer Science,* vol. 22, pp. 475-521, 1997.

[84] J. Glazer, "Dilatometric measurement of the rate of vulcanization of crepe-rubber by sulphur monochloride," *Nature,* vol. 167, pp. 404-405, 1951.

[85] J. Glazer, "Vulcanization of crepe rubber by sulfur monochloride .2. The dilatometric method," *Journal of Polymer Science,* vol. 14, pp. 225-240, 1954.

[86] J. Glazer and J. H. Schulman, "Vulcanization of crepe rubber by sulfur monochloride .1. The gelation method," *Journal of Polymer Science,* vol. 14, pp. 169-179, 1954.

[87] S. H. Kim, M. J. Misner, T. Xu, M. Kimura, and T. P. Russell, "Highly oriented and ordered arrays from block copolymers via solvent evaporation," *Advanced Materials,* vol. 16, pp. 226-+, 2004.

[88] I. W. Hamley, M. D. Gehlsen, A. K. Khandpur, K. A. Koppi, J. H. Rosedale, M. F. Schulz, F. S. Bates, K. Almdal, and K. Mortensen, "Complex layered phases in asymmetric diblock copolymers," *Journal De Physique Ii,* vol. 4, pp. 2161-2186, 1994.

[89] G. J. Liu, X. H. Yan, and S. Duncan, "Polystyrene-block-polyisoprene nanofiber fractions. 1. Preparation and static light-scattering study," *Macromolecules,* vol. 35, pp. 9788-9793, Dec 2002.

[90] L. H. Sperling, *Introduction to physical polymer science*, 4 ed.: John Wiley & Sons, Inc., 2006.

[91] P. J. Carreau, De Kee, D. C. R., and Chhabra, R. P., *Rheology of polymeric systems: Principles and applications*: Hanser/Gardner, 1997.

[92] P. Cassagnau, "Melt rheology of organoclay and fumed silica nanocomposites," *Polymer,* vol. 49, pp. 2183-+, Apr 2008.

[93] L. Elias, F. Fenouillot, J. C. Majeste, and P. Cassagnau, "Morphology and rheology of immiscible polymer blends filled with silica nanoparticles," *Polymer,* vol. 48, pp. 6029-6040, Sep 2007.

[94] C. D. Han and J. K. Kim, "Molecular theory for the viscoelasticity of compatible polymer mixtures .1. A tube model approach," *Macromolecules,* vol. 22, pp. 1914-1921, Apr 1989.

[95] C. D. Han and J. K. Kim, "Molecular theory for the viscoelasticity of compatible polymer mixtures .2. Tube model with reptation and constraint release contributions," *Macromolecules,* vol. 22, pp. 4292-4302, Nov 1989.

[96] M. B. Kossuth, D. C. Morse, and F. S. Bates, "Viscoelastic behavior of cubic phases in block copolymer melts," *Journal of Rheology,* vol. 43, pp. 167-196, Jan-Feb 1999.

[97] R. Krishnamoorti and K. Yurekli, "Rheology of polymer layered silicate nanocomposites," *Current Opinion in Colloid & Interface Science,* vol. 6, pp. 464-470, Nov 2001.

[98] M. Sepehr, L. A. Utracki, X. X. Zheng, and C. A. Wilkie, "Polystyrenes with macro-intercalated organoclay. Part ii. Rheology and mechanical performance," *Polymer,* vol. 46, pp. 11569-11581, Nov 2005.

[99] P. Cassagnau, "Melt rheology of organoclay and fumed silica nanocomposites " *Polymer,* vol. 49, p. 14, 29 April 2008 2008.

[100] C. D. Han, J. W. Kim, and J. K. Kim, "Determination of the order-disorder transition-temperature of block copolymers," *Macromolecules,* vol. 22, pp. 383-394, Jan 1989.

[101] C. D. Han, D. M. Baek, J. K. Kim, T. Ogawa, N. Sakamoto, and T. Hashimoto, "Effect of volume fraction on the order-disorder transition in low-molecular-weight polystyrene-block-polyisoprene copolymers .1. Order-disorder transition-temperature determined by rheological measurements," *Macromolecules,* vol. 28, pp. 5043-5062, Jul 1995.

[102] M. Doi and S. F. Edwards, "Dynamics of concentrated polymer systems .3. Constitutive equation," *Journal of the Chemical Society-Faraday Transactions Ii,* vol. 74, pp. 1818-1832, 1978.

[103] A. J. Kinloch, S. J. Shaw, D. A. Tod, and D. L. Hunston, "Deformation and fracture-behavior of a rubber-toughened epoxy .1. Microstructure and fracture studies," *Polymer,* vol. 24, pp. 1341-1354, 1983.

[104] M. J. Richardson and N. G. Savill, "Volumetric properties of polystyrene - influence of temperature, molecular-weight and thermal-treatment," *Polymer,* vol. 18, pp. 3-9, 1977.

[105] L. G. A. A.I. Andreyeva, and A. S. Kuz'minskii, "Study of the catalytic action of products of treatment of $ticl_3$ with ethanol during the oxidation of 1,4-*cis*-polyisoprene stabilized with n-phenyl-β-naphthylamine and 2,6-di-tert-butyl-4-methylphenol," *Polymer Science, U.S.S.R.,* vol. 10, pp. 2475-2481, 1967.

[106] K. J. Ishizu and A. Onen, "Core-shell type polymer microspheres prepared by domain fixing of block copolymer films," *Journal of Polymer Science Part a-Polymer Chemistry,* vol. 27, pp. 3721-3731, Oct 1989.

[107] G. J. Liu, Z. Li, and X. H. Yan, "Synthesis and characterization of poly styrene-block-polyisoprene nanofibers with different crosslinking densities," *Polymer,* vol. 44, pp. 7721-7727, 2003.

[108] M. L. Williams, R. F. Landel, and J. D. Ferry, "Mechanical properties of substances of high molecular weight .19. The temperature dependence of relaxation mechanisms in amorphous polymers and other glass-forming liquids," *Journal of the American Chemical Society,* vol. 77, pp. 3701-3707, 1955.

[109] W. P. Cox and E. H. Merz, "Correlation of dynamic and steady flow viscosities," *Journal of Polymer Science,* vol. 28, pp. 619-622, 1958.

[110] M. M. Cross, "Rheology of non-newtonian fluids - a new flow equation for pseudoplastic systems," *Journal of Colloid Science,* vol. 20, pp. 417-&, 1965.

[111] R. D.-C. Evaristo Riande, Margarita G. Prolongo, Rosa M. Masegosa, and Catalina Salom, *Polymer viscoelasticity*: Marcel Dekker, 2000.

[112] A. Celzard, E. McRae, C. Deleuze, M. Dufort, G. Furdin, and J. F. Mareche, "Critical concentration in percolating systems containing a high-aspect-ratio filler," *Physical Review B,* vol. 53, pp. 6209-6214, Mar 1996.

[113] A. L. R. Bug, S. A. Safran, and I. Webman, "Continuum percolation of rods," *Physical Review Letters,* vol. 54, pp. 1412-1415, 1985.

[114] X. Zheng, M. G. Forest, R. Vaia, M. Arlen, and R. Zhou, "A strategy for dimensional percolation in sheared nanorod dispersions," *Advanced Materials,* vol. 19, pp. 4038-+, Nov 2007.

[115] F. Hussain, M. Hojjati, M. Okamoto, and R. E. Gorga, "Review article: Polymer-matrix nanocomposites, processing, manufacturing, and application: An overview," *Journal of Composite Materials,* vol. 40, pp. 1511-1575, Sep 2006.

[116] S. Komarneni, "Nanocomposites," *Journal of Materials Chemistry,* vol. 2, pp. 1219-1230, Dec 1992.

[117] L. L. Beecroft and C. K. Ober, "Nanocomposite materials for optical applications," *Chemistry of Materials,* vol. 9, pp. 1302-1317, Jun 1997.

[118] C. Sanchez, B. Lebeau, F. Chaput, and J. P. Boilot, "Optical properties of functional hybrid organic-inorganic nanocomposites," *Advanced Materials,* vol. 15, pp. 1969-1994, Dec 2003.

[119] K. G. Marra, J. W. Szem, P. N. Kumta, P. A. DiMilla, and L. E. Weiss, "In vitro analysis of biodegradable polymer blend/hydroxyapatite composites for bone tissue engineering," *Journal of Biomedical Materials Research,* vol. 47, pp. 324-335, Dec 1999.

[120] R. Gangopadhyay and A. De, "Conducting polymer nanocomposites: A brief overview," *Chemistry of Materials,* vol. 12, pp. 608-622, Mar 2000.

[121] F. Croce, G. B. Appetecchi, L. Persi, and B. Scrosati, "Nanocomposite polymer electrolytes for lithium batteries," *Nature,* vol. 394, pp. 456-458, Jul 1998.

[122] M. Granstrom and O. Inganas, "White light emission from a polymer blend light emitting diode," *Applied Physics Letters,* vol. 68, pp. 147-149, Jan 1996.

[123] J. N. Coleman, U. Khan, and Y. K. Gun'ko, "Mechanical reinforcement of polymers using carbon nanotubes," *Advanced Materials,* vol. 18, pp. 689-706, Mar 2006.

[124] A. J. Crosby and J. Y. Lee, "Polymer nanocomposites: The "Nano" Effect on mechanical properties," *Polymer Reviews,* vol. 47, pp. 217-229, 2007.

[125] S. Y. Hobbs, M. E. J. Dekkers, and V. H. Watkins, "Effect of interfacial forces on polymer blend morphologies," *Polymer,* vol. 29, pp. 1598-1602, Sep 1988.

[126] B. John, K. T. Varughese, Z. Oommen, P. Potschke, and S. Thomas, "Dynamic mechanical behavior of high-density polyethylene/ethylene vinyl acetate copolymer blends: The effects of the blend ratio, reactive compatibilization, and dynamic vulcanization," *Journal of Applied Polymer Science,* vol. 87, pp. 2083-2099, Mar 2003.

[127] S. Ma and Y. Thio, "Melt rheology of polystyrene/elastomeric fiber and sheet nanoparticles"," *Journal of Polymer Science Part B-Polymer Physics,* 2010(Submitted).

[128] S. Ma and Y. Thio, "The effect of crosslinked elastomeric nanoparticle shapes on blends," 2010(To be submitted).

[129] A. Khatory, F. Lequeux, F. Kern, and S. J. Candau, "Linear and nonlinear viscoelasticity of semidilute solutions of wormlike micelles at high-salt content," *Langmuir,* vol. 9, pp. 1456-1464, Jun 1993.

[130] J. H. Tian, W. Yu, and C. X. Zhou, "The preparation and rheology characterization of long chain branching polypropylene (vol 47, pg 7962, 2006)," *Polymer,* vol. 48, pp. 2186-2186, Mar 2007.

[131] D. Graebling, "Synthesis of branched polypropylene by a reactive extrusion process," *Macromolecules,* vol. 35, pp. 4602-4610, Jun 2002.

[132] S. Ma and Y. Thio, "Viscoelastic properties of blend of polystyrene and crosslinked polystyrene-b-polyisoprene nanofiber," *Polymer,* 2010(Submitted).

[133] I. Balberg, "Excluded-volume explanation of archie law," *Physical Review B,* vol. 33, pp. 3618-3620, Mar 1986.

[134] E. Charlaix, E. Guyon, and N. Rivier, "A criterion for percolation-threshold in a random array of plates," *Solid State Communications,* vol. 50, pp. 999-1002, 1984.

[135] L. E. Nielse and R. F. Landel, *Mechanical properties of polymers and composites*, 2nd ed. New York: Marcel Dekker, 1994.

[136] L. H. Sperling, *Physical polymer science*, 3rd ed. New York: Wiley, 2001.

[137] Y. Kobayashi, C. L. Wang, K. Hirata, W. Zheng, and C. Zhang, "Effects of composition and external electric field on positronium formation in a polymer blend system," *Physical Review B,* vol. 58, pp. 5384-5389, Sep 1998.

[138] C. M. Roland, "Rheology of a miscible polymer blend," *Journal of Polymer Science Part B-Polymer Physics,* vol. 26, pp. 839-856, Apr 1988.

[139] Y. Q. Rao and J. M. Pochan, "Mechanics of polymer-clay nanocomposites," *Macromolecules,* vol. 40, pp. 290-296, Jan 2007.

[140] S. Praveen, P. K. Chattopadhyay, S. Jayendran, B. C. Chakraborty, and S. Chattopadhyay, "Effect of nanoclay on the mechanical and damping properties of aramid short fibre-filled styrene butadiene rubber composites," *Polymer International,* vol. 59, pp. 187-197, Feb.

[141] H. Chen, M. L. Cheng, Y. C. Jean, L. J. Lee, and J. Yang, "Effect of co2 exposure on free volumes in polystyrene studied by positron annihilation spectroscopy," *Journal of Polymer Science Part B-Polymer Physics,* vol. 46, pp. 388-405, Feb 2008.

[142] Z. B. Wang, H. T. Pang, G. C. Li, and Z. K. Zhang, "Glass transition and free volume of high impact polystyrene/tio2 nanocomposites determined by dilatometry," *Journal of Macromolecular Science Part B-Physics,* vol. 45, pp. 689-697, 2006.

[143] S. Ma and Y. Thio, "Dynamic mechanical properties of homopolystyrene and elastomeric poly(styrene)-b-poy(isoprene)
block copolymer blends: Morphology and crosslinking density effects," 2010(To be submitted).

[144] T. Heijboar, *Molecular basis of transitions and relaxations*. New York: Gordon and Breach, 1978.

[145] P. C. LeBaron, Z. Wang, and T. J. Pinnavaia, "Polymer-layered silicate nanocomposites: An overview," *Applied Clay Science,* vol. 15, pp. 11-29, Sep 1999.

[146] G. H. Chen, D. J. Wu, W. G. Weng, and W. L. Yan, "Preparation of polymer/graphite conducting nanocomposite by intercalation polymerization," *Journal of Applied Polymer Science,* vol. 82, pp. 2506-2513, Dec 2001.

[147] J. Li, S. J. Guo, Y. M. Zhai, and E. K. Wang, "Nafion-graphene nanocomposite film as enhanced sensing platform for ultrasensitive determination of cadmium," *Electrochemistry Communications,* vol. 11, pp. 1085-1088, May 2009.

[148] A. R. Abramson, W. C. Kim, S. T. Huxtable, H. Q. Yan, Y. Y. Wu, A. Majumdar, C. L. Tien, and P. D. Yang, "Fabrication and characterization of a nanowire/polymer-based nanocomposite for a prototype thermoelectric device," *Journal of Microelectromechanical Systems,* vol. 13, pp. 505-513, Jun 2004.

[149] S. George, K. Ramamurthy, J. S. Anand, G. Groeninckx, K. T. Varughese, and S. Thomas, "Rheological behaviour of thermoplastic elastomers from polypropylene/acrylonitrile-butadiene rubber blends: Effect of blend ratio, reactive compatibilization and dynamic vulcanization," *Polymer,* vol. 40, pp. 4325-4344, Jul 1999.

[150] R. A. Pearson and A. F. Yee, "Toughening mechanisms in elastomer-modified epoxies .3. The effect of cross-link density," *Journal of Materials Science,* vol. 24, pp. 2571-2580, Jul 1989.

[151] J. D. Ferry, *Viscoleastic properties of polymers* 3rd edn. ed.: Wiley, 1980.

[152] D. G. H. Ballard, G. D. Wignall, and J. Schelten, "Measurement of molecular dimensions of polystyrene chains in bulk polymer by low angles neutron-diffraction," *European Polymer Journal,* vol. 9, pp. 965-969, 1973.

[153] J. X. Wu, Y. S. Thio, and F. S. Bates, "Structure and properties of pbo-peo diblock copolymer modified epoxy," *Journal of Polymer Science Part B-Polymer Physics,* vol. 43, pp. 1950-1965, Aug 2005.

[154] J. M. Deitzel, J. Kleinmeyer, D. Harris, and N. C. B. Tan, "The effect of processing variables on the morphology of electrospun nanofibers and textiles," *Polymer,* vol. 42, pp. 261-272, Jan 2001.

[155] A. K. Bledzki and J. Gassan, "Composites reinforced with cellulose based fibres," *Progress in Polymer Science,* vol. 24, pp. 221-274, 1999.

[156] J. R. Dees and J. E. Spruiell, "Structure development during melt spinning of linear polyethylene fibers," *Journal of Applied Polymer Science,* vol. 18, pp. 1053-1078, 1974.

[157] J. W. Leenslag and A. J. Pennings, "High-strength poly(l-lactide) fibers by a dry-spinning hot-drawing process," *Polymer,* vol. 28, pp. 1695-1702, Sep 1987.

[158] P. J. Barham and A. Keller, "High-strength polyethylene fibers from solution and gel spinning," *Journal of Materials Science,* vol. 20, pp. 2281-2302, 1985.

[159] Y. Dzenis, "Spinning continuous fibers for nanotechnology," *Science,* vol. 304, pp. 1917-1919, Jun 2004.

[160] P. W. Gibson, H. L. Schreuder-Gibson, and D. Rivin, "Electrospun fiber mats: Transport properties," *Aiche Journal,* vol. 45, pp. 190-195, Jan 1999.

[161] X. H. Zong, S. F. Ran, K. S. Kim, D. F. Fang, B. S. Hsiao, and B. Chu, "Structure and morphology changes during in vitro degradation of electrospun poly(glycolide-co-lactide) nanofiber membrane," *Biomacromolecules,* vol. 4, pp. 416-423, Mar-Apr 2003.

[162] C. P. Barnes, S. A. Sell, E. D. Boland, D. G. Simpson, and G. L. Bowlin, "Nanofiber technology: Designing the next generation of tissue engineering scaffolds," *Advanced Drug Delivery Reviews,* vol. 59, pp. 1413-1433, Dec 2007.